STATUS REPORTS

to the

PAPERMAKING

and

PROCESS SIMULATION AND CONTROL

PROJECT ADVISORY COMMITTEE

March 20 - 21, 1995

INSTITUTE OF PAPER SCIENCE AND TECHNOLOGY

Atlanta, Georgia

ANNUAL RESEARCH REVIEW

PAPERMAKING
and
PROCESS SIMULATION AND CONTROL

March 20 - 21, 1995

February 15, 1995

TO: MEMBERS OF THE PAPERMAKING AND THE PROCESS SIMULATION AND CONTROL PROJECT ADVISORY COMMITTEE

Attached for your review are the Status Reports for the projects to be discussed at the Papermaking and the Process Simulation and Control Project Advisory Committee meeting. The program review is scheduled for Monday, March 20, 1995, at 1:00 to 5:00 p.m. The Papermaking PAC and the Process Simulation and Control PAC committee meetings will meet separately during the morning of March 21, 1995, from 8:00 a.m. to 12:00 p.m.

We look forward to seeing you at this time.

Sincerely,

David I. Orloff, Ph.D.
Professor of Engineering & Director
Engineering and Paper Materials Division

DIO/map

Attachments

Institute of Paper Science and Technology, Inc.

500 10th Street, N.W.
Atlanta, GA 30318-5794

Telephone 404-853-9500
FAX # 404-853-9510

PAPERMAKING
PROJECT ADVISORY COMMITTEE

IPST Laision: David Orloff (404) 853-1872, FAX (404) 853-9510

Mr. Jack F. Brown *(1994)
Manager, Paper and Coatings
Boise Cascade Corporation
Pulp and Paper Research
4435 North Channel Avenue
Portland, OR 97217-7652
(503) 286-7418
(503) 286-7467 FAX

Mr. James Buob *(1998)
Assistant Paper Mill Manager
Temple-Inland Inc.
P.O. Box 816
Silsbee, TX 77656
(409) 276-1411
(409) 276-3108

Mr. Frank Cunnane *(1996)
Vice President - Marketing
Asten Group, Inc.
Asten Press Fabrics, Inc.
P. O. Box 518
Clinton, SC 29325-0518
(803) 833-3800
(803) 833-6657 FAX

Dr. Eugene V. Hoefs *(1997) (Vice Chairman)
Sr. Research Associate
Appleton Papers Inc.
P.O. Box 359
Appleton, WI 54912-0359
(414) 730-7178
(414) 730-7243 FAX

Mr. George Iverson *(1996)
Supervisor, Papermaking Technology
Eastman Kodak Company
Polymer Processing Division
1669 Lake Avenue
Rochester, NY 14652-3622
(716) 588-3870
(716) 588-2680 FAX

Mr. Jeffrey M. Jensen *(1996)
Production Manager
Westvaco Corporation
Bleached Board Division
104 East Riverside Street
Covington, VA 24426
(703) 969-5000
(703) 969-5486 FAX

Mr. Gurudas Khambadkone *(1997)
The Mead Corporation
Mead Central Research
8th & Hickory Sts.
Chillicothe, OH 45601-0000
(614) 772-3394
(614) 772-3595 FAX

Mr. Joseph P. MacDowell *(1996)
Research Project Supervisor - Coated
and Uncoated
P. H. Glatfelter Co.
228 S. Main Street
Spring Grove, PA 17362-1000
(717) 225-4711
(717) 225-7454 FAX

Dr. Franco Palumbo *(1997)
Riverwood International Corporation
P. O. Box 35800
West Monroe, LA 71294-5800
(318) 362-2000
(318) 362-2133 FAX

Mr. Richard Reese *(1996)
Sr. Paper Machine Engineer
Georgia-Pacific Corporation
P. O. Box 105605
133 Peachtree St., NE
Atlanta, GA 30348
(404) 652-4000
(404) 584-1466 FAX

Mr. John Rogers *(1997)
Technical Director
Sandusky International Inc.
P.O. Box 5012
Sandusky, OH 44870-8012
(419) 626-5340
(419) 626-8674 FAX

Dr. Jay A. Shands *(1997)
Manager, Forming Systems
Beloit Corporation
Rockton Research Center
1165 Prairie Hill Road
Rockton, IL 61072-1595
(608) 364-8501
(608) 364-8600 FAX

* The dates in ( ) indicate the final year of the appointment.

Papermaking PAC (cont.)

Dr. Michael S. Steltenkamp *(1996)
Department Leader
Champion International Corporation
West Nyack Rd.
West Nyack, NY 10994-7228
(914) 578-7228
(914) 578-7175 FAX

Mr. James F. Stewart *(1996)
Division VP Mill Operations
Stone Container Corporation
1979 Lakeside Parkway
Suite 300
Tucker, GA 30084
(404) 621-6700
(404) 621-6747 FAX

Mr. Benjamin A. Thorp *(1997)
Vice President, Process Technology
Consumer Products Business
James River Corporation
P. O. Box 2218
Richmond, VA 23217-2218
(804) 649-4335
(804) 649-4369 FAX

Mr. James C. West *(1995)
Containerboard Manufacturing Manager
Weyerhaeuser Company
5410 79th Avenue Court
Tacoma, WA 98467-3970
(206) 924-2345
(206) 924-2303 FAX

Mr. Lloyd O. Westling *(1996)
Superintendent
Longview Fibre Company
P. O. Box 639
Longview, WA 98632
(206) 425-1550
(206) 425-9877 FAX

Dr. David White *(1997) (Chairman)
Research Associate
Union Camp Corporation
P.O. Box 3301
Princeton, NJ 08543-3301
(609) 896-1200
(609) 844-7366 FAX

* The dates in ( ) indicate the final year of the appointment.

PROCESS SIMULATION AND CONTROL
PROJECT ADVISORY COMMITTEE

IPST Laision: Douglas Coffin (404) 853-9720, FAX (404) 853-9510

Dr. Al al-Shaikh *(1997)
Director, Product Management
Measurex Corporation
One Results Way
Cupertino, CA 95014
(408) 255-1500
(408) 864-7547 FAX

Dr. G.R. (Ron) Brown *(1995)
Director of Laurel Research Laboratory
Westvaco Corporation
11101 Johns Hopkins Road
Laurel, MD 20723-6006
(301) 497-1301
(301) 497-1309 FAX

Mr. Karel K. Cerny *(1995)
Senior Control Systems Engineer
Georgia-Pacific Corporation
133 Peachtree Street, NE
P. O. Box 105605
Atlanta, GA 30348-5605
(404) 652-4603
(404) 584-1466 FAX

Dr. Sanford G. Levy *(1997) (Chairman)
R&D Group Leader - Process
Control Applications
Union Camp Corporation
3401 Princeton Pike
Lawrenceville, NJ 08648
(609) 844-7361
(609) 844-7366 FAX

Mr. Robert E. McIntyre *(1996)
Technical Resource Coordinator
Asten Group, Inc.
209 Brereton Drive
Raleigh, NC 27615
(919) 847-0506
(919) 676-4801 FAX

Mr. Willard M. Reed, Jr. *(1995)
Process Analysis Supervisor
MacMillan Bloedel Inc.
P. O. Box 336
Pine Hill, AL 36769-0336
(205) 963-4391
(205) 963-4513 FAX

Mr. Glen C. Smith *(1995)
Technical Manager
The Mead Corporation
Central Research Labs
8th and Hickory Streets
Chillicothe, OH 45601
(614) 772-3513
(614) 772-3595 FAX

* The dates in ( ) indicate the final year of the appointment.

PAPERMAKING/PROCESS SIMULATION AND CONTROL PROJECT ADVISORY COMMITTEE MEETING

March 20 - 21, 1995
Institute of Paper Science and Technology
Atlanta, Georgia

AGENDA

Papermaking/Process Simulation and Control Program Review (APR)

March 20, 1995

1:00 p.m. - 1:15 p.m.	Opening Remarks and Anti Trust Statement	David White
1:15 p.m. - 2:00 p.m.	Project E00101 Forming Hydrodynamics: Analysis/Optimization and Future Trends	Cyrus Aidun
2:00 p.m. - 2:30 p.m.	Project F004 (3680) Wet Pressing and Project F002 Displacement Dewatering (the work of Zhong Cai)	David Orloff
2:30 p.m. - 3:00 p.m.	Increased Productivity by Improving Steam Box Performance	David Orloff
3:00 p.m. - 3:15 p.m.	Break	
3:15 p.m. - 3:30 p.m.	Project F001 (3470)/3595 Advances in Impulse Drying Research	David Orloff
3:30 p.m. - 4:00 p.m.	Project F003 (3674) Dynamics of Suspensions in Papermaking/Coating: A New Approach	Cyrus Aidun
4:00 p.m. - 4:30 p.m.	Sensor Development for the Paper Industry	Doug Coffin
4:30 p.m. - 5:00 p.m.	Project F006 (3730) Air-Sheet Interactions	Cyrus Aidun P. Neitzel (GT)

March 21, 1995

8:00 a.m. - 12:00 p.m.	Papermaking Committee Discussions	David Orloff

TABLE OF CONTENTS

TABLE FLOW

STATUS REPORT

FOR

PROJECT E00103

Zhong Cai

March 20 - 21, 1995

Institute of Paper Science and Technology
500 10th Street, N.W.
Atlanta, Georgia 30318

TECHNICAL PROGRAM REVIEW

Project Title: TABLE FLOW
Project Code: TABLE
Project No.: E00103
Division: Engineering and Paper Materials
Project Staff: Zhong Cai
Budget (FY ë93-94): $66,097
Reporting Period: September 1994 - January 1995

OBJECTIVE

Process model for the table flow on the fourdrinier.

DISCUSSION

The following discussion of Dr. Cai's work on displacement dewatering was compiled from notes on his computer, after his death.

Dr. Cai considered the following five technical issues to be of importance.
1.) Fiber sheet forming, 2.) Drain flow, 3.) Fiber orientation and thickness variation, 4.) Fiber flocculation and dispersion, 5.) Relationship of the fiber distribution with the headbox jet.

Notes on Table Flow

In a study by Britt and Unbehend [1], they discussed two distinct zones of water removal on the paper machine prior to the press section. One is the forming zone from the slice to the suction boxes, in which the water removal mechanism is drainage flow. The other is the vacuum zone, in which water is displaced in the wet sheet by air in response to vacuum.

Their experimental work included five paper stock samples representing a wide range of freeness values. These samples were defibered newsprint, defibered corrugated board, defibered linerboard, laboratory white stock, and thermomechanical fluff pulp.

They found that the so-called "dry line" on the foundrinier, where the consistency reaches the general range of 4-7%, is the dividing line between the two zones. In the first zone, water forms a continuous phase, and its rate of flow depends on the effective head and its ability to find passages through the suspended stock and forming web. In the second zone, the consistency has reached a point at which appreciable outflow of water occurs only with a high degree of vacuum. The mechanism is largely the displacement of water by air, along with compression and consolidation of the entire system. In the relatively thin paper sheet, some of the air channels through the pores of the sheet rather than pushing out water.

They also found that the addition of polymeric floccullants has a direct effect upon the freeness of a stock. As the drainability is increased by flocculation, there is a loss in vacuum response because of the channeling of air through the thin areas. The loss in response to vacuum also occurs as a result of increased microporosity.

Notes on Retention of Small Articles in Fiber Mats

Han studied the retention of small particles in fiber mats involved in the flow process [2]. First he considered the diffusion in a fiber mat which was conceived as a network of a very large number of interconnected capillaries of varying sizes and lengths. The attenuation process of the particle takes place only in short capillaries between two interconnected points. He found out that the collection efficiency, which is dimensionless and is the fraction of approaching particles collected by fibers, is proportional to the 2/3 power of the diffusion coefficient (in the units of m^2/s). Available experimental data supported this conclusion [3]. He then studied the problem of filtration in which both fibers and particles are to be retained from the suspension. The fiber mat thickness increases with time and is assumed to be at a constant rate. Analytical solutions were derived. Experimental measurements were also used for the comparison.

Han and Chang then studied the filtration process, including the compressibility of fiber mats [4].

Notes on Han's Review

In a report by Han [5], a critical review of the status of the sheet forming process in the table flow section has been presented. The sheet forming process is considered as filtration of a compressible material. The developed mathematical model included the essential features of fiber retention, flow resistance, mat compressibility, and particle distribution. Fiber dispersion is not included.

The mathematical expression for the mat compression is expressed in mat density as a power-law function of compaction pressure. The power index is found to be from 0.22 to 0.45 for cellulosic and synthetic fibers. The ratio of the fiber length to its diameter is found to be about 500 for glass fibers, about 100 for nylon fibers, and less than 100 for cellulose fibers.

Fluid flow through compressible mats involves both viscous and inertial resistance. Therefore, the Forchheimer relationship is used. The suggested porosity function form is, however, slightly different from the Kozeny-Carman form or Ergun form. There are two empirical constants in the porosity function, and an additional empirical constant in the inertial part of the expression.

The filtration expression, without the inertial term, is used for the evaluation of specific surface and volume of cellulosic fibers in constant rate filtration.

When fine particles are collected in a fiber mat formed by filtration, their distribution is exponential. This has been experimentally confirmed for both incompressible and compressible mats formed from simple filtrations.

The fiber retention in mass fraction on a wire screen is deduced from the probability theory and has been experimentally verified under idealized conditions.

Rheology Model of Fiber Suspension

The work by Corey [6] establishes the rheological behavior of suspensions of a single kind of material (asbestos fiber) in various liquids, as a function of fiber concentration,

temperature, and shear rate. Experiments have been designed and conducted to verify various relationships between the viscosity and other parameters.

The classic results suggested equations for the relative viscosity. The relative viscosity of an extremely dilute suspension of spherical particles given by Einstein is

$$\eta_r = 1 + 2.5\, c$$

where c is the volume fraction of spheres. This result is correct up to the extent that binary collisions, long range hydrodynamic interactions, and the mutual volume of exclusion are neglected. Einstein's hydrodynamic approach has been modified by many researchers to account for the factors mentioned above.

Jeffery derived the equation for the viscosity of an infinitely dilute suspension of epplisoids as

$$\eta_r = 1 + \nu\, c$$

where n is a parameter which is a function of the particle shape. Jeffery's result is based on the assumption that particles will tend to adopt that motion which corresponds to the least dissipation of energy. This suggests the existence of a steady state motion of particles.

Fiber length follows normal distribution. These fibers are machine-cut polyester and nylon fibers. The length to diameter ratios for the polyester and nylon fibers are about 83 and 16, respectively.

A method to characterize the state of a concentrated suspension of rod-like particles undergoing flow has been developed [7]. Particle orientation distribution can be predicted with empirically determined constants.

References

1. Britt, K.W. and Unbehend, J.E., "Water Removal during Paper Formation", *TAPPI Journal*, April, 1985, pp.104-107.

2. Han, S.T., "Retension of Small Particles in Fiber Mats", *TAPPI Journal*, Vol. 47, No. 12, December 1964, pp.782-787.

3. Johnson, R.C., "A Study of Particle Retention in Relation to the Structure of a Fibrous Mat", Ph.D. Thesis, The Institute of Paper Chemistry, 1961.

4. Han, S.T. and Chang, N.L., "Retension of Fines in Fiber Mats", *TAPPI Journal*, Vol. 52, No. 4, April 1969, pp.688-693.

5. Han, S.T., "The Status of the Sheet-Forming Process, A Critical Review", Technical Report, The Institute of Paper Chemistry, December 1965.

6. Corey, H., "The Contribution of Fiber-Liquid Interactions to the Rheology of Fibrous Suspensions", Ph.D. Thesis, Dept. of Food Science, Rutgers University, New Brunswick, NJ, 1972.

7. Folgar, F., "Fiber Orientation in Concentrated Suspensions: A Predictive Model", Ph.D. Thesis, Dept. of Mechanical Engineering, University of Illinois at Urbana-Champion, 1983.

DEPLACEMENT OF DEWATERING

STATUS REPORT

FOR

PROJECT F004 (3680)

Zhong Cai

March 20 - 21, 1995

Institute of Paper Science and Technology
500 10th Street, N.W.
Atlanta, Georgia 30318

TECHNICAL PROGRAM REVIEW

Project Title:	DISPLACEMENT DEWATERING
Project Code:	DISPL
Project Number:	F004 (3680)
Division:	Engineering and Paper Materials
Project Staff:	Zhong Cai
Budget (FY '94-95):	$59,904
Reporting Period:	September 1994 - January 1995

OBJECTIVE

Study of the water removal from wet paper sheet using pressurized gas or steam.

DISCUSSION

The following discussion of Dr. Cai's work on displacement dewatering was compiled from notes on his computer, after his death.

Dr. Cai considered the following five technical issues to be of importance:

1.) Fingering phenomenon, 2.) Interaction of the gas or steam jet and the water layer, 3.) Flow distribution in non-uniformly distributed fiber assembly, 4.) Gas or steam property effect (density, viscosity, composition), 5.) Experience with impulse drying and related issues.

First Note

The concept of displacement dewatering is to replace water with gas pushed through the porous media with an applied gas pressure.

In the impulse drying process, a heated roll surface comes into contact with the water, thus, generating water vapor. The pressurized water vapor pushes water out from the porous media.

The problems associated with the displacement dewatering process include fingering phenomenon, or an unstable water-gas interface. Thus, gas can push some part of the water out of the porous layer, creating gas flow channels throughout the porous layer. The dewatering effectiveness is then reduced.

Also the residence time for the displacement dewatering process is relatively long.

Second Note

1. Viscous fingering is inevitable since air or steam vapor is used to replace water, and the viscosity of air or vapor is substantially lower than that of water.

2. With displacement dewatering, bulk can be preserved while water can be blown out from wet paper. Thus, compared with wet pressing, the dewatering mechanism is different. It is possible to apply displacement dewatering to certain grades of paper.

3. With viscous fingering, dewatering can still be achieved to some extent. Since the development of viscous fingering occurs over time, the time scale of the fingering development and that of the operation process become important. In other words, if the process operation time is much shorter than the time needed for the viscous fingering to development, the effectiveness of the displacement dewatering can still be achieved.

4. Even with viscous fingering, part of the water in paper can be replaced or blown out. The level of the dewatering with viscous fingering should be checked out experimentally.

5. Paper permeability is highly anisotropy, with the in-plane permeability being much larger than the transverse permeability. Conceivably, this would reduce the fingering effect to some extent.

6. Paper permeability is strongly related to the compression status of paper. Thus, it is possible to apply some control of the compression pressure to achieve desired permeability state. Also the influence of the compression pressure to the in-plane and transverse permeability are not the same, perhaps having more substantial influence on the in-plane permeability.

7. Water contained in paper is mainly in two forms, water content within individual fibers and water content in space among fibers. Either wet pressing or displacement dewatering will have an effect on water in the space between fibers. Water content within individual fibers can be removed mainly through drying processes where liquid water becomes vapor due to the applied heat. Thus, the expectation of water removal level with displacement dewatering will be close to that of wet pressing, and may not exceed that.

8. With the expectation of the possible water removal level with the displacement dewatering technique, is it still worth doing some development work? The answer is probably yes since pressing and dewatering can be separated. As an alternative to wet pressing, bulk can be preserved through the dewatering process. This cannot be realized with wet pressing.

9. Previous experience and Jeff Lindsay's recent work show that water removal comparable to that of wet pressing can be achieved.

10. With the application of simple Darcy equation, the estimated residence time for the dewatering process is relatively long. However, this can be achieved through modified machine design.

11. Impulse drying applies similar mechanism of displacement dewatering. There are limited theoretical works, but experimental results showed positive effects.

12. Viscous fingering will develop over a certain area. In other words, fingering will be fully developed if enough distance exists in the flow direction. In the paper dewatering process, the flow distance which is the thickness of paper is very small. Thus, fully developed fingering may not be possible.

13. In a general dewatering process, whether wet pressing or displacement dewatering, water contained in spaces between fibers can be removed more effectively, while water contained within individual fibers will not be affected. Therefore, drying with heat, whether impulse drying or traditional evaporating, is the main tool to remove water contained within individual fibers.

14. In Jeff Lindsay's experimental study, the objective of maintaining high bulk has not been demonstrated. He discovered that subjecting paper to low mechanical pressure for

relatively long nip residence time which is required in displacement dewatering may induce creep effects and lead to high densification.

15. Displacement dewatering would be of interest in grades such as linerboard, boxboard, and some printing papers and specialty products where the sheet is too heavy for through drying suitable for lightweight and porous paper, but where bulk is still desired.

Third Note

The process of water removal from a papermaking felt by means of an air-pressure differential across the felt was investigated. The water removal process was found to occur in two phases, of which the first, a "Burst" of water particles, is of worth-while magnitude for papermaking applications. The initial burst occurs at a constant time rate. The amount of water removed depends primarily on initial saturation and applied pressure.

Since the felt was a rather thin porous medium, resulting in short travel paths, the viscous forces resisting water flow were very small compared to the surface tension or capillary type forces. It was these latter which ultimately decided whether or not the water would be "torn loose" from the felt.

The felt samples weighed 0.671 gram per square inch air dry. The purging pressure was maintained at 5.0 in. Hg (2.456 psig) The initial weight was 0.97 gram per square inch. It was seen that the felt saturation drops almost instantaneously to a value of 0.45 gram per square inch. The estimation was that about 91% of the water was removed by the initial burst.

From the experiment observations [1], it was suggested that a better setup would be an apparatus with the pressure maintained constant, but the felt exposed to this pressure for only a short time period, which would be the situation close to an actual machine. Preliminary trials indicated that the burst occurs over an interval of the order of 0.05 sec.

It can be concluded from the experimental observations that Darcy's law is not appropriate to be used to estimate the time interval for displacement dewatering.

The main effect of the air displacement dewatering will be the break of the surface tension in the "burst" process. There is no steady flow which is the base of the Darcy's law.

Since the viscous force effect is not critical, viscous fingering may not be a major obstacle to the process. The "burst" or breaking process will not be uniform anyhow. Thus, local dewatering is expected.

References

1. Riese, J.W., "Water Removal from Felts by Purging with Air Pressure", *TAPPI*, Vol. 42, No. 3, March 1959, pp.192-195.

FUNDAMENTALS OF WATER REMOVAL PROCESSES

STATUS REPORT

FOR

PROJECT F002 (3480)

Zhong Cai

March 20 - 21, 1995

Institute of Paper Science and Technology
500 10th Street, N.W.
Atlanta, Georgia 30318

TECHNICAL PROGRAM REVIEW

Project Title: FUNDAMENTALS OF WATER REMOVAL PROCESSES
Project Code: WETPRESS
Project Number: F002 (3480)
Division: Engineering and Paper Materials
Project Staff: Zhong Cai
Budget (FY'94-95): $59,904
Reporting Period: September 1994 - January 1995

OBJECTIVE

Study of the permeable flow and water-fiber interaction in the wet pressing process.

SUMMARY

Dr. Zhong Cai joined the faculty of the Institute of Paper Science and Technology, as Assistant Professor of Engineering, in September 1994. Over the period of this report, Dr. Cai focused much of his attention on wet pressing, in general, and specifically on developing a better understanding of permeability and its measurement. On January 1, 1995, while driving back from a holiday visit to friends in North Carolina with his wife, Wendy, and his six-year-old son, Jimmy, their car was struck by an out-of-control vehicle. Dr. Cai died at the scene of the accident, while Wendy suffered broken ribs and Jimmy suffered a broken leg. The faculty and staff of the Institute, his friends from MIT, where he went to graduate school, and his friends from Drexel University, where he did research before coming to the Institute, all mourn his loss.

The following discussion of his work was compiled from notes on his computer, after his death. The editor has tried to properly revise the various sections to create a flowing document.

Besides giving a thorough review of wet pressing fundamentals, the work suggests further research in the area of prediction of water permeability from fundamental measurements and efficient ways of deducing water permeability from relatively simple air permeability measurements.

DISCUSSION

1. A. First Note on Wet Pressing

The amount of water which can be removed by wet pressing is limited by the equilibrium moisture content of cellulose.

Laboratory experiments indicate that paper can be pressed to a limit of about 70% solids [1]. In typical paper mills, the sheet is only pressed to a dryness of about 30 to 40% solids [2].

Within a paper structure, there are large pores associated with the space among fibers, and small pores associated with the fiber walls and surface. The distribution of water between the small pores and large pores can be estimated by centrifuging samples of pulp. The water retention ratio as a function of the g-force shows that there is a distinct change in slope near a water retention ratio of 3.0 which indicates a shift in pore size distribution [3].

During wet pressing, the compression force is balanced by the stress within the structural elements or fiber network, and the hydraulic pressure. When most of the force applied is taken by the structural element, or fiber network of the sheet, the compression rate of the fiber network becomes the controlling factor in water removal. On the other hand, when most of the force applied is used in developing a hydraulic pressure to overcome the flow resistance of the sheet, the flow of water through the porous structure becomes the controlling factor. These are the two extremes.

Capillary pressure is a function of the pore size distribution and the saturation level. It can be a very important factor in rewetting of the sheet while the sheet lies on the felt after the press nip.

After leaving the press nip, both the sheet and the felt are in the unsaturated state. The sheet has a much smaller pore size and consequently almost always has a higher capillary pressure than the felt. This causes water to be sucked from the felt into the sheet. This type of rewetting is related to the contact time of the sheet and the felt.

Moisture ratio is commonly used in discussions. It is the weight of the water divided by the weight of the dry components of the sheet [3].

$$\text{Moisture Ratio} = \frac{\text{Weight of Water}}{\text{Weight of Dry Components}} \quad (1)$$

Moisture content is the percent of water by its weight in paper, pulp, paperboard, and chips [4].

$$\text{Moisture} = \frac{\text{Weight of Water}}{\text{Total Weight}} \quad (2)$$

In the press nip, the magnitude of the applied force is substantial, and the paper thickness reduces to a minimum. Fiber to fiber contact points increases, and the fiber network carries a large portion of the load. The magnitude of the load carried by fibers determines the sheet thickness under the nip, and the amount of water within the sheet, assuming that it is saturated.

1. B. Second Note On Pressing

In the wet pressing project at the University of Maine, an indirect measurement method was designed for monitoring the amount of water in the sheet during simulated pressing [5]. Eddy-current proximity gauges were used to measure the thickness of the sheet throughout the compression-expansion cycle. The amount of water removed was calculated from the initial water content of the sheet and the minimum thickness obtained during compression. It was assumed that the sheet was saturated at minimum thickness. The basis weight of the sheet, the initial weight of the sheet, the density of cellulose, and the density of water were used as factors for the calculations.

The compression tester contained a system of cams that allowed the separation of the pressing media from the sheet immediately after the expansion phase, in the range of about 2 ms such as in high-speed conventional presses, to 50 ms such as in extended-nip conditions.

During experiments, high-speed motion pictures of the separation of the porous plate and sheet were also taken. These pictures clearly showed columns of water between the plate

and sheet as they moved apart. Dye tracer experiments were also conducted and showed that some of the water removed from the sheet during compression returned to the sheet as it expanded and separated from the plate. These tests qualitatively established the occurrence of rewet in the expansion side of the nip.

For the furnish in their study, they found about 30% of the water removed during compression was returned to the sheet in rewetting. When two porous plates with pore sizes of 40 mm and 100 mm, respectively, were compared, higher rewet was observed with the 100 mm pore plate as expected.

They found from their observations and computer simulations that as the sheet began to expand on the exit side of the nip, a negative pressure was created at the interface between the sheet and the felt. This negative pressure drew water from the pool in the surface layers of the felt into the space which was beginning to form between the sheet and the felt. Since the felt was much more porous than the sheet, essentially all the water drawn into the gap comes from the felt. Therefore, it appeared that the correlation between the sheet permeability and rewet was weak. As the gap continued to open, the air flow into the gap region reduced and ultimately eliminated the vacuum in the gap. Based on their results, they suggested that reducing the vacuum should be effective in reducing rewet in the nip.

In the modeling work performed by Roux and Vincent in the Centre Technique de L'Industrie Des Papiers in France [6], numerical experiments including a two-dimensional velocity field and a two-dimensional pressure field have been performed. Thus, the problem was considered as a consolidation problem, and the general theory was developed by Biot [7]. The basic concept was that the total pressure was shared by the structure pressure of the porous medium and the hydraulic pressure in the fluid. In their model, the solid skeleton of the fibrous network was considered as an orthotropic elastic body. Fluid flow included both water and air and was assumed to obey Darcy's law. The rigid press roll, in contact with the web, was assumed to be undeformable. Therefore, a known displacement as a function of the roll geometry sets the boundary condition and the fluid particles in contact with the rigid roll had zero relative velocity.

The felt was indirectly taken into account by considering infinite permeability in the first part of the nip, and a limitation on rewetting by the water at the interface between the felt and the sheet of paper in the second part of the nip.

It was assumed that there was a uniform distribution of porosities and saturations over the entire thickness of the sheet ahead of the nip area.

The difference between the transverse and in-plane permeability was taken into account in the modeling. The anisotropic ratio of the machine direction (x) permeability to the transverse (z) permeability was assumed to be constant during the pressing of the wet sheet.

In the model, the nip geometry was the active parameter, and was assumed to progress gradually from an unloaded state to the final geometry of the nip. Therefore, the displacement boundary condition was a function of time and progresses in the z direction.

The elastic hypothesis of the porous medium leads to a paper thickness after the press equal to the incoming sheet thickness.

The distribution of the hydraulic pressure profile from the numerical simulation complies with others found in the literature. The hydraulic pressure reached a maximum before the center line. The maximum hydraulic pressure was located on the paper-roll interface, and the minimum was located on the paper-felt interface. Sheet compaction was higher on the felt side, which implied sheet stratification.

The velocity distribution profile obtained from the numerical results, showed rewetting from the felt to the paper sheet at the diverging part, after the nip. The boundary condition at the felt-paper interface was assumed to be a negative pressure gradient.

1. C. Third Note on Pressing

Wet pressing mainly deals with sheets which have a total water content from one to four times the dry weight of the sheet. At high moisture levels, all parts of the sheet are nearly saturated, and just a few air bubbles are trapped between the fibers in the porous matrix. At low moisture levels, much of the water in the larger voids between the fibers is replaced by air. The remaining water is concentrated at the junctions, on the surface, and within the walls of both fibers and fines. Water held by the large voids between fibers is relatively easy to remove, while water held in the extremely small pores in the fiber wall is difficult to remove.

In Jewett's work on wet pressing [8], a general model describing two-phase flow through a compressible porous media was developed. The model only applies to transverse presses as one-dimensional flow is assumed. The model describes the flow of air and water through a paper mat in response to mechanical force being applied to the mat. The total pressure applied to the paper-felt sandwich was balanced by the sum of the structural pressure and the hydraulic pressure.

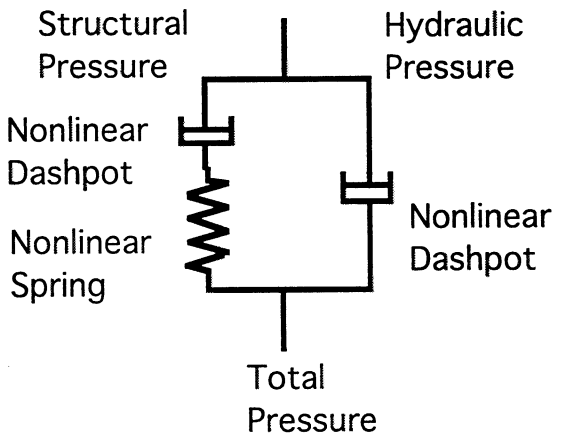

Figure 1. Pressing Model.

The total pressure was the summation of the structural pressure and air pressure, or $p_t = p_s + p_a$. With the equilibrium condition, the water pressure was the summation of the air pressure and the capillary pressure (which was negative), or $p_w = p_a + p_c$.

The volume fraction relationship was $V_w + V_{df} + V_a = 1$ (water volume fraction + dry fiber volume fraction + air volume fraction = 1), and $V_{wf} + V_{fw} + V_a = 1$ (wet fiber volume fraction + free water volume fraction + air volume fraction = 1). Also, the porosity was $1 - V_{wf} = V_a + V_{fw}$. The continuity condition is

$$\frac{\partial V_{fw}}{\partial t} = - \frac{\partial u_w}{\partial z} \qquad (3)$$

where u_w was the superficial water velocity, and z was the coordinate in the transverse direction.

$$\frac{\partial V_{wf}}{\partial t} = -\frac{\partial u_f}{\partial z} \tag{4}$$

where u_f was the superficial fiber velocity.

Since air is compressible, the variation of its density with pressure must be considered. With the ideal gas law, the equation for air was

$$\frac{\partial (p_a V_a)}{\partial t} = -\frac{\partial (p_a u_a)}{\partial z} \tag{5}$$

The permeable flow was assumed to follow Darcy's law as

$$u_{w,f} = u_w - \frac{V_{fw}}{V_{wf}} u_f = -\frac{K_w}{\mu_w} \frac{\partial p_w}{\partial z} \tag{6}$$

$$u_{a,f} = u_a - \frac{V_a}{V_{wf}} u_f = -\frac{K_a}{\mu_a} \frac{\partial p_a}{\partial z} \tag{7}$$

where $u_{W,f}$ and $u_{a,f}$ are the relative velocities (water versus fiber and air versus fiber), K_W and K_a are the permeabilities, and m_W and m_a are the viscosities.

The coordinate system was based on the constant increments of fiber mass. Thus, there was no fiber flow across element boundaries.

The fiber structural deformation was represented by a nonlinear spring-dashpot system, with two empirical functional models for the spring and the dashpot. The permeability is assumed to be a function of the dry fiber concentration with two empirical constants. The

capillary pressure was assumed to be a function of the saturation and the compression level.

A finite difference scheme was developed for the numerical solutions. The initial conditions were the thickness and moisture level of the sheet. The boundary condition was related to the two surfaces of the paper sheet. One surface was pressed against a solid roll in the nip and was modeled as a "no flow" condition. The other surface was against the felt. Free flow was assumed at this boundary. At both boundaries, pressure was specified as a function of time as the driving force for water removal.

All the empirical constants in the model were evaluated through comparison with the dynamic simulation pressing test. Variations in the magnitude of these constants were observed with different types of paper sheets.

The wet pressing project performed at the University of Maine at Orono by Profs. W.H. Ceckler and E.V. Thompson and several graduate students [9,10] includes modeling and computer code development, the design and setup of the compression tester, and some pilot and mill trials.

Compression tests have been performed on the tester for saturated sheets. The two pressing control mechanisms, flow and compression, were verified, and their effects were qualitatively studied.

Empirical compression equations were developed to include a time-dependent effect. The expression contains several empirical constants which were evaluated with experimental measurements.

Sheet permeability was measured experimentally, and the permeability was related to the concentration by using an empirical expression (in the power law form with 2 constants).

Modeling of the flow of air and water through a paper sheet in response to mechanical forces being applied was performed by Jewett [8].

In the case of pulp fibers in the swollen state, in a liquid such as water, a considerable amount of liquid is embedded in the fiber and contained in the fiber lumen. Void fraction

cannot be obtained directly from the mass concentration. The swelling of the fibrous mass will have a direct effect on the void fraction. This is accounted by

$$\varepsilon = 1 - \alpha c \tag{8}$$

The Kozeny-Carman equation becomes

$$K = \frac{1}{k_o s^2} \frac{(1 - \alpha c)^3}{\alpha^2 c^2} \tag{9}$$

With the selection of $k_o = 5.55$, the equation is rearranged as

$$(K c^2)^{1/3} = \left(\frac{1}{5.55 \alpha^2 s^2}\right)^{1/3} (1 - \alpha c) \tag{10}$$

The product of (αs) is the external surface area per mass of fibrous material. If permeability measurements are made at several different concentrations, a plot of $(Kc^2)^{1/3}$ against c will yield a straight line if the Kozeny equation applies. The quantity (αs) may be computed from the c = 0 intercept and the α from the $(Kc^2)^{1/3} = 0$ intercept.

1.D. Fourth Note on Pressing [11] (Capillary Transfer)

In a series of press operations, the paper sheet was first at a saturated state. After some pressing, the paper sheet was at relatively low to medium wetness. Then, capillary suction dominates the water flow process.

In the absence of saturation, surface tension forces tend to dry the paper in the first half of the nip, but then tend to add water to the paper in the second half (rewetting).

It is assumed that there are separate parallel pores in a porous solid, and the little pores are filled with water and the big ones are filled with air. The pressure balance condition is $p_W = p_a + p_c$, where p_W, p_a, and p_c are water, air, and capillary pressures respectively. The capillary pressure p_c is always negative, and the meniscus perimeter arcs tend to encircle the air areas at all saturation levels. The physical reason for this is that the water is preferentially wetting. Thus, p_W is always less than or equal to the air pressure.

The flow equation is

$$-\frac{\mu_w}{K_w}\varepsilon u_w = -\frac{\mu_a}{K_a}\varepsilon u_a + \frac{dp_c}{dz} \qquad (11)$$

Three cases are considered.

(1) $dp_c/dz = 0$. There is uniform capillary pressure everywhere. The seepage velocities are directly proportional.

(2) dp_c/dz = finite but small. The seepage velocities of air and water are not proportional, but the see pages are usually in the same direction.

(3) dp_c/dz = large. In a very transient situation, the seepage velocities may be in opposite directions. This could be the case whenever a fluid soaks into a porous material and the residing air being replaced has no escape route except the one being used by the soaking fluid. The only requirement of the above equation is that both fluids be continuous so that dp_c/dz exists. If 100% saturation occurs, then Darcy's law can be used for the one-component seepage flow. At slightly less than 100% saturation, the flow may be bubbly so that dp_c/dz is discontinuous and cannot influence the seepage across the full material distance.

The traditional view of "pressing," squeezing, or expulsion is valid only if one component (or perhaps bubbly fluid) is present. In that case, fibers enter a volume occupied by fluid, and the fluid has to leave. On the other hand, when enough air is present, the fluid mixture is compressible, and the pressure gradient caused by fibers moving into the fluid mixture is probably small compared to dp_c/dz.

For the conditions of a paper-machine press, p_c is always considered to be continuous. Three arguments were presented.

(1) Both paper and felt enter the press at intermediate wetness levels and probably continuous p_c.

(2) To remove all the air from either material would require overcoming an infinite air seepage resistance.

(3) Air rushing through the air filaments may tend to keep them open longer. It takes a little time for bubbles to form from an unstable air filament.

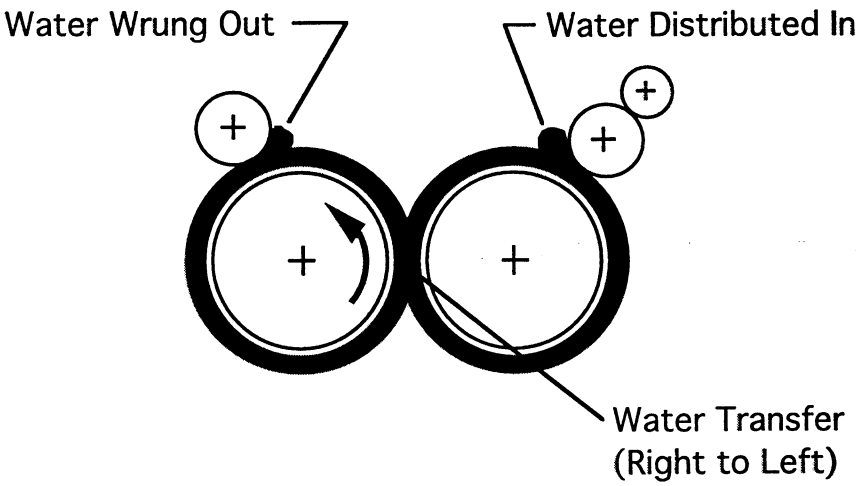

Figure 2.

The proposed relationship is $\delta = B\ \Delta p_c$, where δ is the transfer thickness or the thickness of the water layer transferred between materials, and B is an overall nip conductance factor.

To measure the wetness, the paper was scraped off its roll immediately before the quick release of the felted roll.

The net water transfer was the sum of two parts.

(a) The first part was proportional to the difference between the capillary pressure s in the materials as they first come in contact. Hence, the first part depends on the initial wetness and pore size distribution of each material.

(b) The second part of the net water transfer was more complicated. As the materials pass between rollers, they go through a compression-expansion cycle which generates a cycle of capillary pressure difference. This results in a water flow across the interface which, however, was delayed with respect to the compression-expansion cycle.

1. E. Fifth Note on Pressing

Wet paper was assumed to be a mixture of two continuous phases, a solid fiber phase and a liquid water phase. The mixture was assumed to be elastic. The paper felt and the air phase were excluded from the analysis.

An equation for the compression phase for a felt being pressed in a plain press with nondeformable rolls is

$$\frac{dp}{dx} = \mu U \frac{1}{k} \frac{h - h_o}{h} \tag{12}$$

where x is the distance from mid nip; p is the hydraulic pressure in the nip at x; μ is the viscosity; U is the machine direction velocity of the felt; k is the permeability; h is the thickness of the felt at x; and h_o is the thickness of the felt at the mid-nip. Yih and McNamara [12] solved this equation with the condition of $p = 0$ at the mid-nip. Asklof, et al. [13] found that $p = 0$ before the middle of the nip, and there is a net flow of water in the machine direction.

Wilder [14] modified the above equation as

$$\frac{dp}{dx} = \mu U \frac{1}{k} \frac{h - h_o}{h} - \rho \frac{d(U + v)}{dx} \tag{13}$$

The corresponding mass balance was

$$(U + v)\frac{h - h_o}{h} = q \tag{14}$$

where ρ is the density of water; v is the velocity of water relative to the felt; and q is the flow rate at x. It was found that the inertia term was not significant at lower pressing velocities (below 1500 feet per minute).

The most recent attempt is due to Roux and Vincent [6]. They considered three phases, solid, water, and air. They considered flow velocities in two directions, the machine direction and the thickness direction. They allowed for anisotropic permeability and orthotropic elasticity. Capillary pressure was also included.

The extended nip press (ENP) concept has been successfully applied to the design of presses (Busker [15], Justus and Cronin [16]). The main effect being a longer residence time. In a typical ENP, the residence time varies between 10 to 25 milliseconds. This compares with the 1 to 10 millisecond range in conventional presses.

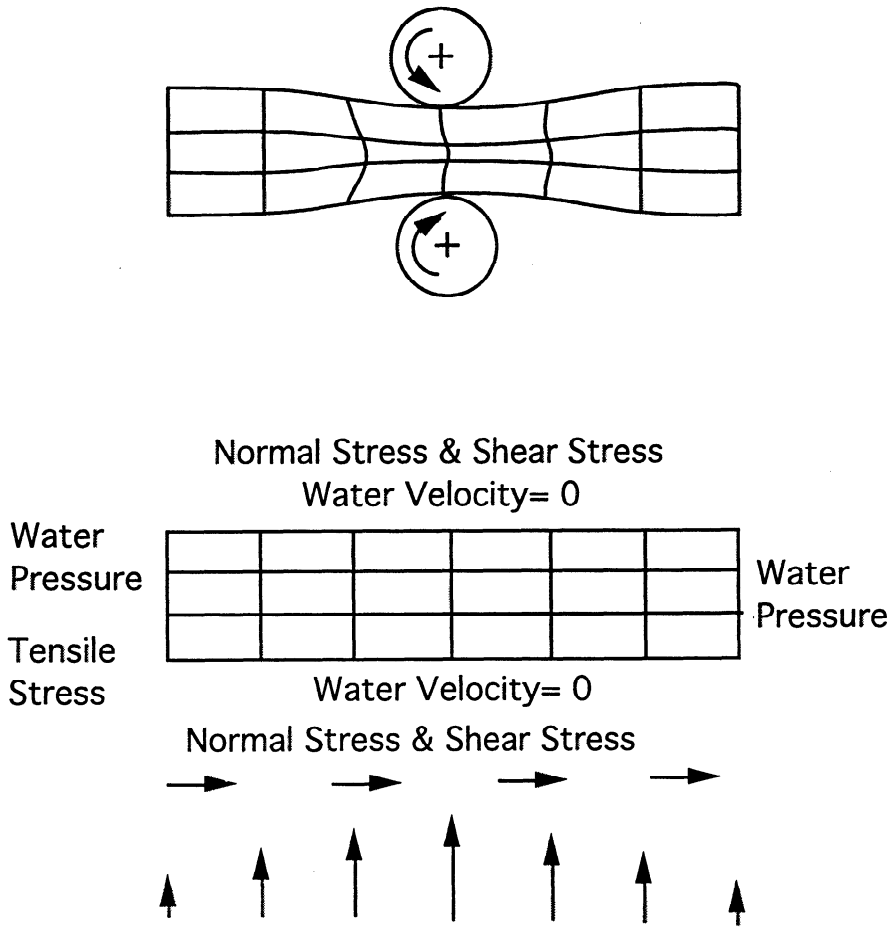

Figure 3. Finite Element Model.

The finite element mesh consists of 2 elements in the thickness direction, and 23 elements in the machine direction. Therefore, there are 3 nodes in the thickness direction and 24 nodes in the machine direction.

A mathematical model for the pressing of wet paper has been formulated, and a finite element program has been developed to solve the governing equations [17]. Computer sensitivity analysis has also been performed.

1. F. Sixth Note on Pressing [18,19] (Rewetting)

A comparison was made with pressing on a wet paper sheet only, and with pressing on the combination of paper and felts. In the latter case, the paper was always wetter, and the felt was always drier than when pressed separately under the same conditions.

Upon the release of pressure, a migration of water from the felt to the paper occurs. If component members are separated, migration cannot take place; the residual moisture was close to that of each being pressed alone.

2.A. Evaluation of Paper Permeability

In the papermaking process, paper permeability is an important variable closely related to many operations, such as drainage flow, wet pressing, and drying. In various papermaking stages, the main task is to efficiently and cost-effectively remove water from wet paper sheets. After the wet sheets are formed at the drainage section, further water removal can be considered as a problem of fluid flow through porous media.

Compared with other porous materials or even other fibrous materials, wet paper sheets show very unique permeability behavior. As these sheets are formed, pressed, and heated, there are tremendous changes within the fibrous material structure. One of the main variables which is crucial to the material permeability behavior is porosity. Since wet sheets are highly compressible, porosity within the wet sheets changes both spatially and over time. Wet sheets contain not only fibers, but also fines which are much smaller and highly migrationable. Local permeability will be strongly affected by these features.

Paper permeability measurements have been performed in many studies related to papermaking processes. Some recent measurement data (Ceckler and Thompson [20], Lindsay, [21]) showed a substantially lower permeability of paper sheets compared with other porous fibrous materials such as textile fabrics at similar porosity. A possible source of this phenomenon was discussed by Lindsay; he suggested dead-end pores as the main reason. However, from the paper fiber structure, it is not very possible to have closed voids within the fiber assembly.

There are three possible sources to account for this phenomenon.

(1) Fiber size distribution including fines within a paper fiber assembly.

(2) Packing structure due to distributed fiber sizes.

(3) Fiber swelling which effectively reduces the free water volume within the assembly, and water contained within individual fibers is difficult to move under the imposed fluid pressure gradient.

The magnitude of the influence of these three factors needs to be determined, either analytically or experimentally.

As shown in the widely used Kozeny-Carman equation, permeability is related to the porosity (ε), the specific surface of the porous material (s), and the fiber packing structure or efficiency which is represented by the Kozeny constant k_o which contains other factors, such as fiber surface condition.

The specific surface is the total solid surface area of the porous material divided by the total solid volume. As the fiber size reduces, the specific surface increases. For a uniform and continuous fiber assembly, the specific surface is inversely proportional to the fiber radius or diameter. For a fiber assembly with distributed fiber sizes, the specific surface can be considered as a function of both the average fiber diameter or radius, and the shape of the distribution in terms of its standard deviation.

Note on Permeability Comparison: When the permeability data of paper (Lindsay) and other fibrous materials are compared, some differences have been observed.

1) The permeability of paper is substantially lower than that of other fibrous materials such as fabrics and aligned fiber bundles used for composite reinforcement. At the similar porosity or fiber volume fraction, the difference is about two orders of magnitude. One significant difference in the structure of the two groups of materials is the fiber dimensions. In paper, not only are there fibers with distributed lengths and diameters, but also a portion of so-called fines. Thus, these fines may play an important role in determining the permeability behavior of paper.

2) The measured data of permeability of paper versus the porosity do not follow the Kozeny-Carman equation predictions, which says the porosity function form is $\varepsilon^3/(1-\varepsilon)^2$. By trial and error, it was found that function form of $\varepsilon^4/(1-\varepsilon)^2$ gives reasonable fit within the range of $\varepsilon = 0.73$ to 0.85 which was the range of Lindsay's experiments.

The original derivation of the Kozeny-Carman equation for aligned fibers uses the hydraulic radius concept (Williams [36]). When fibers are with the same diameter, the Kozeny-Carman form of the expression is derived.

2.B. Evaluation of the Permeability of Paper Materials [22-33]

Abstract: Issues related to the permeability of paper materials are discussed. Unlike other fibrous materials, wood-based paper fibers absorb water and swell when saturated. Thus, the permeability behavior is significantly different. The widely used Kozeny-Carman equation has to be modified for paper materials, but is found to be in reasonable agreement with available measurement data. Other effects due to characteristics of paper fiber assemblies including fiber and fine size distribution and packing efficiency are also discussed.

Nomenclature:

b	=	Dimensionless factor for fiber swelling
c	=	Sheet concentration (kg/m^2)
C	=	Sheet consistency, dimensionless
k_o	=	Kozeny constant, dimensionless
K	=	Permeability (m^2)
M_f	=	Mass of fibers (kg)
M_w	=	Mass of water (kg)
r_f	=	Fiber radius (m)

s = Specific surface area per unit volume of material (kg/m^3)

s_o = Specific surface area ($1/m$)

V = Total material volume (m^3)

V_f = Fiber volume (m^3)

V_w = Water volume (m^3)

α = Specific fiber swelling volume (m^3/kg)

ε = Porosity, dimensionless

ε_e = Effective porosity including the fiber swelling effect, dimensionless

μ = Fluid viscosity ($kg \times m/s$)

ρ_ϕ = Fiber density (kg/m^3)

ρ_ω = Water density (kg/m^3)

Introduction: In several papermaking processes, such as drainage flow, wet pressing, and drying, fluid flow through paper fiber assembly occurs. The efficiency of water removal is affected by the permeable flow through paper fiber materials.

In most of the applications, the permeable flow is assumed to be laminar or viscous dominant. Thus, Darcy's law can be applied to evaluate the paper permeability. Even in the case that inertial flow effect exists, the viscous resistance part is handled similarly.

There are two main categories of permeability of paper materials, dry state and wet state. The former includes the air or gas permeability, which can be measured.

The current research effort seeks to find out if the generally accepted relationships such as the Kozeny-Carman equation are applicable to paper fiber materials, and if so, what modifications are needed. Therefore, data analysis have been performed on available

experimental measurement results. Previous research findings are also compared and summarized.

Background: The exact status of each piece of paper, such as fiber distribution or orientation, is impossible to measure or model in practice. What is interesting is the average or gross features of some variables or properties, such as permeability, porosity, strength, etc. Due to the structural nature of the paper material, the values of these properties vary to some extent even for the "same" type of material. Thus, "exact" solution is not necessary for practical applications. What is needed is a reasonable estimation of the average value and range of these properties or variables. Thus, more rigorous mathematical solutions, either analytical or numerical, are found to have limited values. On the other hand, empirical or semiempirical solutions, such as the Kozeny-Carman equation, have been widely used in practical applications. These solutions usually contain one or more empirical constants which must be determined through relevant experiments. The magnitude of these constants may vary to some extent depending on the particular material or process conditions. Also, there are always some minor effects which cannot be readily included in the analytical expression or numerical modeling. These effects will also be covered in these empirical constants.

For paper materials containing randomly distributed fibers, with a wide range of fiber dimensions, the semiempirical approach is the most efficient one. Thus, many researchers in this area have looked at established equations or formulas, and then modified to include various features of paper materials. The Kozeny-Carman equation for permeability evaluation is in this category. The equation has been used over a wide range of porous materials, including soil, rocks, textiles.

The first question is whether the widely used Kozeny-Carman equation is a reasonable model for predicting paper permeability, and if so, what will be the difference in parameters in the equation for paper materials.

To answer this question, it is necessary to evaluate paper materials with other porous materials. The most similar materials will be fabrics and nonwoven structures since they are also made of fibers. Other studies with these fibrous materials show that the Kozeny-Carman equation is a reasonable tool to be used to estimate the permeability in different orientations at the middle range of the porosity (about 30 to 80%). Beyond that porosity range, the equation needs to be modified when compared with other available experimental and numerical data.

The major elements in the Kozeny-Carman equation consist of a porosity function, a characteristic length which is usually expressed as specific surface area or fiber diameter and which is related to the hydraulic radius of the porous structure, and an empirical constant which includes other effects such as packing efficiency or packing disturbance, fiber orientation, and particle size distributions. Among these variables, both the porosity and the hydraulic radius show very strong influence on the permeability, both can be analyzed according to the physical mechanisms, and both can be measured through experiments. Other variables such as packing disturbance have a relatively small effect on the permeability magnitude, and are usually not easy to measure under practical conditions. Thus, a simplified approach is to use an empirical constant which can then be evaluated for a particular group of materials. The approach has been successfully used for many different types of porous materials including various fibrous structures.

Kozeny-Carman Equation for Paper Materials: For general porous materials, the Kozeny-Carman equation is written as

$$K = \frac{1}{k_o s_o^2} \frac{\varepsilon^3}{(1 - \varepsilon)^2} \tag{15}$$

where ε is porosity; s_o is specific surface with the units of one over length (1/m); and k_o is the Kozeny constant. For fibrous materials with relatively uniform fiber diameter, the Kozeny-Carman equation is written as

$$K = \frac{r_f^2}{4 k_o} \frac{\varepsilon^3}{(1 - \varepsilon)^2} \tag{16}$$

where r_f is the fiber radius or average fiber radius. A constant 4 is introduced so that the Kozeny constant k_o will be the same for both expressions (15) and (16).

For paper material, the equivalent Kozeny-Carman equation is usually written as

$$K = \frac{1}{5.55\ s^2} \frac{(1 - \alpha c)^3}{c^2} \tag{17a}$$

where c is the concentration or density of paper in nits of kg/m^3 and is measured with the dry fiber weight, sheet area and thickness; α is a factor to account for the fiber swelling and other effects and is in units of m^3/kg; s is the specific surface area and is in units of kg/m^2; and the constant 5.55 is equivalent to the Kozeny constant and is empirically determined. When this formula is used for different paper samples, it is assumed that this constant of 5.55 is the same. With the comparison to other forms of the Kozeny-Carman equation (15) and (16), it can be seen that (α c) is equivalent to the porosity. For experimental data processing, expression (17a) is usually written as

$$(K c^2)^{1/3} = (5.55\ s^2)^{-1/3} (1 - \alpha c) \tag{17b}$$

where c and K are measured directly, and α and s are unknown. By plotting the data as $(K\, c^2)^{1/3}$ versus c, if the data distribution follows a straight line, the validity of the Kozeny-Carman equation can be verified, and if so, the values of the other two constants, s and α, can be evaluated.

The Kozeny constant for fibrous materials has been evaluated experimentally. Two extreme cases of the Kozeny constant are flow along the axial or fiber direction of an aligned fiber bundle, and transverse flow or perpendicular to the axial or fiber direction. In the former case, the Kozeny constant is found to be about 0.5, and in the later case, about 11. For other not so oriented fibrous materials such as woven fabrics or fiber mats, the value is found to be about 5.5 or so.

Recently, permeability measurements have been performed on various paper materials. Similar to the fabric material, the in-plane permeability is measured by injecting liquid at the center of a circular sample and then monitoring the expansion of the flow front, while the transverse permeability is measured directly by imposing a fluid pressure gradient across the sample and monitoring the flow rate. In both cases, Darcy's law is used to obtain the apparent permeability of the paper material.

When the apparent permeability is plotted against the porosity, it is clear that the porosity function form, proposed in the Kozeny-Carman equation, cannot follow the permeability trend over the porosity range of interest. Therefore, other empirical formulas are proposed such as an exponential function. However, when the data are plotted against the expression (17b), reasonable data fitting can be observed.

It can be concluded that the Kozeny-Carman equation is reasonable for estimating the permeability of paper materials. However, the usual form of the porosity function must be modified.

There are several benefits of using the Kozeny-Carman equation instead of using other empirical forms of K versus ε. First, the relative permeability of paper material can be compared to that of other porous and fibrous materials on a similar basis. Second, if the Kozeny-Carman form of the porosity function is valid for paper material, further efforts to study paper permeability can be concentrated on other parameters including the specific surface and packing efficiency. Third, the Kozeny-Carman equation has been verified for gas flow through fibrous materials, and it is expected to be also valid for paper materials. It is then possible to use the data of air permeability of paper to predict water permeability since the measurement effort is substantially different.

The comparison of (15) and (16) shows that the term $(1 - \alpha c)$ in (17a) is equivalent to the porosity ε in (15). However, the magnitude of α is usually not known and not easily measured directly. When (15) is used for other fibrous materials, the term s_o can be evaluated such as shown in (16) for uniform fibers. Therefore, k_o becomes an unknown or adjustable variable. On the other hand, in (17a) the value of the Kozeny constant is fixed at 5.55, and the specific surface s becomes the unknown term. With the Kozeny-Carman equation form (15), the unknown constant k_o is dimensionless so that it can be evaluated for different materials on the same basis. With the Kozeny-Carman equation form (17a), both constants α and s have certain units. Therefore, when (17a) is used to estimate values of α and s, they are more or less related to individual material types. Generalization of the measurement data becomes difficult.

It can be seen that the main characteristics of paper material, relevant to the permeability, are its fiber size distribution, ranging from virgin fibers to small fines and added filler particles, and substantial fiber swelling when water permeable flow is considered. The fiber and fine size distribution results in an increase of the specific surface area when compared to other porous medium with more uniform fiber sizes. The swelling of fibers results in a substantially reduced open area to the permeable flow. Both effects will result in the reduction of the paper permeability, which has been observed by comparison of the permeability measurement data of paper and other fibrous materials.

To account for the fiber swelling effect, when water permeability is measured, a dimensionless fiber swelling factor can be introduced. If the total fiber volume fraction before swelling is v_f, and that after swelling is $(1+b)\, v_f$ where b is a dimensionless swelling factor, the corresponding porosity ε' becomes

$$\varepsilon' = \varepsilon - b(1 - \varepsilon) \qquad (18)$$

As expected, ε' is always less than ε. The term ε' reflects the fact that water contained within fibers is much less mobile under the imposed fluid pressure level. Therefore, most of the contribution to the flow resistance, comes from the fluid flow through spaces among fibers. The term ε' is equivalent to the effective porosity concept in the physical sense.

Hence, the corresponding Kozeny-Carman equation becomes

$$K = \frac{1}{k_o s_o^2} \frac{\varepsilon'^3}{(1-\varepsilon')^2} = \frac{1}{k_o s_o^2} \frac{[\varepsilon - b(1-\varepsilon)]^3}{[(1+b)(1-\varepsilon)]^2} \qquad (19)$$

Other terms in this expression are the same as in (15). The porosity ε is the nominal porosity of the paper material, or in other words, is the solid portion of the paper material. Therefore, ε can be measured with the conventional methods. The Kozeny constant k_o is assumed to be unknown, but would be not far away from the selected value of 5.55 that has been used in other studies. In experimental data processing, $(k_o s_o^2)$ can be grouped into one unknown parameter. If s_o can be estimated some way from the fiber size distribution, then k_o can be evaluated. Or, k_o could be assumed as 5.55, and then, s_o could be estimated indirectly from the permeability data.

Similar to equation (17a), if (19) is used for the experimental data processing, K and ε will be measured directly, and $(k_o s_o^2)$ and b can then be evaluated. Both b and $(k_o s_o^2)$ are related only to the geometric change of the paper fiber material and not to the material density. The two variables of s and α in (17a) are, however, related to the paper concentration and thus to the material density implicitly. The shortcoming of the suggested form (19) is that the data processing equation is not linear for b. The estimation of the values b and $(k_o s_o^2)$ will involve more mathematical operations.

To effectively use the Kozeny-Carman equation form (19) for paper permeability estimation, there are three major tasks. First, the magnitude of b needs to be verified, and hopefully, it will be close to a constant for at least a group of similar paper materials. Second, measurement methods to evaluate the specific surface area s_o need to be developed based on the information of fiber and fine size distributions. Third, the magnitude of the Kozeny constant needs to be verified. Presently, the value of 5.55 is used widely in various studies, but the original source is from one study. The variation of

the Kozeny constant for fibrous materials has been reported in other fields, and is a well-known fact. A good guess is that the range of the Kozeny constant is limited, and may be not far away from 5.55, but further study on this issue is needed.

In order to process data with both equations (17a) and (19), the following relationships are needed for the transformation. The nominal porosity ε is related to the sheet consistency C as

$$\varepsilon = \frac{(1 - C)(\rho_f/\rho_w)}{C + (1 - C)(\rho_f/\rho_w)} \tag{20a}$$

or

$$C = \frac{(1 - \varepsilon)(\rho_f/\rho_w)}{\varepsilon + (1 - \varepsilon)(\rho_f/\rho_w)} \tag{20b}$$

where C is dimensionless and is defined as

$$C = \frac{M_f}{M_f + M_w} \tag{21}$$

The relationship between the sheet concentration c and the sheet consistency C is

$$C = \frac{c(\rho_f/\rho_w)}{\rho_f + c(\rho_f/\rho_w - 1)} \tag{22a}$$

or

$$c = \frac{C\,\rho_f}{C + (1 - C)(\rho_f/\rho_w)} \tag{22b}$$

where ρ_W is water density in kg/m^3, and the sheet concentration c is defined as

$$c = \frac{M_f}{V} = \frac{M_f}{V_f + V_w} \tag{23}$$

Therefore, the sheet concentration c is related to the porosity as

$$c = \rho_f (1 - \varepsilon) \tag{24a}$$

or

$$\varepsilon = 1 - \frac{c}{\rho_f} \tag{24b}$$

The variable αin (17a) can be related to the term b in (19) as

$$\alpha = \frac{1 + b}{\rho_f} \tag{25a}$$

or

$$b = \alpha \rho_f - 1 \tag{25b}$$

If b is assumed to be constant or at least close to constant, then α should also be constant. From these relations, the value of b can be obtained through the known value of α which is the slope on the data plot of $(K c^2)^{1/3}$ versus c.

If b can be estimated using the water permeability data, then for a particular group of paper material, it is possible to use (15) for air permeability measurement and (19) for water permeability measurement. Or alternatively, equation (17a) can also be used for both water and air permeability data processing. In the later case, the value of α becomes $1/r_f$. The two groups of data should correlate with each other, but may be somewhat different since other effects are not included in the Kozeny-Carman equation such as surface tension and small particle or fines mobility in water flow case. If the correlation can be established, then the air permeability data can be used for the prediction of the water permeability which otherwise takes more effort to do the measurement.

Comparison of Model with Data: Recently Lindsay and co-workers have performed permeability measurements on paper samples in both in-plane and transverse directions. The data have been plotted as permeability versus porosity as in the case of other

materials. Within the interesting porosity range which is relatively small, log permeability versus porosity plots show that the relationship is close to linear. Therefore, direct application of the Kozeny-Carman equation did not show satisfactory agreement.

When the same data are plotted using the Kozeny-Carman equation with consideration of the swelling effect, or $(Kc^2)^{1/3}$ versus c, the data distribution seems close to a linear relationship, at least within the interesting porosity range.

Other Parameters: With other fibrous materials, which have more uniform fiber diameter distribution, the specific surface of the fibrous material is relatively certain. However, in a paper fiber assembly, there are many broken fibrils due to beating, refining, and other operations, and fines and filler materials for improving finished paper properties. Thus, the situation with respect to specific surface is much more uncertain.

Although the Kozeny constant of 5.55 is used widely in research and modeling of permeability of paper materials, rigorous verifications are not reported. As reported in many other studies on permeability of fibrous materials, the magnitude of the Kozeny constant varies to some extent, and is influenced by numerous factors.

When other fiber assemblies are considered, usually the specific surface can be deducted from the fiber geometry. Thus, the Kozeny constant is left as the adjustable parameter. With the paper fiber material, the specific surface is not known; then, the Kozeny constant is assumed to be known as 5.55, and then, the specific surface area becomes an adjustable parameter.

Conclusions: The Kozeny-Carman equation seems to be a good approximation and practical solution for estimating paper permeability. When water permeability of paper is

considered, the fiber swelling effect is significant and has to be included in the model. Thus, a swelling factor is introduced for the modification. When compared with available permeability measurement data, reasonable agreement has been observed.

2.C. Permeability (September 23, 1994)

On September 23, members of the impulse drying team came to see me and discussed some issues about the paper permeability related to their project. Among the data plots, one showed the specific surface (m^2/g) versus the consistency (%). These data showed very weak dependence of the two variables.

The question that was asked was whether the observed results were expected from the physical model such as the Kozeny-Carman equation. The following summarizes my results. The specific surface defined in the measurement is a very weak function of the consistency within the range of the consideration. In other words, the magnitude of the defined specific surface varies only a few percent within the interested consistency range. With the increase of the consistency value, the defined specific surface decreases slightly. The plotted data clearly support this conclusion although data scattering is relatively large.

Notes on the Paper Permeability Data: The permeability formula used in the experimental data processing is [34].

$$(k\, c^2)^{1/3} = (5.55\, s^2)^{-1/3} (1 - \alpha\, c) \qquad (26)$$

where k is the water permeability (m^2) or permeability measured on samples saturated with water; c is the sheet concentration or density (kg/m^3 or g/m^3); s is the flow-exposed surface area of the fibers based on per unit mass (m^2/kg or m^2/kg); and α is the specific volume of the water swollen fibers (m^3/kg or m^3/g). The constant 5.55 is used for the so-called Kozeny constant in the Kozeny-Carman equation.

From the definition of these terms, $(1-\alpha c)$ is the so-called flow porosity associated with water. In other words, $(1-\alpha c)$ is the porosity with the swollen fibers assuming these fibers themselves are impermeable. The sheet concentration c is calculated as $c=m/AL$, where

m is the mass of the dry sheet (kg or g); A is the sheet area (m^2); and L is the sheet thickness (m).

The permeability formula used can be also written as

$$k = \frac{1}{5.55\ s^2} \frac{(1 - \alpha c)^3}{c^2} \tag{27}$$

As a comparison, the widely used Kozeny-Carman equation for porous fibrous materials is usually written as [35-37].

$$k = \frac{1}{k_o\ S_o^2} \frac{\varepsilon^3}{(1 - \varepsilon)^2} \tag{28}$$

where ε is the average porosity of the material; k_o is a dimensionless and empirical constant and also called Kozeny constant; and S_o is the specific surface, or the surface area per unit volume of solid material. Therefore, S_o is calculated as the total surface area exposed to flow divided by the total volume of the solid material in a porous medium, and is with the units of one over the length (1/m). For general fibrous and textile materials, it has been suggested that the Kozeny constant $k_o = 5.5$ is a good estimation [38]. However, other reported data also show large variations on the Kozeny constant data.

In the experimental result plot, the specific surface s is in the units of [m^2/kg] or [m^2/g]. According to the definition [34], s is equivalent to the specific surface S_o divided by the density of the paper material ρ which is with the units of [kg/m^3] or [g/m^3], or

$$s = \frac{S_o}{\rho} \tag{29}$$

With this relationship, the Kozeny-Carman equation formula (27) can be rewritten as

$$K = \frac{1}{\left[5.55/(\rho\ \alpha)^2\right] S_o^2} \frac{(1 - \alpha c)^3}{(\alpha c)^2} \tag{30}$$

This is equivalent to the widely-used form as equation (28), with the Kozeny constant replaced by $[5.55/(\rho\ \alpha)^2]$ which is also dimensionless.

To find out the relationship between the defined specific surface s and the consistency C, the definition of the specific surface S_0, and the relationship between the paper density ρ and the consistency C will be discussed.

The definition of S_0 is the total surface area exposed to flow divided by the total solid volume of the porous medium. For fibrous materials with uniform diameter and different lengths in an arbitrarily selected volume with N fibers, the total surface area A_f neglecting the end surfaces of fibers is

$$A_f = \sum_{i=1}^{N} (2\pi r_f) L_i = (2\pi r_f) \sum_{i=1}^{N} L_i \tag{31}$$

where r_f is the fiber radius, and L is the fiber length. Similarly, the total fiber volume is

$$V_f = \sum_{i=1}^{N} (\pi r_f^2) L_i = (\pi r_f^2) \sum_{i=1}^{N} L_i \tag{32}$$

S_0 can be obtained from the definition as

$$S_0 = \frac{A_f}{V_f} = \frac{2}{r_f} \tag{33}$$

Thus, in this case, S_0 is only related to the fiber radius r_f. For a more general case when r_f is not constant within a paper fiber assembly, S_0 can be obtained similarly as

$$S_0 = \frac{A_f}{V_f} = \frac{2 \sum_{i=1}^{N} (r_f)_i L_i}{\sum_{i=1}^{N} (r_f)_i^2 L_i} \tag{34}$$

If the distributions of the fiber radius and fiber length are known, S_0 can be calculated with a more rigorous mathematical approach. When the distributions are within a limited range, S_0 is expected to be related to the average fiber radius $\overline{r_f}$ in the similar form as equation (33), but with a modified constant. However, S_0 is *not* related to the

consistency C. In other words, if two paper samples made from the same furnish are at different consistencies, the values of S_0 will be the same or be very close.

The consistency C is defined as the mass fraction of fibers in a water-saturated paper structure. C can be expressed as

$$C = \frac{M_f}{M_f + M_w} \tag{35}$$

or

$$\frac{M_w}{M_f} = \frac{1}{C} - 1 \tag{36}$$

where M_f is the mass of the fibers (kg) and M_W is the mass of water (kg). The volume relationship of fibers, water, and the total can be expressed as

$$V_f = \frac{M_f}{\rho_f} \tag{37}$$

$$V_w = \frac{M_w}{\rho_w} \tag{38}$$

$$V = \frac{M_f}{\rho_f} + \frac{M_w}{\rho_w} \tag{39}$$

where ρ_f and ρ_W are the density of fiber and water, respectively (kg/m^3); V is the total volume (m^3); V_f is the volume of fibers (m^3); and V_W is water volume (m^3). The density of paper ρ can be obtained as

$$\rho = \frac{M_f + M_w}{V_f + V_w} = \frac{\rho_f\left(1 + \frac{M_f}{M_w}\right)}{\left(1 + \frac{\rho_f}{\rho_w}\frac{M_f}{M_w}\right)} = \frac{\rho_f}{C + \frac{\rho_f}{\rho_w}(1 - C)} \tag{40}$$

Thus, the average density of paper ρ is related to the consistency C. If the fiber radius is assumed to be constant with the use of equations (29), (33), and (40), the defined specific surface s in the data plot is

$$s = \frac{S_o}{\rho} = \left(\frac{2}{r_f}\right) \frac{\left[C + \frac{\rho_f}{\rho_w}(1 - C)\right]}{\rho_f} \qquad (41)$$

As discussed earlier, with the distributions of both fiber radius and length, the term $(2/r_f)$ becomes another constant related to $\overline{r_f}$. With certain types of fiber composition, ρ_f is also a constant. Thus, s becomes a function of C, and also the functional form is linear.

With the available data range of C from 0.35 to 0.53, and with the estimation of ρ_f/ρ_w of about 1.1 to 1.3, the variation of s is very limited. An intermediate variable F is introduced as

$$F = \left[C + \frac{\rho_f}{\rho_w}(1 - C)\right] \qquad (42)$$

Therefore, s is proportional to F. The values of F with corresponding C and r_f/r_w are listed in the following table. Since the relationship of F versus C is linear, only the maximum and minimum values in each set are listed. The difference between the maximum and the minimum is also listed as the percentage of the minimum value.

Table 1: F values versus different values of C and ρ_f/ρ_w

F Value	C = 0.35	C = 0.53	Difference
$\rho f/\rho w = 1.1$	1.065	1.047	1.7%
$\rho f/\rho w = 1.2$	1.130	1.094	3.3%
$\rho f/\rho w = 1.3$	1.195	1.141	4.7%

It can be seen from the results listed in the table that although the defined specific surface s (m^2/g) is a function of the consistency C (%), the dependence in the range of interest is very limited, with changes of s of about 1.7 to 4.7% in the selected range of ρ_f/ρ_W and C. In other words, with the increase of the consistency value, the defined specific surface decreases slightly in a linear manner. Available plotted data clearly support this conclusion, although data scattering is relatively large.

In summary, the defined specific surface s (m^2/g) is a linear function of the consistency C (%) as shown in equation (41), but the dependence in the range of interest is very weak, only about a few percent of the magnitude difference. With the increase of the consistency value, the defined specific surface value decreases slightly. The finding is in a good agreement with the available experimental data.

Appendix: As an additional note, the average porosity ε widely used in the permeability formula can also be expressed as a function of the density ratio ρ_f/ρ_W and the consistency C as

$$\varepsilon = \frac{V_w}{V_f + V_w} = \frac{\frac{M_w}{\rho_w}}{\frac{M_f}{\rho_f} + \frac{M_w}{\rho_w}} = \frac{\frac{\rho_f}{\rho_w}\frac{M_w}{M_f}}{1 + \frac{\rho_f}{\rho_w}\frac{M_w}{M_f}} = \frac{\frac{\rho_f}{\rho_w}(1 - C)}{C + \frac{\rho_f}{\rho_w}(1 - C)} \qquad (43)$$

where V_W and V_f are the volume of water and fiber, respectively; ρ_W and ρ_f are the density of water and fiber, respectively; and M_W and M_f are the mass of water and fiber, respectively. In the case of $\rho_f/\rho_W = 1$, the porosity $\varepsilon = 1 - C$.

The derivative of the porosity ε with the two variables ρ_f/ρ_W and C is

$$\frac{\partial \varepsilon}{\partial(\rho_f/\rho_w)} = \frac{C(1 - C)}{[C + (\rho_f/\rho_w)(1 - C)]^2} \qquad (44)$$

$$\frac{\partial \varepsilon}{\partial C} = \frac{-(\rho_f/\rho_w)}{[C + (\rho_f/\rho_w)(1 - C)]^2} \qquad (45)$$

Therefore, ε decreases with the increase of C, while ε increases with the increase of $\rho f/\rho w$.

2.D. Permeability (December 8, 1994):

A few of my thoughts follow.

1. As stated before, the equation used for determining α and s by our data processing is

$$(k\,c^2)^{1/3} = (5.55\,s^2)^{-1/3}(1 - \alpha\,c) \qquad (46)$$

where k is the water permeability (m^2) or permeability measured on samples saturated with water; c is the sheet concentration or density (kg/m^3 or g/m^3); s is the flow-exposed surface area of the fibers based on per unit mass (m^2/kg or m^2/kg); and α is the specific volume of the water swollen fibers (m^3/kg or m^3/g). The constant 5.55 is used for the so-called Kozeny constant in the Kozeny-Carman equation.

There are four variables in the formula. Among them k is measured in the current test, and c is measured by the sample supplier. Therefore, both are from the direct measurements and are used for further data processing. Then, by using the data plotting, s and α are assessed through the measured values of k and c.

The sheet concentration c is related to the sheet density including both fiber and water components. Therefore, c is based on the average density ρ, as stated in equation (40) of the previous notes.

Since the calculation of s is based on k and c, s will be related to the average density ρ through c. Therefore, in equation (29) in the previous notes when s is written as $s = S_o/\rho$, the term ρ is the average sheet density, not the fiber or solid density, although S_o which is the conventional specific surface term is related to the fiber or solid only.

In other words, without introducing the term S_o for the discussion, s is related to c and the average density ρ through the data processing calculations. When s is written as s =

S_0/ρ, the term S_0 is assumed to be a property of the fiber or solid material only, and ρ is then the average sheet density. Both s and c are based on the same variable ρ.

Since in both equations (29) and (40) of the previous notes the density ρ is the average sheet density, the derivation is consistent.

2. Although S_0 is assumed to be a property, related to fiber only, it may be somewhat related to the pressing process. The definition of the specific surface S_0 is the total surface area of the fiber material divided by the total volume of the fiber material. At different values of c, the sheet concentration, both the surface area and the volume of the fiber material are the same theoretically since the dry fiber mass or volume is the same for samples pressed at different levels. The difference is the sheet thickness when c is measured and calculated.

In a real pressing process, with a greater pressure which results in higher c, there must be more fiber-to-fiber contacts. Even after the pressure is released, a sheet with high c will probably have more fiber-to-fiber bonds. Thus, the exposed surface area of fibers may be reduced somewhat, resulting in a change of the permeability k. On the other hand, with more fiber-to-fiber contacts, the flow path will probably be more tortuous, which also results in some change of the permeability. These two effects would somewhat cancel with each other.

At the current stage, the magnitude of either of these effects, related to the change of c, is not known. However, since the variation range of c is limited, it may be reasonable to assume that these two effects are relatively small.

2. E. Notes on Permeability (December 20, 1994)

The following are some new exploratory results of the issue of s versus C (specific surface area in m^2/kg versus the sheet consistency C).

The "traditional" way of writing the Kozeny-Carman equation is

$$K = \frac{1}{k_o s_0^2} \frac{\varepsilon^3}{(1 - \varepsilon)^2} \qquad (47a)$$

where ε is the average porosity of the material; k_o is a dimensionless and empirical constant and also called Kozeny constant; and s_o is the specific surface, or the surface area per unit volume of solid material. The term s_o is calculated as the total surface area exposed to flow divided by the total volume of the solid material in a porous medium, and is with the units of one over the length (1/m). For general fibrous and textile materials, it has been suggested that $k_o = 5.5$ is a good estimation.

For the water permeability of paper material with swelling, the porosity is replaced with the "effective" porosity ε', and the modified Kozeny-Carman equation is

$$K = \frac{1}{k_o s_o^2} \frac{\varepsilon'^3}{(1 - \varepsilon')^2} \tag{47b}$$

This effective porosity can be considered as $\varepsilon'=1-\alpha c$, where c is the sheet concentration or density (kg/m^3 or g/m^3) and is the dry fiber weight divided by the sheet volume (sheet area times sheet thickness), and α is the specific volume of the water swollen fibers (m^3/kg or m^3/g). That leads to the alternative expression of the Kozeny-Carman equation as

$$K = \frac{1}{5.55\ s^2} \frac{(1 - \alpha c)^3}{c^2} \tag{47c}$$

where s is the flow-exposed surface area of the fibers based on the per unit mass of fibers (m^2/kg or m^2/g). In the experiment, s and α are not directly measured. Instead, K and c are measured, and s and α are then derived from the data plot. Also, the Kozeny constant k_o in (47a) is assumed to be 5.55 as expressed in (47b).

The question is whether the flow-exposed surface area of fibers, s, is a function of the sheet consistency, C. The definition of the consistency C is

$$C = \frac{M_f}{M_f + M_w} \tag{48}$$

where M_f and M_W are the mass of fiber and water, respectively. The answer to the question involves the interpretation of equations (47a) and (47b), and will be discussed below.

To account for the fiber swelling effect when water permeability is measured, a dimensionless fiber swelling factor can be introduced. If the total fiber volume fraction before swelling is v_f, and that after swelling is $(1+b)\,v_f$ where b is a dimensionless swelling factor, the corresponding effective porosity ε' becomes

$$\varepsilon' = \varepsilon - b(1 - \varepsilon) \tag{49}$$

Hence, the expression (47a) becomes

$$K = \frac{1}{k_o s_0^2} \frac{\varepsilon'^3}{(1 - \varepsilon')^2} = \frac{1}{k_o s_0^2} \frac{[\varepsilon - b(1 - \varepsilon)]^3}{[(1 + b)(1 - \varepsilon)]^2} \tag{50}$$

The sheet concentration can be expressed as

$$c = \frac{M_f}{V} = \frac{M_f}{V_f + V_w} = \rho_f (1 - \varepsilon) \tag{51}$$

where V is the total volume; V_f and V_W are the volume of fiber and water, respectively; and ρ_f is the fiber density. Since the term $(1-\alpha c)$ in (47b) is equivalent to ε' in (47a), with the use of (49) and (51), the new variable b is related to the swollen factor α as

$$1 + b = \alpha \rho_f \tag{52}$$

Thus, equation (50) can be further written as

$$K = \frac{1}{k_o s_0^2} \frac{(1 - \alpha c)^3}{\alpha^2 c^2} \tag{53}$$

Compared with (47b), it can be found that $s = (s_o \alpha)$ if k_o is assumed to be 5.55. Since s_o is assumed to be a property of dry fibers only, the problem becomes to find out whether α is related to the sheet consistency C. This can be solved with the definitions of ε and c. The two variables are related to C as

$$\varepsilon = \frac{V_w}{V_w + V_f} = \frac{M_w/\rho_w}{M_w/\rho_w + M_f/\rho_f} = \frac{(1 - C)(\rho_f/\rho_w)}{C + (1 - C)(\rho_f/\rho_w)} \tag{54}$$

$$c = \frac{C \rho_f}{C + (1 - C)(\rho_f/\rho_w)} \tag{55}$$

where ρ_w is the density of water, and ρ_f/ρ_w becomes the specific ratio of fiber. When α is solved and expressed as a function C, the expression is

$$\alpha = \frac{1}{2\rho_f}\left[\frac{1}{C}\left(\frac{\rho_f}{\rho_w}\right) - \left(\frac{\rho_f}{\rho_w} - 1\right)\right] \tag{56}$$

Thus, the specific surface area s is related to C as

$$s = s_o\left\{\frac{1}{2\rho_f}\left[\frac{1}{C}\left(\frac{\rho_f}{\rho_w}\right) - \left(\frac{\rho_f}{\rho_w} - 1\right)\right]\right\} \tag{57}$$

It can be seen that s is a function of C, and decreases when C increases. Since the range of C in the consideration is relatively limited, the decrease of s is also very limited.

2.F. The Effect of Fines on the Permeability of Paper

In a paper fiber assembly, there is some percentage of fines content due to refining and other operations. The sizes of these fines are much smaller than fibers. The existence of these fines within a paper fiber assembly may greatly change the magnitude of the permeability.

The major effect of fines on the permeability comes from two aspects. One is the substantial increase of the specific surface area of the fiber assembly, and the other is the change of the packing structure.

The detailed analysis of these two effects is difficult because of the random distribution of fibers and fines within a paper fiber assembly. The evaluation of these two effects, however, can be conducted using a simplified analysis. The results can provide valuable insight into the physical mechanism of the problems, and assist further exploration of solutions.

Effect of fines on the Specific Surface Area: The existence of fines within a paper fiber assembly can increase the specific surface area, which results in lower permeability. In order to assess the effect of fines on the specific surface area, a simplified case was studied by comparing two paper fiber assemblies with and without fine contents.

Fiber assembly 1 contains fibers with uniform radius. Therefore, the specific surface area $s_1 = 2/r_{f1}$. Fiber assembly 2 contains fibers with radius r_{f1} and some portion of fines with radius r_{f2}. The volume percentage of fines versus the total solid volume is *c*, which is assumed to be in the range of 5 to 20%. The fine radius is assumed to be r_{f2}. The ratio of the two radii is $b = r_{f2}/r_{f1}$. If in a selected representative volume there are n_1 fibers and n_2 fines, the volume percentage of fines is

$$c = \frac{n_2 \pi r_{f2}^2}{n_1 \pi r_{f1}^2 + n_2 \pi r_{f2}^2} = \frac{n_2 b^2}{n_1 + n_2 b^2} \tag{58}$$

If fiber end areas are neglected, and the total fiber length and fine length are assumed to be the same, the specific surface area of the fiber assembly 2 is

$$s_2 = \frac{n_1 2\pi r_{f1} + n_2 2\pi r_{f2}}{n_1 \pi r_{f1}^2 + n_2 \pi r_{f2}^2} \tag{59}$$

From these expressions, the specific surface area s_2 for the fiber assembly 2 can be related to *b* and *c* as

$$s_2 = \frac{2}{r_{f1}}\left(1 - c + \frac{c}{b}\right) \tag{60}$$

The ratio of the specific area $s^* = s_2/s_1$ becomes a function of *b* and *c* as

$$s^* = 1 - c + \frac{c}{b} \tag{61}$$

It can be seen that s* increases with the increase of c or the decrease of b. The relationship of s* versus selected values of b and c is plotted in Fig. 4 It can be seen that if the fine percentage is relatively high, the influence can be substantial. For example, if there is 20% fine volume for the fiber radius ratio of 5 and 10, s* is about 2.8 and 4.8, respectively. Since the permeability K is related to the square of the specific surface s, K can reduce significantly with the presence of the fines.

Although these two cases are greatly simplified, the results can provide valuable information about the influence of fines on the permeability of paper fiber assembly.

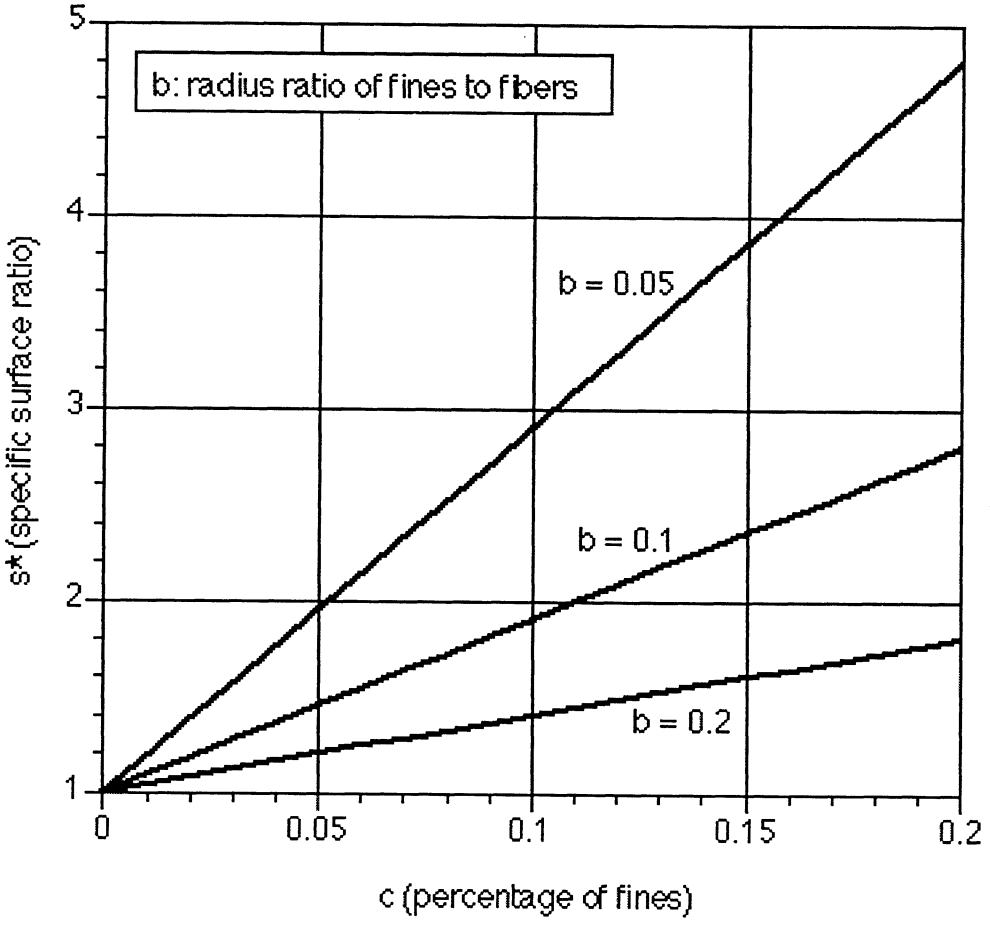

Figure 4. Specific Surface Area Versus the Fine Percentage and Fine Size.

2.G. Note on Permeability of Mixed Fibers

The well-known permeability estimation equation for fibrous materials is the Kozeny-Carman equation. In the Kozeny-Carman equation, three main factors are considered. First is the porosity. A functional form of the porosity effect has been suggested. Second is the specific surface effect. If fibers have relatively uniform diameter, the specific surface is related to the fiber diameter or radius. Third is the packing and orientation effect, which is not clearly characterized, but is included in an empirical constant, the

Kozeny constant. Since the Kozeny constant is adjustable under different structural and flow situations, it is useful in practical applications where the value of the constant can be estimated.

The Kozeny-Carman equation has been applied to various porous materials, including the ones with various pore sizes. The porosity and the specific surface are based on the averaged or macrolevel structure of the porous material. Both are properties of the material and can be measured or estimated. The adjustable Kozeny constant then takes care of the pore distributions and other effects. In the fibrous material case, fiber packing patterns are closely related to the magnitude of the Kozeny constant and the permeability.

At a particular porosity level, the permeability of mixed fibers is expected to be different from that of either fiber species. For example, fiber species A and B show permeability magnitudes of K_A and K_B, respectively. The mixture of both species would show a permeability somewhere in between.

To investigate the permeability of a mixture of fibers, the specific surface and the packing structure will be considered.

The Kozeny-Carman equation is written as

$$K = \frac{1}{k_o s^2} \frac{\varepsilon^3}{(1-\varepsilon)^2} \tag{62}$$

where K is the permeability in the units of length squared; k_o is the Kozeny constant which is dimensionless; s is the specific surface; and ε is the average porosity.

The specific surface of a fiber assembly can be calculated. For fibers with uniform sizes, s can be obtained as

$$s = \frac{A_f}{V_f} = \frac{\sum 2\pi r_f L_f}{\sum \pi r_f^2 L_f} = \frac{2}{r_f} \tag{63}$$

where A_f is the total surface area; V_f is the total volume; r_f is the fiber radius; and L_f is the fiber length. When fiber surface area is calculated, the end area of fibers is neglected. The summation sign represents the total area or volume calculations.

If two species of fiber with the same length but different fiber radius are considered, the specific surface of the mixture s_m can be obtained as

$$s_m = \frac{2\left(\frac{m_{f1}}{\rho_{f1}\, r_{f1}} + \frac{m_{f2}}{\rho_{f2}\, r_{f2}}\right)}{\frac{m_{f1}}{\rho_{f1}} + \frac{m_{f2}}{\rho_{f2}}} \tag{64}$$

where subscripts f1 and f2 refer to two species of fibers; m_f is the mass fraction; and r_f is the fiber density. The definition of the mass fraction gives $m_{f1} + m_{f2} = 1$. If both fibers have the same fiber density, then the estimation of s_m can be simplified as

$$s_m = 2\left(\frac{m_{f1}}{r_{f1}} + \frac{m_{f2}}{r_{f2}}\right) \tag{65}$$

Therefore, if r_{f1} and r_{f2} are known, s is a linear function of m_{f1} or m_{f2}. Also, if the specific surface of the fiber type 1 is $s_1 = 2/r_{f1}$, and that of fiber type 2 is $s_2 = 2/r_{f2}$, then the specific surface of the mixture s_m is related to s_1 and s_2 with a simple rule of mixture as

$$s_m = m_{f1}\, s_1 + m_{f2}\, s_2 \tag{66}$$

Since the permeability K is proportional to $(1/s^2)$, the influence of the s on K is nonlinear. Thus, if the permeability of fiber type 1 is K_1 at a particular porosity ε and with an assumed Kozeny constant k_o, and that of fiber type 2 is K_2 similarly, the estimation of K_m of the fiber mixture at the *same porosity* and with the *same Kozeny constant* is not a simple rule of mixture. The expression of K_m can be derived as

$$K_m = \frac{1}{\left(m_{f1}\sqrt{\frac{1}{K_1}} + m_{f2}\sqrt{\frac{1}{K_2}}\right)^2} \tag{67}$$

This relationship is plotted in Fig. 5 with selected values of K_1 and K_2. As shown in the figure, the permeability of the fiber mixture K_m is always less than that of the simple rule of mixture of using K_1 and K_2. When the difference of K_1 and K_2 becomes larger such as in case 2 of the figure, the difference of K_m and the average of K_1 and K_2 become larger.

Since the permeability of K_1 or K_2 is proportional to the square of the fiber radius r_{f1} or r_{f2}, respectively, the difference of K_1 and K_2 is larger than the difference of fiber diameters.

The above discussion is based on the assumption of using the same Kozeny constants for the fiber mixture and for uniform fiber size assemblies. Since the magnitude of the Kozeny constant is closely related to the fiber packing structure, the assumption is apparently oversimplified. When two types of fibers are mixed together, smaller fibers tend to fill into the spaces among larger fibers, resulting in a "better" packed structure. Thus, the flow resistance of the mixed fiber assembly even at the same porosity level would be higher because of the packing structure. In other words, if the Kozeny-Carman equation is used to describe the permeability of mixed fiber assemblies, the Kozeny constant would be larger.

In order to estimate the packing structure influence on the overall permeability, simplified numerical simulation can be performed.

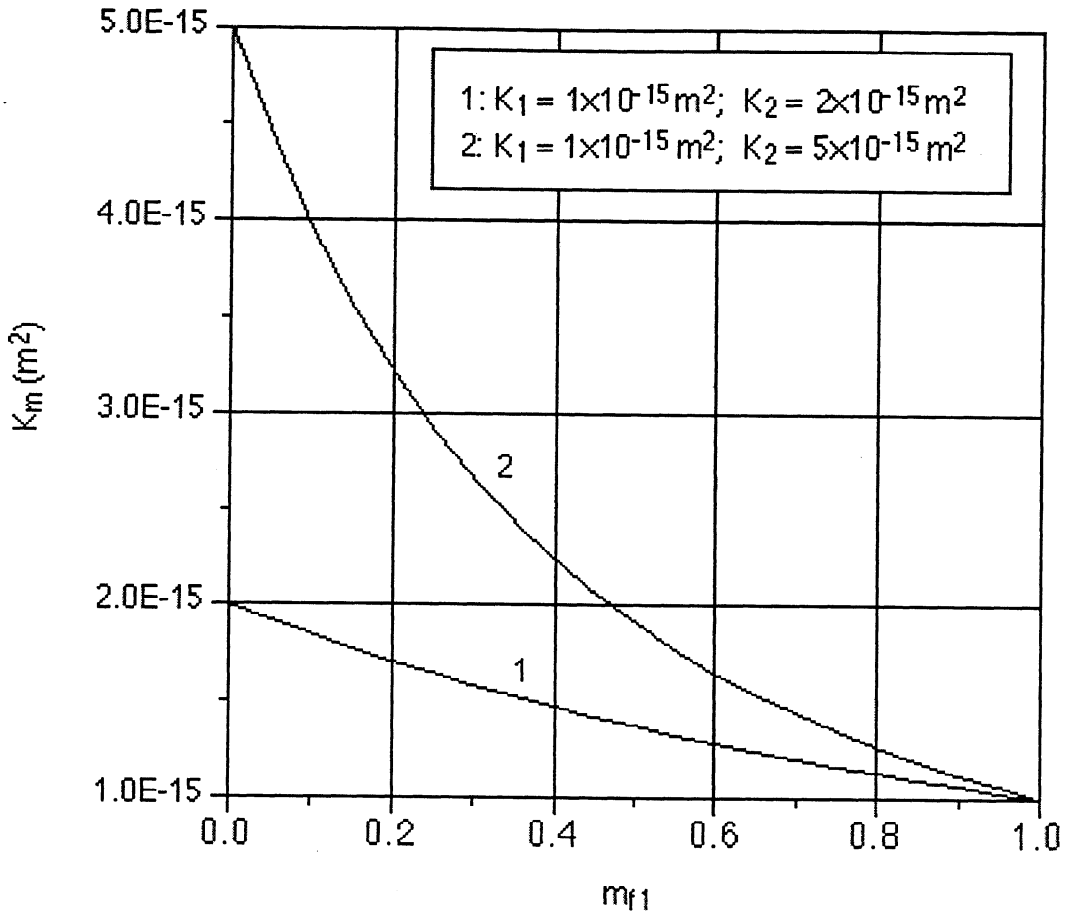

Figure 5. Comparison of K_m Versus K_1 and K_2 with the Assumption of Same Kozeny Constant.

2.H. Note on Porosity Characterization

In a recent study about the pore size distribution of the cellulosic pulps by Allan, Ko, and Ritzenthaler [39], it was found that in never-dried or reswollen, natural or regenerated cellulosic materials, the voids have a log-normal size distribution. The two parameters for the log-normal pore size distribution model are the median pore width and the standard deviation. Both parameters are accessible from the experimentally measured data when the percentage normalized cumulative pore volume F and the natural logarithm of the pore width w are plotted on a normal probability function scale.

3. Air Permeability and Water Permeability (December 19, 1994)

From my experience on the permeability issue, I think that the air permeability of a paper material will be somewhat related to its water permeability. It also has great potential for a more efficient permeability measurement method.

In the past two weeks, I studied the permeability from the impulse drying project. Isaak Rudman did some air permeability measurements upon his own initiative. I developed some formulas to correlate air permeability with water permeability based on the Kozeny-Carman equation. Using these available data and after carrying out some data processing calculations, I found out that my assumption stands. Figure 6 is a plot showing the comparison of the calculated specific surface area with these two groups of data. It is reasonable to assume a linear correlation between the two sets of values, which actually implies the difference in the magnitude of the Kozeny constant in the two cases.

I have written a draft version of a technical report about the theoretical part of this derivation, which gives detailed discussion about various related issues. Also I would like to pursue this topic since it can provide a useful tool for estimating the water permeability of paper materials. It seems to me that I can develop a good proposal based on my observation of the available data.

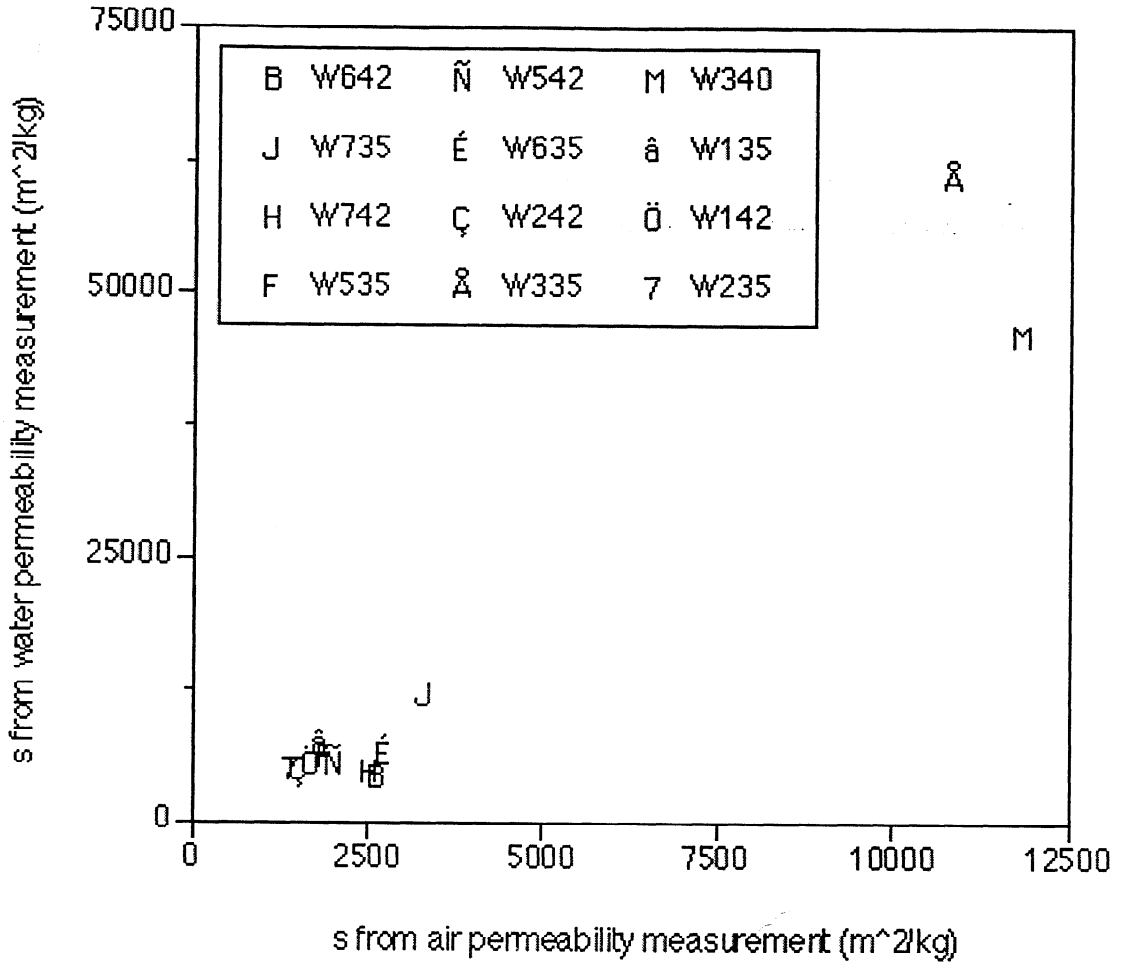

Figure 6. Correlation Between Air and Water Permeability Measurements.

4. References

1. Heller, H.H. and Tweksbury, C.G., "What Are the Limits of Paper Dryness Obtained in a Wet Press"?, TAPPI, Vol. 55, No. 6, June 1972.

2. McCarrol, T.H.M. and Wiseman, N., "Survey Examines Press Section Performance of Newsprint Machines," Pulp and Paper Magazine of Canada, December 1968.

3. Jewett, K.B., "The Application of a Model for Two Phase Flow through a Compressible Porous Media to the Wetpressing of Paper," Ph.D., Thesis, University of Maine, 1984.

4. Lavigne, J.R., Pulp and Paper Dictionary, Miller Freeman Books, 1993.

5. Jaavidaan, Y., Ceckler, W.H., and Thompson, E.V., "Rewetting in the Expansion Side of Press Nips," *TAPPI Journal*, March 1988, pp. 151-155.

6. Roux, J.C. and Vincent, J.P., "A Proposed Model in the Analysis of Wet Pressing," *TAPPI Journal*, February, 1991, pp. 189-195.

7. Biot, M.A., "General Theory of Three-Dimensional Consolidation," *Journal of Applied Physics*, Vol. 12, February 1941, pp. 155-164.

8. Jewett, K.B., "The Application of a Model for Two Phase Flow through a Compressible Porous Media to the Wetpressing of Paper," Ph.D. Thesis, Dept. of Chemical Engineering, University of Maine at Orono, 1984.

9. Ceckler, W.H. and Thompson, E.V., The University of Maine at Orono Wet Pressing Project, Final Report, (Under Contract No. AC02-78CS40064, Dept. of Energy), August 24, 1982, DOE/CS/40064-3 (DE83009342).

10. Ellis, E.R., Jr., "Compressibility and Permeability of Never Dried Bleached Softwood Kraft Pulp and Its Application to the Prediction of Wet Press Behavior," Ph.D. Thesis, Dept. of Chemical Engineering, University of Maine at Orono, 1981.

11. Wilder, J.E., "Paper Drying: Capillary Transfer between Porous Compressible Materials," Ph.D. Thesis, Dept. of Mechanical Engineering, M.I.T., 1967.

12. Yin and McNamara.

13. Asklof, Larsson, Linderoth, and Wahlstrom.

14. Wilder, J.E., "Paper Drying: Capillary Transfer between Porous Compressible Materials," Ph.D. Thesis, Dept. of Mechanical Engineering, M.I.T., 1967.

15. Busker, 1971.

16. Justus and Cronin, 1981.

17. Singh, K.M., "Mathematical Analysis of the Wet Pressing of Paper," Ph.D. Thesis,

College of Environmental Science and Forestry, State University of New York, 1990.

18. White, R.E. and Berdux, F.W., "Static Pressing of Wet Sheets and Felts," *TAPPI,* Vol.
43, No. 6, June 1960, pp. 580-586.

19. Jewett, K.B., "The Application of a Model for Two Phase Flow through a Compressible Porous Media to the Wetpressing of Paper," Ph.D. Thesis, Dept. of Chemical Engineering, University of Maine at Orono, 1984.

20. Ceckler, W.H. and Thompson, E.V., "The University of Maine at Orono Wet Pressing Project, Final Report," (Under Contract No. AC02-78CS40064, Dept. of Energy), August 24, 1982, DOE/CS/40064-3 (DE83009342).

21. Lindsay, J.D., "The Anisotropic Permeability of Paper," *TAPPI Journal*, May 1990, pp. 223-229.

22. Brown, J.C. "Determination of the Exposed Surface Area of Pulp Fibers from Air Permeability Measurement, Using a Modified Kozeny Equation," Ph.D. Thesis, The Institute of Paper Chemistry, 1949.

23. Brown, G.R., "Creeping Flow of Fluids through Assemblages of Elliptic Cylinders and Its Application to the Permeability of Fiber Mats," Ph.D. Thesis, The Institute of Paper Chemistry, 1975.

24. Chen, F.J., "The Permeability of Compressed Fiber Mats and the Effects of Surface Area Reduction and Fiber Geometry," Ph.D. Thesis, The Institute of Paper Chemistry, 1982.

25. Han, S.T., "Compressibility and Permeability of Fiber Mats," *Pulp and Paper Magazine of Canada*, Vol. 70, No. 9, May 1969, pp. 65-77 (T134-146).

26. Hordtmann, D.H., Lindsay, J.D., and Stratton, R.A., "Using Edge-Flow Tests to Examine the In-plane Anisotropic Permeability of Paper," *TAPPI Journal*, Aprial 1991, pp. 241-247.

27. Ingmanson, W.L., "An Investigation of the Mechanism of Water Removal from Pulp Slurrues," *TAPPI Journal*, Vol. 35, No. 10, October 1952, pp. 439-448.

28. Lindsay, J.D., "The Anisotropic Permeability of Paper," *TAPPI Journal*, May 1990, pp. 223-229.

29. Lindsay, J.D. and Brady, P.H., "Studies of Anisotropic Permeability with Applications to Water Removal in Fibrous Webs, Part I: Experimental Methods, Sheet Anisotropy, and Relationships to Freeness," *TAPPI Journal,* Vol. 76, No. 9,

FUNDAMENTALS OF DRYING

STATUS REPORT

FOR

PROJECT F001 (3470)

David I. Orloff

March 20 - 21, 1995

Institute of Paper Science and Technology
500 10th Street, N.W.
Atlanta, Georgia 30318

TECHNICAL PROGRAM REVIEW

Project Title:	FUNDAMENTALS OF DRYING
Project Code:	DRYING
Project No.	F001 (3470)
Division:	Engineering and Paper Materials
Project Staff:	David I. Orloff
Budget (FY '94-95):	$142,435

OBJECTIVE

To develop an understanding and a database for commercialization of advanced water removal systems, based on high intensity drying principles. This new technology will reduce capital costs, increase machine productivity, reduce the amount of energy used, and improve properties.

GOAL

To commercialize the impulse drying process by 1998.

SUMMARY

Over the past year, the impulse drying team has concentrated on expanding our knowledge of impulse drying and related technology to serve as a framework for decision making regarding its commercialization.

Key accomplishments for the period include:

- *Joint Research and Development Agreement* - The Institute continued to try to form a three-way research and development agreement between the Institute, Union Camp Corporation, and Beloit Corporation for the commercialization of impulse drying of board grades of paper. In December 1994, an impasse was reached between Beloit and Union Camp with regard to royalty payments. The Institute and Beloit Corporation are currently working to put a two-way agreement into effect. That agreement would focus on press roll surface durability experiments at the Institute, continuous commercial speed impulse drying experiments on the Beloit No. 4 pilot paper machine, and converting trials at the Institute.

- *External Funding* - The impulse drying project is partly funded by the U.S. Department of Energy Office of Industrial Programs and by in kind contributions from Beloit Corporation and Union Camp Corporation. U.S. DOE impulse drying funding to the Institute for FY '94 was $495,000. U.S. DOE funding in FY '95 is expected to be $287,000 for the Institute and $550,000 for Beloit Corporation (for the purchase of induction heating equipment to be installed on its #4 pilot paper machine).

- *Numerical Modeling* - Lubrication and heat transfer modeling of the inside of the proposed crown-compensated impulse drying press roll has been completed. The results may be used to predict internal loading of the press roll and heat transfer from the lubricant to the press roll and loading shoe.

- *Durability Test Facility* - The Institute's pilot impulse dryer has been modified so that it can serve as a commercial speed press roll surface durability test facility (DTF). Tensile testing of alternate plasma-sprayed surfaces was conducted. Shear testing is in progress. Test results will be used to identify three coatings for future testing on the DTF.

- *Thermal Mass* - Laboratory-scale experiments were conducted to assess the advantages of various press roll coatings having a range of thermal mass. The work showed that as the thermal mass of the coating decreases its thermal efficiency increases. The work also showed that an intermediate value of thermal mass resulted in maximum water removal and property development.

- *Steam Box Fundamentals* - A steam box comparator was constructed that can serve as a means for evaluating various strategies for web preheating. Preliminary experiments showed that a vacuum box placed under a steam box can substantially improve the penetration of heat into the web.

- *Impulse Drying Operating Window Expansion* - The Institute's laboratory-scale impulse drying simulator has been rebuilt to allow impulse drying in an environment where the ambient pressure can be controlled.

- *Commercial Furnish Evaluation* - Laboratory and sheet-fed pilot experiments were performed in cooperation with Beloit Corporation and Union Camp Corporation. The experiments were designed to determine the relationships between refining, prepressing, and water permeability for commercial pulps. In addition, mill-refined pulp and machine paper were compared to laboratory samples with regard to water permeability and impulse drying performance.

- *Patents & Papers* - The impulse drying team has been active in publishing and presenting papers dealing with issues that have previously been communicated to IPST member companies and are relevant to impulse drying technology.

DISCUSSION

Joint Research and Development Agreement

The Institute continued to try to form a three-way research and development agreement between the Institute, Union Camp Corporation, and Beloit Corporation for the commercialization of impulse drying of board grades of paper. In December 1994, an impasse was reached between Beloit and Union Camp with regard to royalty payments. The Institute and Beloit Corporation are currently working to put a two-way agreement

into effect. That agreement would focus on press roll surface durability experiments at the Institute, continuous commercial speed impulse drying experiments on the Beloit No. 4 pilot paper machine, and converting trials at the Institute.

Numerical Modeling

A constant viscosity lubrication model of the inside of the proposed crown compensated impulse drying press roll has been completed, and has been reported to member companies [1]. The results of the model were found to compare well with experimental measurements made by Beloit Corporation on its small crown-compensated roll flow loop. Analysis of a large diameter roll showed that the mechanical power required to operate the roll increased with increased roll speed while being relatively insensitive to increases in press load. The analysis also resulted in required lubricant flow rates and internal pressure distributions that, in the future, may be incorporated into finite element models to predict the thermal stress distribution within the roll coating.

Parametric studies were also carried out to determine the sensitivity of the lubrication model to variations in oil viscosity, shoe angle, and shoe radius. Oil viscosity and shoe angle were found to be sensitive variables. The results showed that the required oil flow rate was relatively insensitive to oil viscosity when the oil viscosity was between 50 and 100 centistokes. However, when the oil viscosity was reduced below 20 centistokes, the required oil flow rate increased almost exponentially. The simulations also showed that

the mechanical power, required to drive the press roll, increased linearly with oil viscosity.

Shoe angle, while not as important as oil viscosity, was shown to be an important variable. In particular, it was found that both mechanical power and oil flow rate increased with increased shoe angle.

More recently, the constant viscosity model has been extended to evaluate the heat transfer from the roll shell to the lubricant as well as the heat transfer from the lubricant to the hydrostatic shoe [2]. Calculations for a large press roll (R_s=R=0.508 m) were made over a range of applied load (300-1100 KN/m), roll speed (300-1100 m/min), shoe temperature (100-160°C), and inner roll surface temperature (100-300°C). The work showed that, because of the viscous nature of the lubricant, and the large tangential speed of the roll, the direction of heat transfer was generally from the oil to the inner surface of the roll. Hence, the temperature of the oil between the shoe and the roll shell was generally higher than the temperature of the inner surface of the roll.

The heat transfer from the oil to the roll was found to decrease linearly with increased inner roll surface temperature, and increase linearly with increased shoe temperature. In addition, the heat transfer model showed that heat transfer from the oil to the shoe increased linearly with increased inner roll surface temperature and decreased linearly with increased shoe temperature.

A major conclusion of the heat transfer work was that by holding the shoe temperature significantly below that of the inner surface of the roll the effects of viscous heating can be significantly reduced.

Durability Test Facility

The Institute's pilot impulse dryer has been modified so that it can serve as a commercial speed press roll surface durability test facility (DTF). The facility will allow the testing of roll coatings at conditions that simulate the thermal and loading cycles expected during commercial impulse drying. The apparatus can be operated at speeds of 2500 ft/min and at surface temperatures of 250°C. An infrared thermal imaging system has been purchased to allow continuous monitoring of the integrity of roll coatings during simulated high-speed impulse drying.

Tensile testing of alternate plasma sprayed surfaces was conducted to identify three coating for future testing on the DTF.

The five coatings selected for strength testing were the two coatings, C and A, that have been previously evaluated on Beloits' impulse drying shoe press, and three newly developed coatings. The new coatings included an improved strength version of the A coating, designated IA; a coating made of a low concentration of NiCr blended with Z_rO_2, designated LNCC, and a coating made from a higher concentration of NiCr blended with Z_rO_2, designated MNCC. Nine test specimens were fabricated to determine

the tensile strength at failure of each of these coatings. A modified version of ASTM C633-79 was utilized. The modification consisted of the use of a stronger, more viscous adhesive, Miller Stephenson 907, in the preparation of samples.

Two modes of tensile failure were observed; they were failure in the coating and failure at the interface between the coating and the base metal substrate. A summary of the mean tensile failure stress for each failure mode is recorded in Table 1. Also shown is the probability of observing each of the modes of failure.

Table 1. Tensile Testing Alternate Plasma-Sprayed Surfaces.

Coating Type	Coating Failure		Interface Failure	
	Probability, %	Avg. Failure Stress, psi	Probability, %	Avg. Failure Stress, psi
A	44	2538	56	791
C	100	1484	0	na
IA	56	2472	44	2642
LNCC	100	1928	0	na
MNCC	100	2158	0	na

Thermal Mass

Laboratory-scale experiments were conducted to assess the advantages of various press roll coatings having a range of thermal mass. The work showed that as the thermal mass of the coating decreases its thermal efficiency increases. The work also showed that an intermediate value of thermal mass resulted in maximum water removal and property development.

In these experiments [3], the following hypothesis was tested:

HYPOTHESIS: If similar sheets are impulse dried with roll surfaces having different "thermal mass," then the onset of delamination will occur such that the energy transferred from each roll surface is the same.

Energy transfer during impulse drying, at the onset of delamination, was measured for both a steel and a ceramic-coated platen. For both low and high specific surface sheets, and over a wide range of press loads, the steel surface transferred substantially more energy than the ceramic-coated surface. This result invalidates the hypothesis, suggesting that something other than energy transfer controls the onset of sheet delamination.

It has previously been reported that sheet permeability, as measured by hydrodynamic specific surface, influences the temperature at which the onset of delamination occurs. Hence, we have asked the question of whether choice of platen surface controls the permeability of the sheet at nip opening. To test this idea, sheets impulse dried, at temperatures just below the onset of delamination, using three surfaces having different "thermal mass" were sectioned through the thickness of the sheets. The results of these sectioning measurements are expected to be ready for the spring PAC meeting.

Interestingly, the experiments [3] confirmed that energy transfer is pressure dependent for steel surfaces while being pressure independent for the ceramic surface. This suggests that the local thermal properties of the moist sheet control heat transfer when a high

"thermal mass" steel surface is used, while a ceramic-coated surface controls heat transfer independent of the local thermal properties of the moist sheet.

Steam Box Fundamentals

A steam box comparator was constructed that can serve as a means for evaluating various strategies for web preheating. Preliminary experiments showed that a vacuum box placed under a steam box can substantially improve the penetration of heat into the web.

Previous work [Orloff, D.I., and Lindsay, J.D, Proceedings: 1992 TAPPI Papermakers Conference, Book 1, pp. 85-93] has shown that impulse drying performs optimally when the sheet is prepressed, as much as possible, before entering the impulse dryer. An effective way to increase the press dryness, entering the impulse dryer, is to preheat the sheet as much as possible before each press that is upstream to the impulse dryer.

Figure 1, taken from previously published data [Orloff, D.I., Journal of Pulp and Paper Science, 18(1), 23-32] shows the effect of preheat temperature on press dryness for a simulated single-felted roll press operating at a press impulse of 5.4 psi sec. It is observed that percent outgoing solids increases by about 3% with an increase of sheet temperature from 120°F to 180°F. A general rule of thumb is that for every 1% increase in dryness, at the press section, a 4% increase in machine productivity should be expected. Hence, by increasing the sheet temperature from 120°F to 180°F, a machine productivity increase

of 12% should be realized. This result demonstrates that improved design and utilization of preheating devices could have significant bottom-line implications.

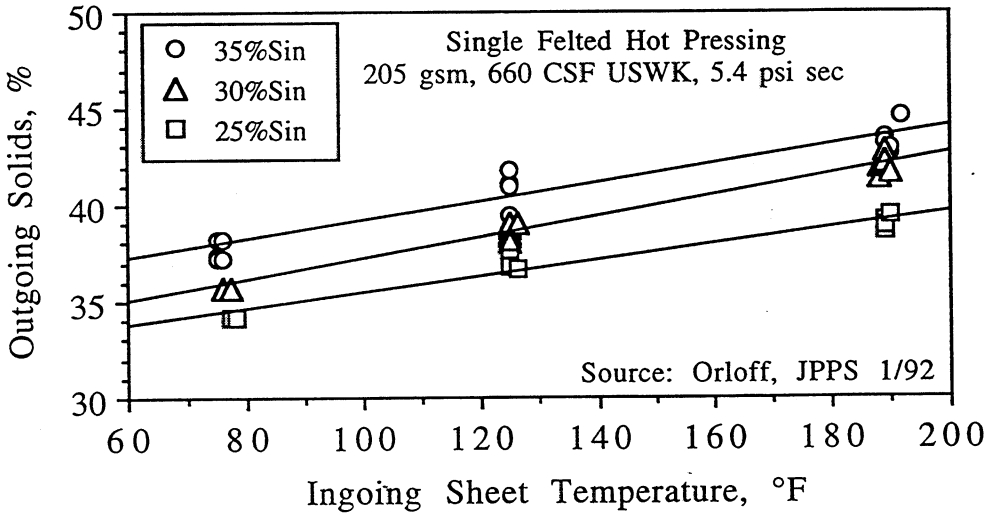

Figure 1. Preheating Improves Single-felted Hot Pressing.

Discussion with a number of member company representatives suggested that web preheating, usually through the use of steam boxes, is poorly understood. Some companies report improved pressing efficiency by using steam boxes. Other companies report that they have removed steam boxes because either they never worked, or through changes in furnish, they no longer work as well as previously. Review of the preheating literature suggests that very little engineering heat transfer data exist for steam boxes.

Over the past year, the Institute has constructed an apparatus for evaluating the performance of web preheating devices. The experimental apparatus, methods, and some

preliminary data have also been reported [4]. In these preliminary experiments, z-directional temperature profiles were measured as 42 lb/1000ft^2 sheets carried on a press felt traverse between a steam box and a vacuum box at commercial speeds. The experiments showed that the vacuum box can significantly increase the ability of the steam box to uniformly raise the temperature of the sheet. Figure 2 shows the effect of vacuum on the mean sheet temperature exiting the steam box.

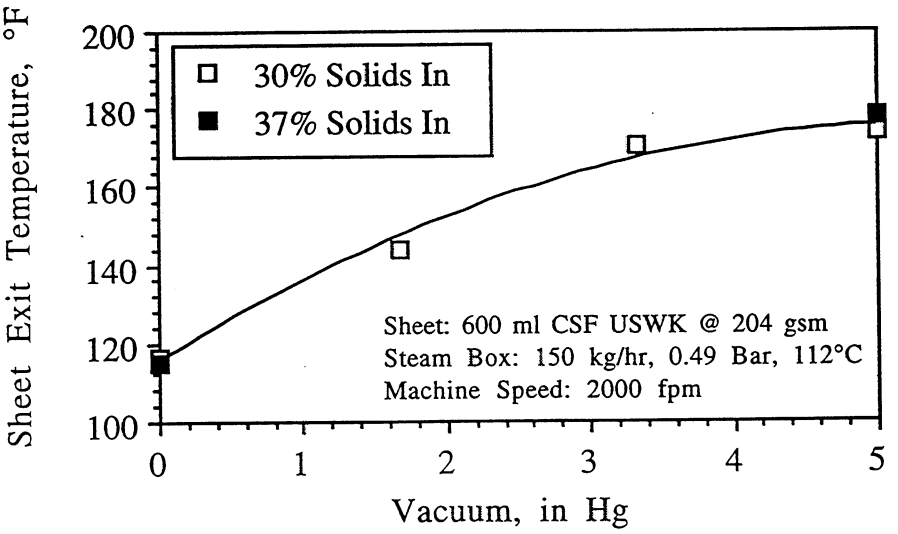

Figure 2. Mean Exit Sheet Temperature vs. Vacuum.

It is clear from these results that proper use of a vacuum box under the press felt can significantly improve the performance of the steam box. It is also clear that the vacuum applied to the bottom of the sheet, rather than the vacuum in the vacuum box, is the controlling factor. With this in mind, the apparatus has also been equipped with vacuum transducers that will allow instantaneous measurement of the vacuum between the sheet and the felt as well as the vacuum applied to the bottom of the felt. It is expected that

some felt structures may perform better in transmitting vacuum to the underside of the sheet than others. Future experiments may prove helpful in assessing this effect. Additional preheat work is ongoing in the form of two Masters theses. In one project, we are developing a method to measure the thermal conductivity of moist paper as a function of refining, pressing, and temperature. In the other project, we are investigating steam preheating of simpler noncellulosic porous structures to learn how to interpret our paper preheating data in the form of nondimensional correlations.

Impulse Drying Operating Window Expansion

The Institute's laboratory-scale impulse drying simulator has been rebuilt to allow impulse drying in an environment where the ambient pressure can be controlled [5]. This work is being conducted as a Master's thesis, and preliminary experiments are expected to be completed by May 1995.

Commercial Furnish Evaluation

Handsheets formed from various combinations of softwood and hardwood were produced by Union Camp. These samples were then prepressed on pilot presses by Beloit. Prepressed samples were then impulse dried on Beloit's pilot roll press (HRP), pilot shoe press (ENP-HRP), and impulse drying simulator (Beloit- MTS); and the Institute's impulse drying simulator (IPST-MTS). Prepressed sheets were tested by the Institute for

hydrodynamic specific surface, and impulse dried sheets were ultrasonically tested to detect sheet delamination [6].

Measurements of hydrodynamic specific surface confirmed previous observations that reduced refining and increased prepressing tend to reduce the hydrodynamic specific surface of commercial pulps. Mill-refined pulp and machine paper were found to be comparable to laboratory prepared samples with regard to hydrodynamic specific surface and impulse drying performance. Infralaboratory comparisons indicated consistent trends with IPST results being the most conservative.

Patents & Publications

Over the past year, the Institute has been granted two additional patents [7, 8] dealing with various aspects of impulse drying technology.

A paper describing joint IPST/Beloit impulse drying experiments was published [9] in *Tappi Journal*, and additional papers have been submitted for publication [10, 11].

GOALS FOR FY: 1995-1996

The ultimate objective of the impulse drying program is to commercialize the technology for heavy weight grades of paper and to expand the usefulness of the technology for a wider range of furnishes and paper grades. To accomplish this objective, the Institute will

seek finalization of a formal agreement with the Beloit Corporation to develop the technology for board grades on a pilot paper machine. In addition, the Institute will pursue research that will lead to expanded application of the technology.

Work planned for FY '95-96 Will Focus on These Major Objectives.

- Conduct commercial speed roll surface durability experiments to determine the plasma spray coating composition that yields the best durability. {U.S. DOE Funding}.

- Assist Beloit Corporation in conducting high-speed, continuous, impulse drying experiments on its No. 4 pilot paper machine, and convert the linerboard product into corrugated board and corrugated boxes. {U.S. DOE Funding}.

- Continue variable ambient pressure impulse drying experiments to determine commercially viable ways of extending impulse drying to a wider range of furnishes and grades. {IPST Member Dues Funding}.

- Continue steam box comparator experiments to improve our understanding of the variables influencing preheating efficiency. {IPST Member Dues Funding}.

REFERENCES

1.) Bloom, F., Hojjatie, B., Orloff, D.I., "Modeling of Fluid Flow and Heat Transfer in a Crown Compensated Impulse Drying Press Roll: I. The Lubrication Problem," IPST Member Report No. 8, (August 1994).

2.) Bloom, F., Hojjatie, B., Orloff, D.I., "Modeling of Fluid Flow and Heat Transfer in a Crown Compensated Impulse Drying Press Roll: II. The Heat Transfer Problem," IPST Member Report No. 12, (February 1995).

3.) Phelan, P., Kerschner, C., and Orloff, D.I., "An Investigation of the Effect of Thermal Mass and Peak Pressure on Impulse Drying," IPST Member Report No. 9, (October 1994).

4.) Patterson, T., and Orloff, D.I., "Improved Understanding of Web Preheating Technology Part I: Methods, Apparatus, and Preliminary Data" IPST Member Report No. 10, (October1994).

5.) Orloff, D.I., "Commercialization of Impulse Drying," Setting Precedents For Global Leadership, 1994 IPST Executives' Conference Proceedings, (May 1994).

6.) Orloff, D.I., Phelan, P., and Rudman, I., "Progress Report on Furnish Evaluations for Impulse Drying Commercialization Demonstration", IPST Member Report No. 11, (February 1995).

7.) Orloff, D.I., et al., "Method and Apparatus for Drying Web," U.S. Patent: 5,327,661, (Issued July 12, 1994).

8.) Orloff, D.I., et al., "Method and Apparatus for Drying Web," U.S. Patent: 5,353,521, (Issued October 11, 1994).

9.) Orloff, D.I., Phelan, P., and Crouse, J., "Linerboard Drying On A Sheet-fed Pilot Impulse Drying Shoe Press," Tappi Journal, 78(1):129-141(1995).

10.) Bloom, F., Hojjatie, B., and Orloff, D., "The Lubrication Problem In Crown-Compensated Impulse Drying Press Roll", IPST Technical Paper Series Number 549, (January 1995), also submitted for publication to Journal of Pulp and Paper Science.

11.) Bloom, F., Hojjatie, B., and Orloff, D., "Modeling of Fluid Flow and Heat Transfer in a Crown-Compensated Impulse Drying Press Roll: I. The Lubrication Problem," submitted to the SIAM J. Appl. Math.

FUNDAMENTALS OF COATING SYSTEMS

STATUS REPORT

FOR

PROJECT F003 (3674)

Cyrus K. Aidun

March 20 - 21, 1995
Institute of Paper Science and Technology
Atlanta, Georgia 30318

PROJECT TITLE: Fundamentals of Coating Systems
PRINCIPAL INVESTIGATOR: Cyrus K. Aidun
DIVISION: Engineering and Paper materials
BUDGET (FY 94-95): $45,000
PROJECT NO.: 3674

OBJECTIVES: (1) To investigate the cause and origin of coat weight nonuniformities reported in high-speed blade coating of paper and board, (2) to explore novel coating systems for application of a more uniform coat weight profile at higher machine speeds.

SUMMARY OF RESULTS and TASKS COMPLETED:

One of the objectives of this project is the development of new and novel coating systems. This objective has been completed. In this section, we refer to a novel coating system as the *vortex-free* coater [1,2]. The *single layer* and *double layer* coaters imply coater heads that apply a single layer of coating or two layers of wet-on-wet coatings, respectively. A list of the major tasks that have been completed are provided below.

1. Flow visualization studies of air entrainment with short-dwell coater head installed on IPST's current coating flow visualization facilities have been completed (maximum speed = 3300 fpm).

2. The computational studies and optimization of the single layer vortex-free coater including the rheological properties of the coating color have been completed.

3. An initial version of the single layer vortex-free coater head has been constructed and installed on the experimental flow visualization facilities. Preliminary flow visualization studies have been completed.

4. During the Fall 1994 meeting, PAC members stated that the new design is superior to other coating systems. Based on the PAC recommendation, the cost of pilot trials have been estimated and presented below.

BUDGET FOR PILOT TRIALS

YEAR 1:

Fabrication of the initial pilot unit[1], 18" wide (design, drawing & manufacturing)	$75,000
Pilot machine time @ $6,000 per day[1] (40 days)	$240,000
Modifications to the design	$50,000
Principal Investigator & Assistant Engineer	$45,000
Travel (5 trips for 2)	$15,000
IPST overhead (185% of Personnel)	$83,250
TOTAL	$508,250

The purpose of these new designs is to eliminate the flow instabilities and the air entrainment problems associated with pressurized pond coating systems. The preliminary details of these designs have been published in the previous reports. A copy of the patents [1,2] granted for these designs will be provided upon request from IPST.

In the last report, we outlined various physical mechanisms that we have found to result in macroscopic coating defects in blade coating. In summary, there are three dominant mechanisms by which coating film thickness can be adversely affected. These are:

(1) pressure fluctuations upstream of the blade,
(2) flow instability upstream of the blade, and
(3) air entrainment at the wetting line.

The interrelation between these effects are summarized in the report. Also, the results from: (a) recent flow visualization experiments with an experimental short-dwell coater head, experiments with the first prototype vortex-free coater, and further interfacial stability analysis of air/liquid interfaces as applies to air entrainment at the contact line have been reported.

GOALS FOR 1994-95

The goals for the next period are to enhance the flow visualization facility by adding a new pump and instrumentation and to plan for pilot trials. If funding for the pilot trials become available, work will start in that direction.

---

[1] cost estimate provided by a machine manufacturing company

INDUSTRY IMPACT

High quality coated paper products are a significant segment of the total paper market. The goal of this research project is to contribute to the development of a cost- effective coating process for products with superior quality and more flexibility. This will provide the industry with a competitive edge in an ever growing market.

A METHOD FOR RHEOLOGICAL ANALYSIS OF COATING SUSPENSIONS AT HIGH SHEAR

(C. K. Aidun and Y. Lu)

ABSTRACT

The lattice Boltzmann method, an alternative approach to solving a fluid flow system, is used to analyze the dynamics of particles suspended in fluid. The interaction rules between the fluid particles and the suspended particles are developed for real suspensions where the particle boundaries are treated as no-slip impermeable surfaces. This method correctly and accurately determines the dynamics of single particle and multi-particles suspended in the fluid. With this method, computational time scales linearly with the number of suspensions, N, – a significant advantage over other computational techniques which solve the continuum mechanics equations where the computational time scales as N^3.

INTRODUCTION

Understanding the macroscopic transport behavior of particles or fibers suspended in a fluid medium is important to many industries that deal with slurries, colloids, polymers, ceramics, etc. In the paper and photographic film industries, the flow of suspensions occur in important manufacturing processes including paper formation, coating and printing applications. Effective experimental methods, such as magnetic resonance imaging, are being developed for investigation of the macroscopic behavior of suspensions. There is a great need for a theoretical approach to accurately analyze and predict the microstructural dynamics of flow in many manufacturing processes. The flow of suspensions under the blade in coating paper and film is a prime candidate. The small scale structure of the coating layer on the surface of the paper and photographic films is of critical importance for the industry. Controlling and improving the surface quality and physical properties depend on understanding the microstructure of the pigment particle formation, binder migration, and interactions with the porous substrate.

One of the methods that has been successful for analysis of suspensions is the Stokesian

Dynamics [3,4]. This method solves the Stokes equations for the fluid phase and the N-body Langevin equation to obtain the motion of N particles. With this method, however, the computational time scales as N^2, if the mobility matrix is directly constructed, and N^3, if the hydrodynamic interactions are included. Also, the method is limited to suspensions with simple geometries such as spheres or spheroids in simple shear layers. Considering that in practice, the suspensions are irregularly shaped and the flow characteristics are three-dimensional, other more effective methods need to be developed for analysis of various particulate transport processes.

We are developing a more practical method for microdynamical analysis of suspended particles in liquids. This method is based on the solution of the lattice Boltzmann equation [5] for the fluid phase which reduces to the Navier-Stokes equations with appropriate equilibrium distribution function. The equations describing the interaction of the fluid with the suspended particles are derived based on the conservation of mass and momentum. The suspended particles move based on the Newton's equation of motion.

In this study, we examine the accuracy of this method with known solutions of flow over circular suspensions using the finite element solution of the Navier-Stokes equations. We also compare the effective viscosity of dilute suspensions with the Einstein's relation for multi-particle flow system. In all cases, the results agree very well with the known solutions. We have also examined the computational speed as a function of the number of suspensions, N. The computational time increases linearly with N making it possible to obtain macroscopic behavior by considering a large number of suspensions.

The reason for the remarkable computational speed is the local nature of time evolution operation with the lattice Boltzmann method [5]. At each time step, the distribution function is updated in two steps. One is the collision operation which is completely local at each lattice and independent of the surrounding lattices. The other step involves the streaming where mass and momentum is transported to neighboring lattice sites. This step also involves local communication between immediate lattice neighbors. The time evolution of the solution is explicit and, therefore, involve no matrix solution or inversions.

Ladd et al. [6,7] first applied the lattice gas automaton [8,9] to the two-dimensional suspen-

sions. Recently, Ladd [10,11] combined the lattice Boltzmann method for the fluid phase with the Newtonian dynamics of the colloidal suspension system for analysis of short-time motion of colloidal particles. Ladd's method [10,11], however, allows small amount of mass transfer across the surface of the suspensions. In other words, the lattice nodes inside and outside the particles are treated in an identical manner so that the fluid occupies the whole computational domain, inside and outside the suspended particles.

We have developed new boundary conditions for the interaction between the surface of impermeable suspensions and the fluid particles. The new rules treat the suspensions as solid particles and prevent mass exchange across the suspension boundary, while taking account of the momentum exchange between the fluid and the solid particle. The particles have solid boundaries and their motion relative to the fluid phase is governed by the Newton's law of motion. Following an outline of the problem formulation and the new particle/fluid interaction rules, we present the numerical results and we examine the accuracy of this method.

In this analysis, we use the Bhatnagar-Gross-Krook [12] single relaxation time approximation to replace the linear operator of Higuera et al. [13] in the lattice Boltzmann equation, proposed by McNamara and Zanetti [5]. The results are obtained with a two-speed square lattice where on each node there are a total of eight directions. The velocity vectors $\mathbf{e}_{1i}$, $\mathbf{e}_{2i}$ $(i = 1, \cdots, 4)$ are defined as

$$\mathbf{e}_{1i} = (\cos\frac{i-1}{2}\pi, \sin\frac{i-1}{2}\pi), \tag{1}$$

$$\mathbf{e}_{2i} = \sqrt{2}(\cos(\frac{i-1}{2}\pi + \frac{\pi}{4}), \sin(\frac{i-1}{2}\pi + \frac{\pi}{4})), \tag{2}$$

along the perpendicular and diagonal directions, respectively. The lattice Boltzmann equation is given by

$$f_{\sigma i}(\mathbf{x} + \mathbf{e}_{\sigma i}, t+1) - f_{\sigma i}(\mathbf{x}, t) = -\frac{1}{\tau}[f_{\sigma i}(\mathbf{x}, t) - f^{(0)}_{\sigma i}(\mathbf{x}, t)], \tag{3}$$

where $f_{\sigma i}$ $(\sigma = 1, 2; i = 1, \cdots, 4)$ is the single-particle distribution function, $f^{(0)}_{\sigma i}(\mathbf{x}, t)$ is the equilibrium distribution at $(\mathbf{x}, t)$ and τ is the single relaxation time. In our simulations, $f^{(0)}_{\sigma i}(\mathbf{x}, t)$ is taken as

$$f^{(0)}_{\sigma i}(\mathbf{x}, t) = A_\sigma + B_\sigma(\mathbf{e}_{\sigma i} \cdot \mathbf{u}) + C_\sigma(\mathbf{e}_{\sigma i} \cdot \mathbf{u})^2 + D_\sigma u^2 \quad , \tag{4}$$

with

$$A_1 = \frac{\rho}{6}, \quad B_1 = \frac{\rho}{3} \quad C_1 = \frac{\rho}{2}, \quad D_1 = -\frac{\rho}{2}$$
$$A_2 = \frac{\rho}{12}, \quad B_2 = \frac{\rho}{12} \quad C_2 = \frac{\rho}{8}, \quad D_2 = \frac{\rho}{8} \tag{5}$$

where ρ is the mass density at the node. For this model, the sound speed is $c_s = \sqrt{2/3}$, and the kinematic viscosity is $\nu = (2\tau - 1)/6$. With this equilibrium distribution, the Navier-Stokes equations can be derived using the Champan-Enskog expansion.

BOUNDARY RULES AND DYNAMICS

The physical boundary condition for solid-fluid system is the no-slip condition, that is the fluid adjacent to the surface moves with the solid surface and the velocity normal to the surface is zero. There are several methods to implement the no-slip boundary conditions [14]. Here we are using a modified bounce-back method with appropriate momentum exchange between the solid and the fluid.

The solid boundary can be located on the lattice node or at a distance equal to one-half the lattice space away from the lattice point. In the latter case, the fluid particles collide onto the solid boundary and bounce back along the same link, as shown in Figure 1. This bounce back process involves zero mass transfer. It works only if the boundary is stationary. Ladd [10,11] proposed the following rule for moving boundary problems. This rule applies only to the bounce-back links that are opposite to the incident links and is given by

$$f_{\sigma i'}(\mathbf{x}, t+1) = f_{\sigma i}(\mathbf{x}, t_+) + 2B_\sigma(\mathbf{e}_{\sigma i'} \cdot \mathbf{u}_b), \tag{6}$$

where $\mathbf{x}$ is the position of the node adjacent to the wall which is moving with velocity $\mathbf{u}_b$, i' denotes the bounce-back link and i the incident link pointing the opposite direction to i'. The last term in above equation, $2B_\sigma(\mathbf{e}_{\sigma i'} \cdot \mathbf{u}_b)$, is an additional term to the bounce back rule mentioned before. It correctly accounts for the momentum transfer between the fluid and the moving boundary. However, it also introduces extra amount of mass into the boundary node $\mathbf{x}$. The total amount of the extra mass at the node is just the summation of these terms over

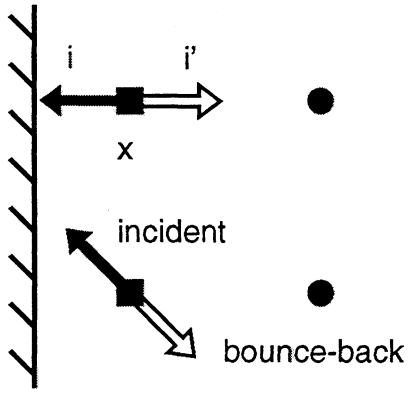

FIGURE 1: LOCATION OF BOUNDARY NODES (SOLID SQUARES) FOR A FLAT SOLID SURFACE. THE INCIDENT LINK IS INDICATED BY SOLID ARROW, WHILE THE BOUNCE-BACK LINK IS SHOWN BY A HOLLOW ARROW.

all the bounce-back links, defined as

$$\delta\rho(\mathbf{x}) = 2\sum_{\sigma}\sum_{i'} B_{\sigma}(\mathbf{e}_{\sigma i'} \cdot \mathbf{u}_b), \tag{7}$$

where i' denotes the bounce-back link. In most cases, $\delta\rho(\mathbf{x})$ is nonzero. Consequently, with Ladd's rule, the mass at the boundary node is not conserved and there has to put fluid inside the suspensions to allow mass transfered across the boundary. Here we propose a new rule which conserves mass at the boundary nodes as well as correctly conserving momentum transfer or the momentum flux across the boundary. Therefore the suspensions are treated as realistic solid particles. The new rule for links that are along the bounce-back directions is

$$f_{\sigma i'}(\mathbf{x}, t+1) = f_{\sigma i}(\mathbf{x}, t_+) + 2B_{\sigma}(\mathbf{e}_{\sigma i'} \cdot \mathbf{u}_b) + \epsilon_{\sigma}\delta\rho(\mathbf{x}), \tag{8}$$

where $\delta\rho(\mathbf{x})$ is the total extra mass at the node, ϵ_{σ} is a constant depending on the lattice form. For the two-speed square lattice considered here, we have $\epsilon_{\sigma} = (-1/2)^{\sigma}$. For the links other than the bounce-back ones, the rule reads

$$f_{\sigma j}(\mathbf{x}, t+1) = f_{\sigma j}(\mathbf{x} - \mathbf{e}_{\sigma j}, t_+) + \epsilon_{\sigma}\delta\rho(\mathbf{x}). \tag{9}$$

The last terms of the above equations are isotropic. By addition of these terms, not only momentum transfer is correctly accounted for, but also mass is conserved along the boundary and no fluid mass is transfered into the suspension, since

$$2\sum_{\sigma}\sum_{i'} B_{\sigma}(\mathbf{e}_{\sigma i'} \cdot \mathbf{u}_b) + \sum_{\sigma}\sum_{i} \epsilon_{\sigma}\delta\rho(\mathbf{x}) = 0. \tag{10}$$

With this rule, solid particals are treated as realistic impermeable solid objects. An alternate way to balance the extra mass $\delta\rho(\mathbf{x})$ at the boundary node is to include the rest particles. The extra mass is thus distributed to the rest particle at the boundary node.

The fluid particles collide with each other at each time step while the interaction between the fluid and the suspensions takes place in the middle of the convection time step. The suspension boundary is impermeable and therefore, no fluid particles can penetrate into it. For the interactions between suspension and fluid, there are two basic steps. The first one is the impact of fluid particles on the wall of the moving suspension. The other step is the

displacement of the fluid particles due to the motion of the suspension. The first step is the "driving" process while the second is the 'damping' process. The hydrodynamic (lubrication) force becomes significant as two suspensions approach each other.

The velocity vector $\mathbf{u}_b$ depends not only on the translational and the angular velocity of the suspension, but also on the position, where the fluid particles collide with the suspension, and the colliding directions, that is

$$\mathbf{u}_b = \mathbf{U} + \mathbf{\Omega} \times (\mathbf{x} + \frac{1}{2}\mathbf{e}_{\sigma i} - \mathbf{X}), \tag{11}$$

where $\mathbf{U}$ is the translational velocity of the suspension, $\mathbf{\Omega}$ the angular velocity with respect to the center of mass, and $\mathbf{X}$ is the position vector of the center. In the second step, as the suspension moves through the cells, mass is displaced, accordingly.

For a given link (σi) at a node, the force on the suspension is given by

$$\mathbf{F}_{\sigma i} = \begin{cases} 2(f_{\sigma i} + B_\sigma \mathbf{u}_b \cdot \mathbf{e}_{\sigma i})\mathbf{e}_{\sigma i} & , \text{ incident links,} \\ \\ 0 & \text{otherwise,} \end{cases} \tag{12}$$

whereas the torque, $\mathbf{T}_{\sigma i}$ with respect to the center of mass, $\mathbf{X}$, is given by

$$\mathbf{T}_{\sigma i} = (\mathbf{x} + \frac{1}{2}\mathbf{e}_{\sigma i} - \mathbf{X}) \times \mathbf{F}_{\sigma i}. \tag{13}$$

Knowing the net force and the torque, the motion of the suspension is governed by the Newtonian equations, given by

$$\mathbf{U}(t + \frac{1}{2}) - \mathbf{U}(t - \frac{1}{2}) = M^{-1} \sum_{BN} \sum_{\sigma} \sum_{i} F_{\sigma i}(\mathbf{x}, t + \frac{1}{2}), \tag{14}$$

for translation where BN stands for the boundary nodes, and

$$\mathbf{\Omega}(t + \frac{1}{2}) - \mathbf{\Omega}(t - \frac{1}{2}) = I^{-1} \sum_{BN} \sum_{\sigma} \sum_{i} T_{\sigma i}(\mathbf{x}, t + \frac{1}{2}), \tag{15}$$

for rotation. Here M is the mass of the suspension and I is the moment of inertia. Equations (11) to (15) completely prescribe the motion of the suspended particles in the fluid. In the following section we use several examples to show the accuracy and robustness of this method.

RESULTS AND DISCUSSION

The new collision rules between the fluid particles and the suspended particles satisfy the conservation of mass and momentum with the no-slip condition. Furthermore, the suspended particles are treated as real solid particles with impermeable boundaries. To demonstrate the validity of this method, we present the application of this method to several problems.

To examine the correctness of the collision rules, we apply this method to two different forms of the same hydrodynamic problem. Consider the flow over a cylinder placed at the middle of a straight channel, as shown in Figure 2. If the cylinder is fixed and the channel walls move in the x-direction with constant velocity, u_w, then the problem has no moving boundaries (i.e., the domain is fixed) and conventional methods can be applied. An alternative form of this problem is to fix the coordinate system with the channel walls and to allow the cylinder to move freely inside the channel as a suspended particle would (Figure 2b). If the body force exerted on the freely moving cylinder is equal to the force that the fixed cylinder experiences when the channel walls move with velocity u_w, then the terminal velocity of the moving cylinder, u_c, should be equal to $-u_w$. To examine the collision rules for a moving particle, we apply the lattice Boltzmann method and solve the fixed cylinder problem first to compute the hydrodynamic force per unit area of the cylinder. We then apply the same force on the freely moving cylinder and compute the cylinder's terminal velocity using the lattice Boltzmann method with the new boundary collision rules presented above. We also solve the fixed cylinder problem directly from the Navier-Stokes equations using finite element discretization with Galerkin projection [15] to examine the accuracy of the Lattice Boltzmann method, in general.

The drag on the surface is computed for cylinders with radius 5.4, 10.4, and 30.4 lattice dimensions. The width of the channel is 128 in all cases. The periodic boundary conditions are imposed on both ends of the channel as shown by the dashed lines in Figure 2. For each case, the time relaxation parameter, τ, is adjusted to keep the Reynolds number, defined as

$$R_e \equiv \frac{2u_w r}{\nu} \tag{16}$$

equal to 1. The hydrodynamic force on the cylinder and the shear stress on the wall are listed in Table 1 along with results from finite element solutions of the Navier-Stokes equations. For each

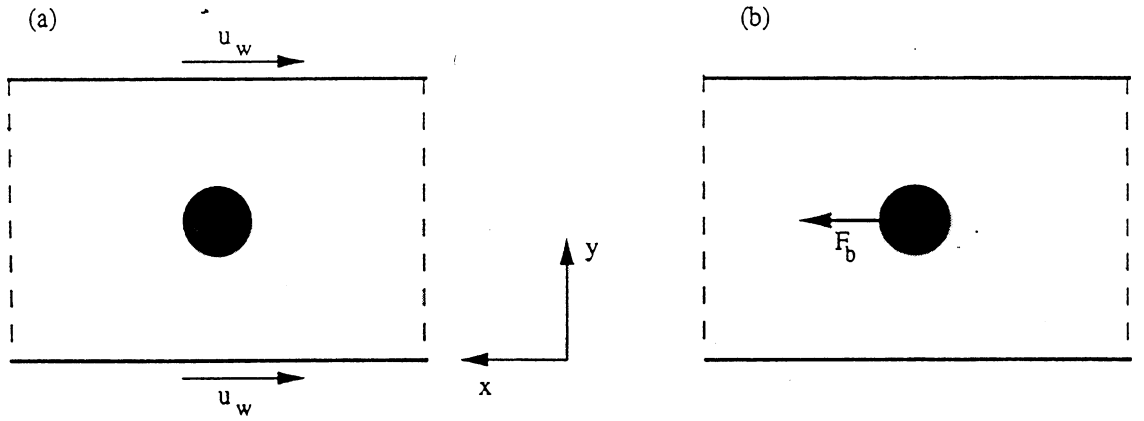

FIGURE 2: FLOW OVER A CIRCULAR CYLINDER IN A STRAIGHT CHANNEL, (a) FIXED CYLINDER WHERE THE CHANNEL WALLS MOVE WITH VELOCITY u_w, AND (b) THE CYLINDER IS FREE TO MOVE UNDER THE BODY FORCE $F_b = -f_c A$, WHERE A IS THE SURFACE AREA OF THE CYLINDER.

Table 1: COMPARISON OF THE FINITE ELEMENT SOLUTION OF NAVIER-STOKES EQUATION FOR THE FIXED CYLINDER CASE WITH THE LATTICE BOLTZMANN SOLUTION OF THE FIXED AND MOVING CYLINDERS. THE REYNOLDS NUMBER, $Re = 1$ FOR ALL CASES. THE FORCE f_w ON THE WALL OR f_c ON THE CYLINDER IS MEASURED PER UNIT AREA OF THE SURFACE. SUBSCRIPT a STANDS FOR RESULT OF THE FINITE ELEMENT SOLUTION, b RESULT FOR THE MOVING CYLINDER WHERE THE INPUT IS THE BODY FORCE IN THE x DIRECTION, AND THE OUTPUT IS THE TERMINAL VELOCITY.

case		τ	ρ_c/ρ_f	u_w	u_c	f_w	f_c
I	Fixed	N/A[a]	∞	-0.04	0.0	0.137	0.966
	cylinder	1.796	∞	-0.04	0.0	0.132	1.022
r=5.4	Moving	1.796	2.0	0.0	0.040[b]	0.133	1.022
II	Fixed	N/A[a]	∞	-0.02	0.0	0.316	1.158
		1.748	∞	-0.02	0.0	0.313	1.229
r=10.4	Moving	1.748	2.0	0.0	0.020[b]	0.307	1.229
III	Fixed	N/A[a]	∞	-0.01	0.0	1.543	2.067
		2.324	∞	-0.01	0.0	1.532	2.054
r=30.4	Moving	2.324	2.0	0.0	0.010[b]	1.523	2.054

case, the first and second rows correspond to the solution of the Navier-Stokes equation and the lattice Boltzmann equation, respectively. f_w and f_c represent the nondimensional force per unit area of the channel wall and the cylinder surface, respectively. The pressure scale, $\rho_f u_w^2$ is used to nondimensionalize the stress at the wall and the cylinder. The agreement between the Navier-Stokes solution and the lattice Boltzmann solution is within the numerical deviation of $\pm 5\%$. The error is mainly due to numerical descretization. As grid size decreases, the relative error decreases, as well. To examine the new collision rules for the moving particles, we impose a body force on the moving cylinder equal to the force computed for the fixed cylinder case and solve for the terminal velocity of the moving cylinder. The results for each case are listed in Table 1. Again, in all cases the results agree very well. This example confirms the correctness and the reliability of our boundary collision rules.

As a second verification problem, we use our method to simulate the sedimentation of a circular particle in a 2D channel. A circular particle of diameter d is released along the central line, with zero volocity, in a channel of width $4d$. The x-axis is vertically down on the left wall, and the y-axis horizontal to the right. The density of the solid particle is two times larger than the fluid density. The inlet of the domain is always $10d$ upstream of the moving particle, where zero velocity is applied uniformly, while the outlet is $15d$ downstream of the particle, where traction free boundary condition are applied. Feng, Hu and Joseph [16] recently simulated the same process by solving the Navier-Stokes equation for fluid phase and implementing Newtonian dynamics for the solid particle. Our simulation results of drag coefficients are compared, in Figure 3 with theirs, as well as the exact solution [17] of Stokes approximation. The agreement is very good.

HIGH SHEAR VISCOSITY OF SUSPENDED SPHERICAL PARTICLES

The extension of the lattice Boltzmann method and the boundary rules to three-dimensional cases is straightforward. With extension of our method to the three-dimensional cases, we have simulated the dynamics of a monolayer of spheres suspended in a Couette flow, similar to a blade coating system. The fluid is between two parallel surfaces, where one surface moves in the x direction with a constant velocity, relative to the lower surface. The y-axis is vertically

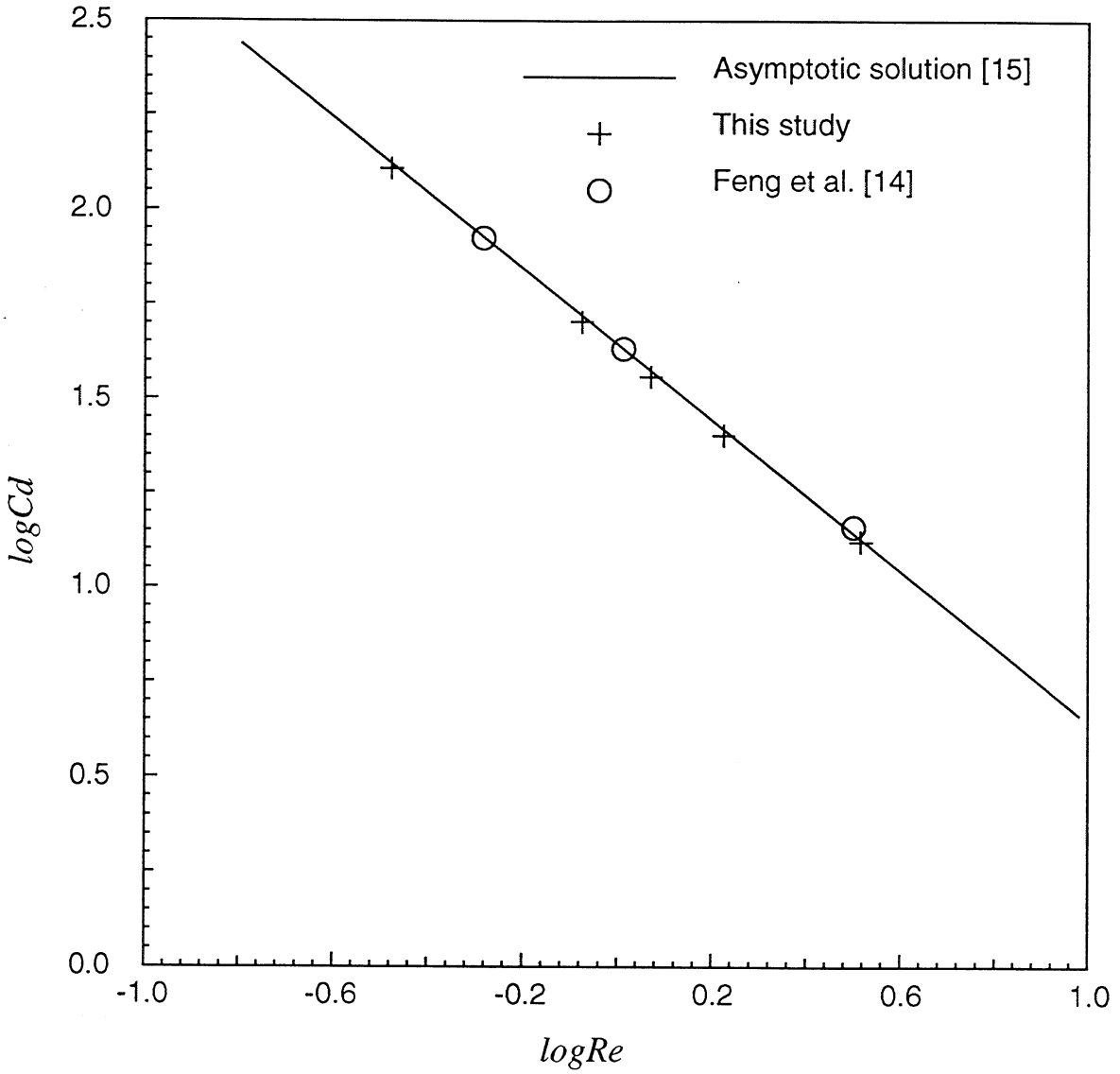

FIGURE 3: DRAG COEFFICIENTS OF A CIRCULAR PARTICLE SETTLING IN A 2D CHANNEL AS COMPARED TO THE NUMERICAL RESULT OF FENG ET AL. [14] AND THE EXACT RESULT OF THE ASYMPTOTIC SOLUTION [15].

up. Periodic boundary condition is used in both x and z directions. In our calculations, the fluid phase viscosity is set to 0.039 Pa.sec. In dimensional form, the parameters in the calculations correspond to a typical blade coating system, *i.e.*,

surface speed	20 m/sec.
distance between two parallel surfaces	20 μm
fluid density	1000 kg/m^3
solid density	2000 kg/m^3
shear rate	10^6 1/sec.

Figure 4 compares our simulation results on the effective viscosity with numerical simulations by Brady [18], and three correlations from the experimental data, by Chong et al. [19] and Krieger [20]. The exact asymptotic results for low concentrations by Einstein [21] and by Batchelor and Green [22] are also shown in Figure 4 for comparison. The lattice Boltzmann simulations agree very well with the experiments. Therefore the new boundary rules outlined in the paper can very effectively be used for simulation of solid particles suspended in fluid. Furthermore, this method is more practical for analysis of suspensions because of the linear relation between the cpu time, t_{cpu}, and the number of suspensions, N. This relation is given by $t_{cpu} = 600 + 3.4N$ (sec) for a 128×128 system with 10,000 time steps on IBM RS/6000. Comparing with the Stokesian Dynamics where the cpu time increases with N^3, the lattice Boltzmann method has a significant advantage. The other advantage is that it is very easy to implement the lattice Boltzmann simulation to multidispersed, irregular shaped suspension flows.

In conclusion, we have developed a new boundary rule for lattice Boltzmann simulations of solid particles suspended in fluid. Lattice Boltzmann simulations with the new boundary conditions have been carried out for 2D and 3D flow of suspensions in parallel channels. Results of the simulations with the new method are in good agreement with direct solutions of the Navier-Stokes equations and the exact asymptotic results.

ACKNOWLEDGEMENTS

This study has been supported by the National Science Foundation's Presidential Young Investigator Award (CKA) through grant CTS-9258667, and by industrial matching contributions. The calculations were conducted, in part, using the National Center for Supercomputing Applications, a resource at the University of Illinois at Urbana-Champaign which is funded by the National Science Foundation.

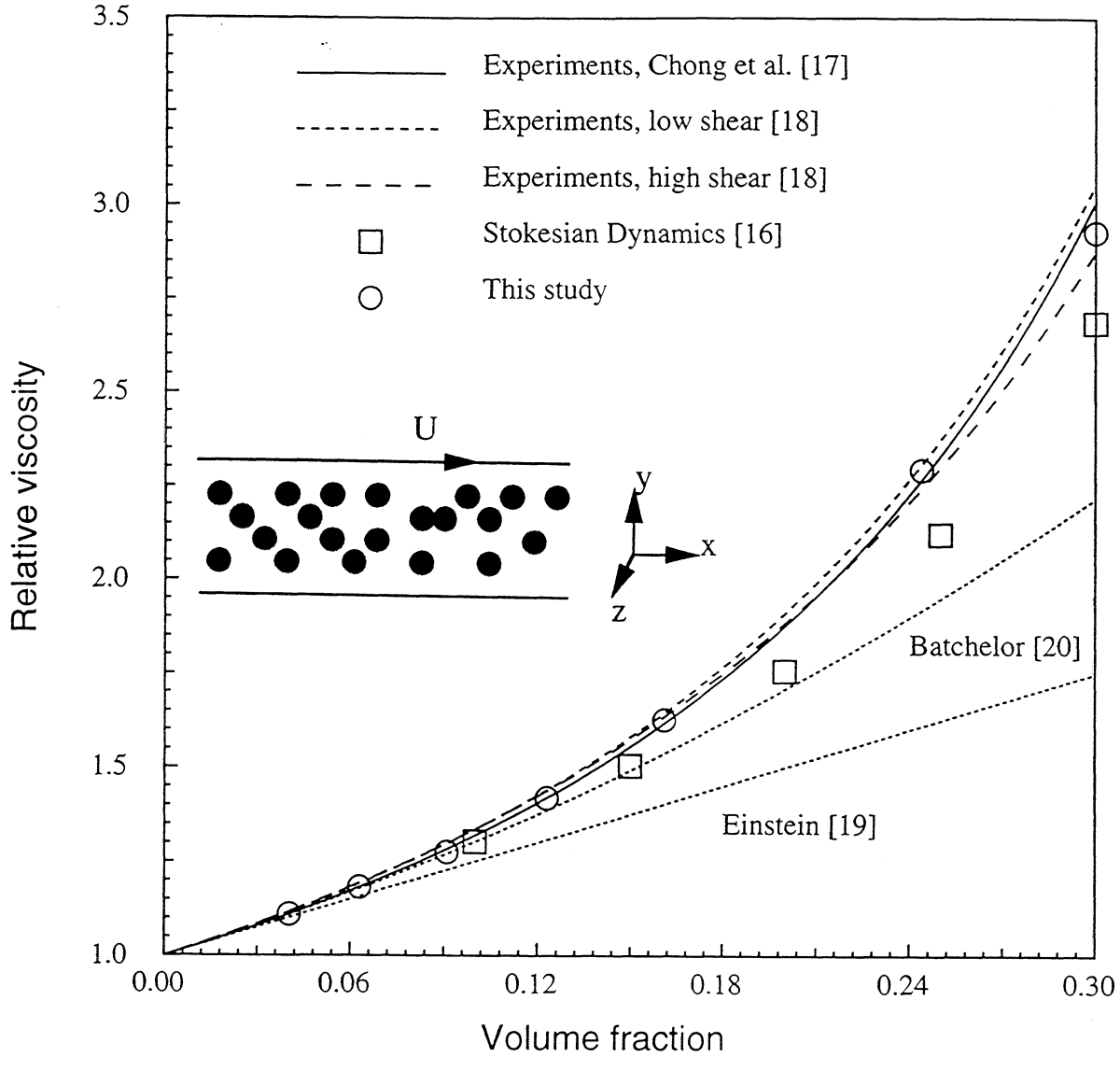

FIGURE 4: RELATIVE VISCOSITY OF MONODISPERSED SPHERICAL SUSPENSIONS IN A COUETTE FLOW AS A FUNCTION OF VOLUME RATIO. THE SIMULATIONS ARE CARRIED OUT FOR SYSTEMS WITH $128 \times 128 \times 16$ AND $256 \times 256 \times 32$ LATTICE NODES. THE NUMBER OF SUSPENDED PARTICLES RANGE FROM 16 TO 64.

REFERENCES

1. Aidun, C.K., Institute of Paper Science and Technology, "Coating Device for Travelling Webs", U.S. Patent No. 5,366,551; Issued on Nov. 22,1994.

2. Aidun, C.K., Institute of Paper Science and Technology, "Flotation Coating Device for Travelling Webs", U.S. Patent No. 5,354,376; Issued on Oct. 11,1994.

3. Brady, J.F., and Bossis, G., *Ann. Rev. Fluid Mech.*, "Stokesian Dynamics," **20**: 111 (1988).

4. Ziler, Z., and Bousfield, D.W., *TAPPI Coating Confrence Proceedings*, "The Motion of Disk-shaped Pigments in Transient Shear Flows," 373 (1992).

5. McNamara, G., and Zanetti, G., *Phys. Rev. Lett.*, "Use of the Boltzmann Equation to Simulate Lattice-Gas Automaton," **61**: 2332 (1988).

6. Ladd, A.J.C., Colvin, M.E., and Frenkel, D., *Phys. Rev. Lett.*, "Application of Lattice-Gas Cellular Automata to the Brownian Motion of Solids in Suspension," **60**: 975 (1988).

7. Ladd, A.J.C., and Frenkel, D., *Phys. Fluids A*, "Dissipative hydrodynamic interactions via lattice-gas cellular automata," **2**: 1921 (1990).

8. Frisch, U., Hasslacher, B., and Poemeau, Y., *Phys. Rev. Lett.*, "Lattice-Gas Automaton for the Navier-Stokes Equation," **56**: 1505 (1986).

9. Wolfram, S., *J. Stat. Phys.*, "Cellular Automaton Fluids 1: Basic Theory," **45**: 471 (1986).

10. Ladd, A.J.C., *J. Fluid Mech.*, "Numerical simulations of particulate suspensions via a discretized Boltzmann equation, Part I," **271**: 285 (1994).

11. Ladd, A.J.C., *J. Fluid Mech.*, "Numerical simulations of particulate suspensions via a discretized Boltzmann equation, Part II," **271**: 311 (1994).

12. Bhatnagar, P., Gross, E.P., and Krook, M.K., *Phys. Rev.*, "A Model for Collision Processes in Gas: I. Small amplitude Processes in Charged and Neutral One-Component Systems," **94**: 511 (1954).

13. Higuera, F., Succi, S., and Benzi, R., *Europhys. Lett.*, "Lattice Gas Dynamics with Enhanced Collisions," **9**: 345 (1989).

14. Ziegler, D.P., *J. Stat. Phys*, "Boundary Conditions for Lattice Boltzmann Simulations,"

71: 1171 (1993).

15. Engelman, M.S., *Fluid Dynamics International, Inc.*, "Fidap: fluid dynamics analysis package," Vol. 6.0.

16. Feng, J., Hu, H.H., and Joseph, D.D., *J. Fluid Mech.*, "Direct simulation of initial value problems for the motion of solid bodies in a Newtonian fluid," **261**: 95 (1994).

17. Faxen, H., *Proc. Roy. Swedish Inst. Eng. Res.*, No. 187 (1946).

18. Phillips, R.J., and Brady, J.F., *Phys. Fluids*, "Hydrodynamic transport properties of hard-sphere dispersions," **31**: 3462 (1988).

19. Chong, J.S., Christiansen, E.B., and Haer, A.D., *J. Appl. Polymer Sci.*, "Rheology of Concentrated Suspensions," **15**: 2007 (1971).

20. Krieger, I.M., *Advan. Colloid Interface Sci.*, "Rheology of Monodisperse Lattices", **3**: 111 (1972).

21. Eistein, A., *Annln. Phys.*, "Eine neue Bestimmung der Moleküldimensionen," *19*: 289 (1909).

22. Batchelor, G.K., and Green, J.T., *J. Fluid Mech.*, "The dtermination of the bulk stress in a suspension of spherical particles to order c^2," **56**: 401 (1972).

HEADBOX AND FORMING HYDRODYNAMICS

STATUS REPORT

FOR

PROJECT E00101

Cyrus K. Aidun

March 20 - 21, 1995

Institute of Paper Science and Technology
500 10th Street, N.W.
Atlanta, Georgia 30318

DATE: Fall 1994
PROJECT TITLE: Headbox and Forming Hydrodynamics
PROJECT LEADER: Cyrus K. Aidun
PROJECT NUMBER: E00101 (NEW)

GOALS AND OBJECTIVES

The goals of this project are to (1) investigate and optimize the paper and board formation process and to (2) develop novel methods for analysis and control of paper formation.

Short-term objectives are:

- to investigate the effect of various parameters on cross-stream and secondary flow in the headbox and effects on fiber orientation and mass formation,

- to investigate the effects of the forming section (on the table) hydrodynamics on fiber orientation, basis-weight, CD profile, MD/CD ratio, and STFI compressive strength,

- to explore mechanisms for increasing the CD and STFI strength properties in the forming section.

VALUE TO INDUSTRY

The immediate value to the industry is in terms of a better understanding of the hydrodynamic effects on fiber orientation in the forming section. This information can be utilized to control the polar angle and consequently improve properties such as twist-warp and crush strength.

In general, the computational results along with the flow visualization studies will provide the key information for improving formation in terms of paper and board properties. The proposed research aims at pinpointing the origin of these problems, providing a better understanding of their effects on pertinent properties, and seeking techniques for improving the forming process in general. Minimizing stock disturbances at higher machine speeds results in higher productivity and better product quality.

Several results are expected from this project. In the short term, we will show the effect of a flow pattern specific to a headbox system on fiber orientation and local mass formation. This information can be used to identify what feature(s) of the flow in the forming section is (are) contributing to the undesirable fiber distribution and fiber orientation. This information will be used for adjusting the flow parameters in a way to improve product qualities such as formation uniformity, twist-warp, and crush strength.

SUMMARY OF RESULTS

A method has been developed to examine the source of secondary flows in the headbox. Although computational analysis show the location and the magnitude of the secondary flows, the physical origin of these flows often remain hidden. We outline a method that can be used to determine the specific feature of the headbox that is responsible for the secondary flows. In the following section, we explain this method.

A METHOD TO DETERMINE THE PHYSICAL ORIGIN OF SECONDARY FLOWS

Uniformity of the physical properties in the cross-machine direction (CD) is one of the most important properties in manufacturing paper and board. Nonuniformities in average fiber orientation and mass distribution, two of the most common quality problems, could be the result of: (1) imperfect setup of the forming section or (2) hydrodynamic effects. Examples of an imperfect setup are unbalance pressure in the manifold or distributor, plugging of the tubes in the tube bank, flow injection or ejection into and out of the headbox from the side walls, misalignment of the headbox with the wire, nonuniform slice profile, and nonuniform wire permeability (drainage properties). All of the effects from an imperfect setup will to some degree result in nonuniform properties in CD. The effects of these imperfections on the forming properties are relatively simple to understand and resolve. However, even if the setup of the forming section is perfect, there are purely hydrodynamic issues which may result in significant nonuniformities in paper and board formation properties.

The hydrodynamic effects could be in the form of flow instability, where a base flow becomes unstable and is replaced by another flow pattern with qualitatively different flow characteristics, or, secondary flows where a weak flow pattern is superimposed on the

primary flow. Although hydrodynamic instability is very important in paper making processes, in this project we focus on the secondary flows and their effects on nonuniform CD properties.

Secondary flows generate CD flow components which result in misalignment of the forming jet with the wire near the side walls. Consequently, the fibers forming near the side walls experience shear in CD on the forming table and form with an average orientation different from the fiber orientation near the mid-section of the forming table. .

In this section, we outline the method for capturing the secondary flows that are the source of nonuniform fiber orientation in the forming section. The secondary flows are weak relative to the main stream flow (i.e., flow component in MD) and, therefore, difficult to compute and visualize. Experimental measurements of these weak currents on the commercial machines are next to impossible. We have formulated a method to computationally decompose the flow into its primary and secondary components. From observing the secondary component of the flow, the physical mechanism of the cross-flow in the headbox can be better understood.

The method is to compute the flow field inside the headbox by excluding the effect of the side wall on the flow. This is accomplished by relaxing the no-slip condition of the side wall to the free-slip condition. The no-slip condition states that the fluid velocity adjacent to the side wall is the same as the velocity of the wall. In our case, the wall is stationary and, therefore, the fluid velocity adjacent to the wall is zero. Because of this condition, the side wall imposes a shear stress on the fluid which results in boundary layer development and growth. The free-slip condition states that although there cannot be any fluid penetration into the boundary, the surface does not impose a shear stress on the fluid. Let's refer to this case as the *ideal* flow field since without the wall effect, the flow field will be two-dimensional (excluding the turbulent fluctuations). The secondary flow is defined as the difference between the real case, with no-slip boundary conditions at the side wall, and the ideal case. In other words,

$$\mathbf{U}_s(x,y,z) = \mathbf{U}(x,y,z) - \mathbf{U}_i(x,z), \tag{1}$$

where $\mathbf{U}$ represents the actual flow field with three velocity components (u,v,w). The flow fields represented by $\mathbf{U}_s$ and $\mathbf{U}_i$ are the secondary and the ideal ($\mathbf{U}_i$ = (u,w)) flow fields, respectively. The contour plot of the cross-flow, v, for the real flow field, $\mathbf{U}$, is

presented in Fig. 1. As before, the left wall is a symmetry plane and the other side is bounded by the no-slip side wall. We compute the ideal state using the same geometry and subtract it from the primary flow to get the secondary flow field. The secondary flow, $\mathbf{U}_s$, is visualized in Fig. 2 where the fluid particle trajectories are plotted inside the headbox. The top and side views are also presented in the same figure for better visualization.

The secondary flow forms a vortex inside the headbox with its source of energy concentrated near the side wall. To visualize this, we have computed the energy of the secondary flow inside the headbox by projecting the velocity field onto itself, that is

$$E(x,y,z) = \frac{\mathbf{U}_s \bullet \mathbf{U}_s}{U_{av}^2(x)} \qquad (2)$$

where $U_{av}^2(x)$ is the square of the average mass flux at location x inside the headbox. The contour plot of the energy, E, presented in Fig. 3, clearly shows the location of the source of secondary flow and, consequently, the cross-flow inside the headbox. In previous meetings we attributed the cross-flow to the boundary layer development and the shear exerted on the fluid from the side wall and the slice without providing any proofs. This analysis serves as a proof of our previous explanation of the physical mechanism generating the cross-flow inside the headbox.

In general, this method of analyzing the associated energy with the secondary flow is most effective in practical situations to pinpoint the source of flow nonuniformities. Very often, computation of the flow field alone will not readily reveal the source of the problem. The method established can be used to pinpoint the origin of the flow nonuniformities inside a headbox.

FUTURE TASKS

The physical characteristics of the sheet are formed on the wire due to jet/wire interactions, shear, and drainage characteristics of the forming section. We are working on a closed form solution of a forming model that can explain the shear profile on the wire. From the results, we establish the degree of fiber orientation as the sheet forms on the table. The MD/CD strength ratio can be improved by manipulation of the fiber

orientation on the forming table. Mechanisms to enhance the CD properties, as well as, STFI and ring crush values will be explored.

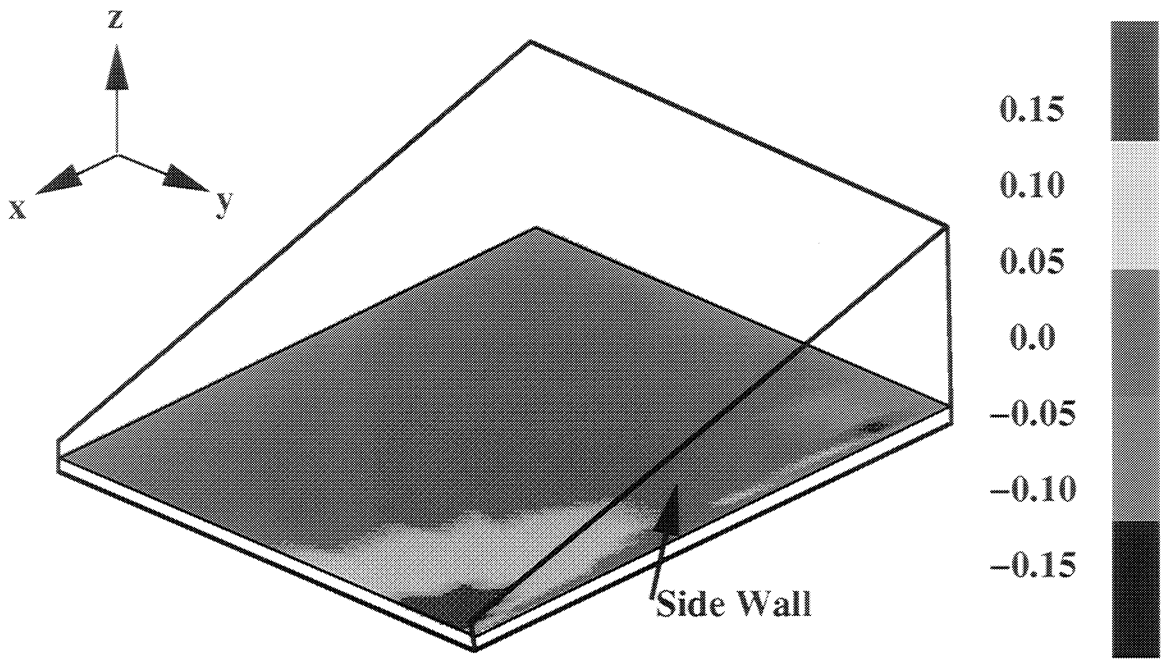

Figure 1. The contour plot of the cross−flow, v, for the real flow field.

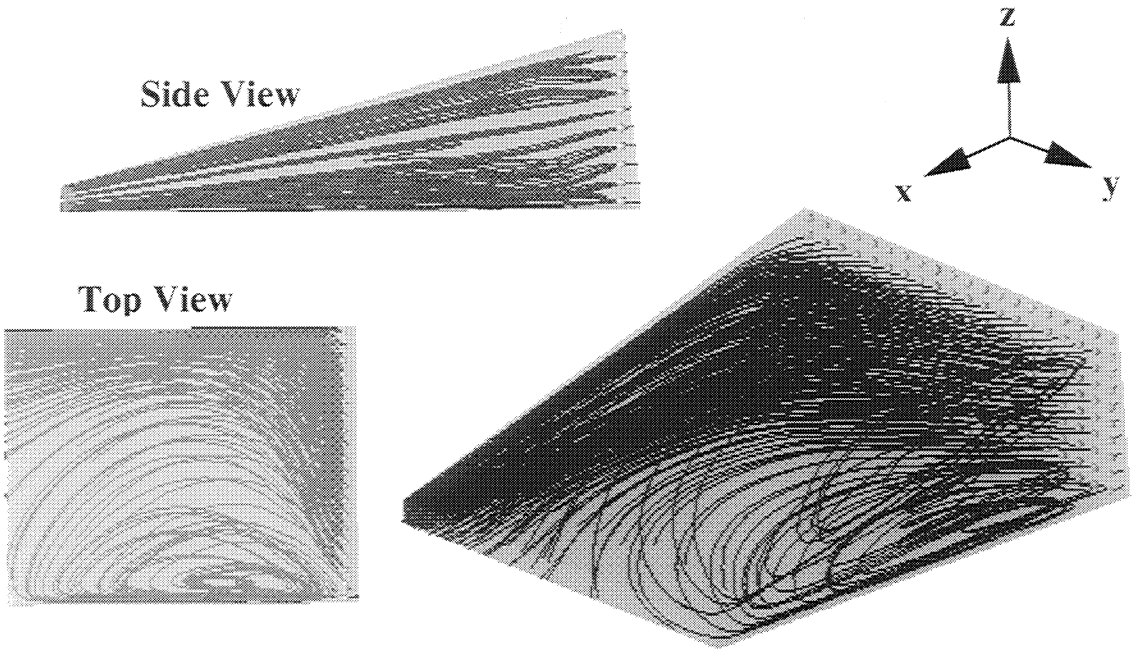

Figure 2. The fluid particle trajectories of the secondary flow.

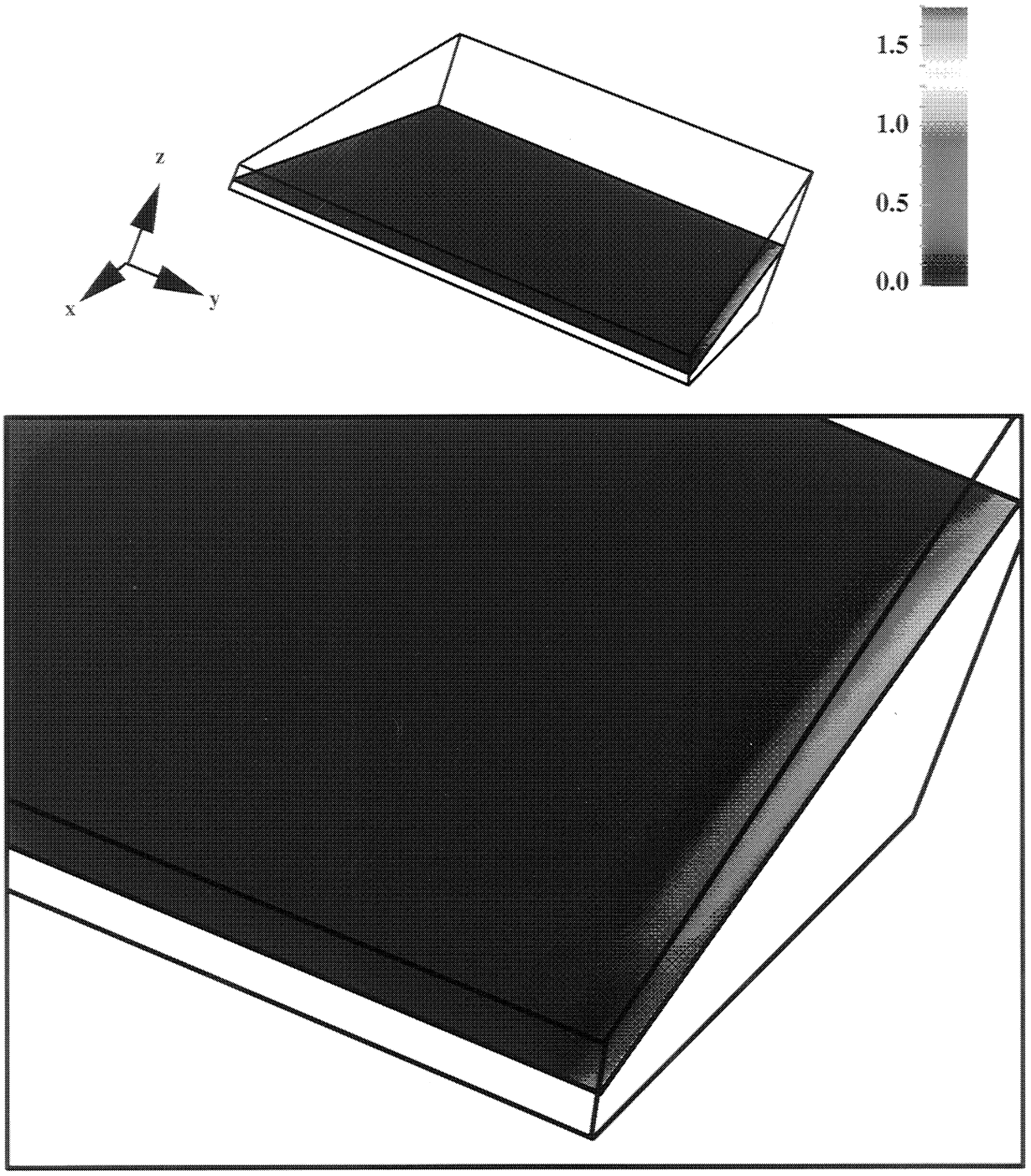

Figure 3. Contour plot of the energy of the seconday flow showing the source of the mechanism generating cross-flow in the headbox.

AIR/SHEET INTERACTIONS

STATUS REPORT

FOR

PROJECT F006 (3730)

Cyrus K. Aidun
G. Paul Neitzel

March 20 - 21, 1995

Institute of Paper Science and Technology
500 10th Street, N.W.
Atlanta, Georgia 30318

Technical Program Review Report

DATE: Spring 1995
PROJECT TITLE: Air/Sheet Interactions
PRINCIPAL INVESTIGATORS: Cyrus K. Aidun and G. Paul Neitzel
BUDGET (FY 93-94): $145,000
PROJECT NO.: 3730

PROGRAM OBJECTIVES and GOALS:

The objectives of this project are to: a) gain a better understanding of the fluid dynamics and the structural mechanics of sheet flutter; b) correlating the onset of break or sheet damage ("pain threshold") with the sheet flutter characteristics (e.g., frequency, speed, ...) and the sheet's structural properties; and c) extend the results to analysis of blade deformation and vibration in coating processes.

The interactions between fluid flow and flexible solid boundaries will be examined with applications to processes in paper manufacturing. The primary application is in sheet vibration induced by interactions between the sheet and the adjacent air stream which results in operational difficulties and web breaks.

SUMMARY OF PROGRESS FOR THE PAST PERIOD:

The initial tasks involving development of the techniques required for computational and experimental studies of the air/sheet interactions have been completed.

We are developing a computational program to evaluate the three-dimensional deformation of the substrate under load and transform of coordinates from global to the local surface deformation system. The initial computational experiments demonstrated the potential of this approach in terms of air/sheet interactions, as well as, optimization of moisture removal from the dryer section.

In previous reports, we have outlined the results from a series of wind tunnel experiments to evaluate the system for an in-depth study of sheet fluttering and mechanisms of reducing the vibration and consequent sheet breaks. Problems with these experiments were identified and resolved. The samples used in the wind-tunnel experiments were Bond #4 printing paper, Letter

Print (IPST Letterhead) paper, unbleached paperboard (Corrugating Medium), and light-weighted "trace" paper. Once the computational methods are fully developed, the experimental data can be used to evaluate the solution.

We have started the design and fabrication of the test section for the new wind tunnel. We anticipate installation by March of 1995 and start of the experiments during the same month.

In parallel to the computational and experimental studied outlined above, we are developing the principles for incluidng the physical properties of paper into the computations. The physical properties of the paper can be obtained from the physical properties of the fiber, the fiber orientation, the pore structure, and density. The preliminary analyses are presented below followed by an application to an ideal flow situation for edge flutter. The extension of this method to full computational analysis including the solution of the complete fluid flow equations is presented at the end of this report. The two-dimensional program for the solution of the full equations governing the fluid flow with rigid and deformable boundaries has been completed. Several sample problems have been solved to confirm the correctness and accuracy of the formulation and the solution methodology.

GOALS FOR FY 1995-96

To further develop the computational methods by including the physical properties of the web into the the sheet fluttering analysis and to perform the wind tunnel experiments.

Free Edge Flutter Based on 3-D Structural Characteristics of Paper

(Cyrus Aidun and Dewei Qi)

In order to study the effects of micro-structure of sheets on the onset of fluttering, we have added a 3-D angular distribution function into Cox's structural model of sheets. This model is used to predict the critical speed of air flows for the onset of fluttering in terms of single fiber properties, z-directional orientation of the fibers and voids in the sheet. As an initial analysis, we assume air flow irrotational and make use of potential theory. Based on this analysis, the critical speed of air for sheet fluttering decreases as z-directional orientation of fibers increases and that critical speed decreases as porosity increases and the fiber length decreases.

1 Introduction

In a high-speed paper machine, air flows strongly interact with paper and cause the paper to vibrate in an out-of-plane direction. The vibration or flutter normally causes quality and runnability problems. If these problems are severe enough, then the possibility of crease and breaking greatly increases.

Fundamental knowledge and understanding of the interaction between sheets of paper and air will lead to a better design for the dry section of the paper machine and reduce product costs. Mujumdar and Douglas [1] have investigated the dynamic instability of sheets by using a threadline model. Later, Pramila [2] modified the model by adding additional mass due to the boundary layer of surrounding air. Chang and Moretti [3] incorporated the potential flow theory into the model to estimate the added mass. Wind tunnel experiments have been conducted by Chang and Moretti [4] to seek the critical speed of air flows under different conditions. When the tension of the sheets is much larger than stiffness, the effect of the structure of sheets

on flutter is neglected. However, when sheets are thick enough and tension is small, the effects of the structure of sheets at flutter become significant, particularly at the free edges.

In order to study the effects of sheet structure at the onset of sheet fluttering, a 3-D angular distribution function has been introduced into Cox's model [5]. Then, critical speeds of air flows for onset fluttering have been predicted in terms of single fiber properties, z-directional orientation of the fibers, and voids.

2 Free edge flutter of the paper

The motion of a web or sheet in air can be described by the following equation,

$$m\frac{\partial^2 w}{\partial t^2} + 2mV\frac{\partial^2 w}{\partial x \partial t} + (mV^2 - T)\frac{\partial^2 w}{\partial x^2} + D[\frac{\partial^4 w}{\partial x^4} + 2\frac{\partial^4 w}{\partial y^2 \partial x^2} + \frac{\partial^4 w}{\partial y^4}] = p^- - p^+ \tag{1}$$

where m is the mass per unit area of web, w displacement in z (thickness) direction, t time, V velocity of moving web, T tension of web, D bending

stiffness of web, $p^- - p^+$ is aerodynamic pressure difference between the bottom surface of the sheet and the top surface. In sheet flutter experiments inside a wind tunnel, where the velocity of the sheet is equal to zero, this equation reduces to

$$m\frac{\partial^2 w}{\partial t^2} - T\frac{\partial^2 w}{\partial x^2} + D[\frac{\partial^4 w}{\partial x^4} + 2\frac{\partial^4 w}{\partial x^2 \partial y^2} + \frac{\partial^4 w}{\partial y^4}] = p^- - p^+ \qquad (2)$$

The stiffness D is given by

$$D = Eh^3/12(1-\nu) \qquad (3)$$

where E is Young's modulus of sheet, h thickness of sheet, ν poisson's ratio. If tension T is much larger than D, the term with the fourth-order derivatives can be neglected. However, when the sheet is stretched by using a uniform force at the ends, the distribution of the tension is not uniform. The tension close to the free edges becomes very small. This can be simply confirmed by a finite element analysis. The free edge effects may cause large-amplitude flutter on the sheet at a very low critical speed. This dynamic instability has been investigated by Chang and Moretti [4]. The effects of the microstructure

of the paper on the flutter have not been studied by them. In our work, we analyze the effects of the microstructure of the sheet, such as voids, z-directional orientation of fibers, and single fiber properties on the dynamic stability of the sheet. A model of the microstructure of the fiber network is first introduced in order to incorporate structure of the sheet into the above equation through E, and ν.

3 Microstructure of paper

3.1 3-D angular distribution function

Paper is made of a three-dimensional random fiber network. Macromechanical properties of the paper, such as elastic constants, $C_{\alpha\beta\nu\mu}$, essentially depend on properties of a single fiber and its distribution in space. Angular distribution function can be defined as the possibility of finding a fiber per unit solid angle at polar angle (θ, ϕ). Thus,

$$f(\theta,\phi) = \frac{1}{n}\sum_i \delta(cos\theta - cos\theta_i)\delta(\phi - \phi_i), \tag{4}$$

where n is the total number of fibers; subscript i indicates the ith fiber in the system. The angular distribution function may be expanded in the series of spherical harmonic functions in real number space,

$$f(\theta,\phi) = \sum_{l=0}^{l=\infty} \sum_{m=0}^{m=l} [Q^c_{lm} Y^c_{lm}(\theta,\phi) + Q^s_{lm} Y^s_{lm}(\theta,\phi)], \tag{5}$$

where Y^c_{lm} is defined as

$$Y^c_{lm} = P_{lm}(cos\theta) C_m(\phi) \tag{6}$$

and

$$Y^s_{lm} = P_{lm}(cos\theta) S_m(\phi) \tag{7}$$

with

$$C_m(\phi) = \frac{1}{\sqrt{\pi}} cosm\phi, \quad m \neq 0$$

$$C_0 = \frac{1}{\sqrt{2\pi}},$$

$$C_s(\phi) = \frac{1}{\sqrt{\pi}} sinm\phi.$$

Q^c_{lm} and Q^s_{lm} are expansion coefficients. $P_{lm}(cos\theta)$ is a normalized Associated Legendre function; l and m are integers. Substituting equation (4) into (5),

multiplying it by Y_{lm}^c or Y_{lm}^s, integrating both sides of this equation, and making use of the orthogonality properties of the basis functions, we get

$$Q_{lm}^c = \frac{1}{n}\sum_i P_{lm}(cos\theta_i)C_m(\phi_i), \tag{8}$$

and

$$Q_{lm}^s = \frac{1}{n}\sum_i P_{lm}(cos\theta_i)S_m(\phi_i).$$

Because of the orthogonality of harmonic functions, the terms with l larger than 4 do not contribute any physical property to the paper. Therefore, we can truncate the series at $l = 4$. Furthermore, if a symmetrical invariance of inversion for the fiber network is imposed, we can delete all odd l terms because the parity of the spherical harmonic functions is l. Assuming that the fiber-orientational distribution is symmetric with respect to the mid-plane, machine direction, and crossmachine direction of the sheet, we can drop all terms which contain $sinm\phi$. Therefore, the 3-D angle distribution function for machine-made paper is proposed as

$$f(\theta,\phi) = \frac{1}{4\pi} + Q_{20}P_{20}(cos\theta)C_0 + Q_{40}P_{40}(cos\theta)C_0 + Q_{22}P_{22}(cos\theta)C_2(\phi)$$

$$+ \quad Q_{42}P_{42}(cos\theta)C_2(\phi) + Q_{44}P_{42}(cos\theta)C_4(\phi). \tag{9}$$

Five independent coefficients are required to describe the distribution of fibers in a 3-D space; we will address these in future reports.

If we focus on how z-directional distribution of fibers affects the in-plane mechanical properties of paper, and assume the distribution of fibers is isotropic in the x-y plane, such as handsheets, then the angular distribution function is reduced to a simpler form, given by

$$f(\theta,\phi) = \frac{1}{4\pi} + Q^c_{20}P_{20}(cos\theta)C_0 + Q^c_{20}P_{40}(cos\theta)C_0. \tag{10}$$

In order to use the orthogonality of spherical harmonic functions, we have normalized $f(\theta,\phi)$ to 1 by integrating θ from 0 to π and ϕ from 0 to 2π. In this way, we have moved the end of the fiber to the original point of the coordinate system to determine the angular distribution function. Any mechanical quantity, say B, is calculated by

$$< B >= \frac{\int_0^{\pi}\int_0^{2\pi} Bf(\theta,\phi)sin\theta d\theta d\phi}{\int_0^{\pi}\int_0^{2\pi} f(\theta,\phi)sin\theta d\theta d\phi} = \frac{\int_0^{\frac{\pi}{2}}\int_0^{2\pi} Bf(\theta,\phi)sin\theta d\theta d\phi}{\int_0^{\frac{\pi}{2}}\int_0^{2\pi} f(\theta,\phi)sin\theta d\theta d\phi}$$

The final results for mechanical properties in the assumed symmetry should

be the same for normalizing $f(\theta, \phi)$ to 1 by integrating θ either from 0 to π or from 0 to $\pi/2$.

3.2 Structural model of paper

Using a model of 3-D sheets, proposed by Cox [5], and the 3-D angular distribution function introduced above, we may predict the anisotropic properties of the sheet. If the sheet is subjected to tensile strains $e_{\alpha,\beta}$, then strain along a fiber with polar angle (θ, ϕ) is given by

$$\begin{aligned} e_f &= sin^2\theta cos^2\phi e_{xx} + sin^2\theta sin^2\phi e_{yy} + cos^2\theta e_{zz} \\ &+ sin^2\theta cos\phi sin\phi e_{xy} + sin\theta cos\theta cos\phi e_{xz} + sin\theta cos\theta sin\phi e_{yz}, \end{aligned} \quad (11)$$

where engineering strains are employed. The energy density W can be written as

$$\begin{aligned} W &= \frac{1}{2}\int_0^{\pi}\int_0^{2\pi} \sigma_f e_f V_f N f(\theta,\phi) sin\theta d\theta d\phi \\ &= \frac{1}{2}\int_0^{\pi}\int_0^{2\pi} E_f(1-\Omega)e_f^2 f(\theta,\phi) sin\theta d\theta d\phi \end{aligned} \quad (12)$$

where σ_f is the stress on the fiber; V_f represents the volume of a single fiber; N is the total number of fibers per unit volume; and Ω is the porosity of the

sheets. All elastic constants of the sheet can be calculated from

$$\sigma_{\alpha\beta} = \frac{\partial W}{\partial e_{\alpha\beta}} = C_{\alpha\beta\mu\nu} e_{\mu\nu}, \quad \alpha, \beta = x, y, z \tag{13}$$

where $\sigma_{\alpha\beta}$ is the stress tensor of the sheet; $C_{\alpha\beta\nu\mu}$ is the elastic constant tensor.

The elastic constants required for this study are given by

$$\begin{pmatrix} C_{xxxx} & C_{xxyy} & C_{xxzz} \\ & C_{yyyy} & C_{yyzz} \\ & & C_{zzzz} \end{pmatrix}$$

with

$$C_{yyyy} = C_{xxxx} = K(\frac{1}{5} - \frac{4\sqrt{5\pi}}{35} Q^c_{20} + \frac{2\sqrt{\pi}}{35} Q^c_{40}) \tag{14}$$

$$C_{xxyy} = K(\frac{1}{15} - \frac{4\sqrt{5\pi}}{105} Q^c_{20} + \frac{2\sqrt{\pi}}{105} Q^c_{40}) \tag{15}$$

$$C_{xxzz} = C_{yyzz} = K(\frac{1}{15} + \frac{2\sqrt{5\pi}}{105} Q^c_{20} - \frac{8\sqrt{\pi}}{105} Q^c_{40}) \tag{16}$$

$$C_{zzzz} = K(\frac{1}{5} + \frac{8\sqrt{5\pi}}{35} Q^c_{20} + \frac{16\sqrt{\pi}}{105} Q^c_{40}) \tag{17}$$

where $K = E_f(1 - \Omega)$. If paper is completely isotropic in 3-D space, then all $Q^{c,s}_{lm}$ are zero except Q_{00}, and the above results for C are correctly obtained for this case as expected. The relation between normal stress tensor σ and normal strain tensor e can be expressed as a matrix form, $\sigma = Ce$ or $e =$

$C^{-1}\sigma$. Therefore, Young's modulus E and poisson's ratio ν of the sheets in equation (3) are calculated by

$$E = \frac{1}{(C^{-1})_{xxxx}} \tag{18}$$

$$\nu = -\frac{(C^{-1})_{xxyy}}{(C^{-1})_{xxxx}} \tag{19}$$

3.3 Finite fiber length model

When fibers are short and the fiber "end effect" cannot be neglected, we have to use a finite fiber length model. Let us consider a single fiber with finite length l_0 embedded in the fiber network where fibers are bonded together. Assume that the fiber is rod-like with radius r_0, and the mean separation of the fibers normal to their length is r_1. If the fiber network (sheet) is subjected to strain $e_{\alpha\beta}$, then strain e_s in the sheet along the fiber direction at a distance r_1 from the fiber centroid is governed by the same equation as in (11) except e_f is replaced by e_s. Shear stress τ may transfer from the fiber surrounding to the fiber. We can balance the shear forces in the network with the shear forces at the interface of the fiber and the network, where shear stress is τ_0,

that is

$$2\pi r\tau d\xi = 2\pi r_0\tau_0 d\xi,$$

where $d\xi$ is a small segment considered in the fiber. Using $\tau = Gdu/dr$, where du/dr is shear strain, G is mean shear transfer constant, we obtain

$$\frac{du}{dr} = \frac{r_0\tau_0}{G}\frac{1}{r}$$

After integrating the above equation from r_0 to r_1, we have

$$\tau_0 = \frac{G}{r_0 ln\frac{r_1}{r_0}}(u_s - u_f),$$

where u_s is displacement of the fiber network along the fiber direction at r_1, and u_f is axial displacement of the fiber. Balancing the shear forces at the interface with the tensile force in the fiber, we can write

$$dF + 2\pi r_0\tau_0 d\xi = 0.$$

Using the above two equations, we can write

$$\frac{d^2F}{d\xi^2} + H(e_s - \frac{1}{E_f A}F) = 0$$

where $e_s = du_s/d\xi$ has been used; A is the cross-sectional area of the fiber; F is the tensile force in the fiber; and $H = \frac{2\pi G}{ln(r_1/r_0)}$. The solution for the equation with boundary condition $F = 0$ at $\xi = 0$ and $\xi = l_0$ is given by

$$F = E_f A e_s [1 - \frac{ch\lambda_0(l_0/2 - \xi)}{ch\frac{\lambda_0 l_0}{2}}],$$

where $\lambda_0 = \sqrt{H/E_f A}$ and l_0 is the fiber length. The energy density W_1 due to tensile stresses can be calculated following the same procedure as those in section 2.2. The result is given by

$$\begin{aligned} W_1 &= \frac{1}{2} A E_f N \int_0^{l_0} \int_0^{\pi} \int_0^{2\pi} e_s^2 [1 - \frac{ch\lambda_0(l_0/2 - \xi)}{ch\frac{\lambda_0 l_0}{2}}]^2 f(\theta, \phi) sin\theta d\theta d\phi d\xi \\ &= \frac{1}{2} A E_f N (l_0 - \frac{3}{\lambda_0} th\frac{\lambda_0 l_0}{2} + \frac{2}{2ch^2\frac{\lambda_0 l_0}{2}}) \int_0^{\pi} \int_0^{2\pi} e_s^2 f(\theta, \phi) sin\theta d\theta d\phi \quad (20) \end{aligned}$$

The energy density W_2 due to shear stress transmitted is, similarly, given by

$$\begin{aligned} W_2 &= \frac{1}{2} N \int_0^{l_0} \int_{r_0}^{r_1} \tau \frac{du}{dr} 2\pi r dr d\xi \int_0^{\pi} \int_0^{2\pi} f(\theta, \phi) sin\theta d\theta d\phi \\ &= \frac{1}{2} A E_f N \int_0^{l_0} \int_0^{\pi} \int_0^{2\pi} e_s^2 \frac{sh^2\lambda_0(l_0/2 - \xi)}{ch^2\frac{\lambda_0 l_0}{2}} f(\theta, \phi) sin\theta d\theta d\phi d\xi \\ &= \frac{1}{2} A E_f N (\frac{th\frac{\lambda_0 l_0}{2}}{\lambda_0} - \frac{l_0}{2ch^2\frac{\lambda_0 l_0}{2}}) \int_0^{\pi} \int_0^{2\pi} e_s^2 f(\theta, \phi) sin\theta d\theta d\phi \end{aligned}$$

Total energy is written as

$$W = W_1 + W_2 = \frac{1}{2}E_f(1-\Omega)(1-\frac{th\frac{\lambda_0 l_0}{2}}{\lambda_0 l_0/2})\int_0^{\pi}\int_0^{2\pi} e_s^2 f(\theta,\phi)sin\theta d\theta d\phi$$

Final results for elastic constants are similar to equations (14) (15) (16) (17), where K is now replaced by $E_f(1-\Omega)(1-\frac{th\frac{\lambda_0 l_0}{2}}{\lambda_0 l_0/2})$ for the finite fiber length model.

4 Analysis of flutter

Chang and Moretti [3,4] have conducted wind tunnel experiments to investigate the free edge flutter. In their experiments, tension is applied across flow direction. They analyze and predict the dynamic instability for the free edge fluttering by using potential flow theory. We briefly review their procedure here and refer the reference [4] for more details. The air flow is assumed to be two-dimensional in their analysis. The aerodynamic pressure on the sheet is expressed by the Bernoulli equation

$$p_{\pm} = -\rho[\frac{\partial\varphi}{\partial t} + V\frac{\partial\varphi}{\partial y}]_{z=0\mp}$$

where φ is the flow potential; y is in the primary flow direction; ρ is the density of air. The deflection of the sheet can be assumed as

$$w = \hat{w}cos(\frac{\pi x}{L})e^{i(\omega t - \kappa y)}.$$

where, $\hat{w}$ is the amplitude of vibration; L is the length of the paper tested; and κ is a wave length. Boundary conditions for step change in pressure across the sheet are given by

$$p_+ - p_- = 2p_+$$

and

$$p_+ = -\rho\hat{w}\frac{(\omega - \kappa V)^2}{\kappa}e^{i(\omega t - \kappa y)}.$$

Therefore, the governing equation becomes

$$-\omega^2 m + D[(\pi/L)^2 + \kappa^2]^2 + (\pi/L)^2 T\hat{w}e^{i(\omega x - \kappa y)} - 2\rho\hat{w}e^{i(\omega - \kappa y)}(\omega - \kappa V)^2/\kappa = 0$$

where the x-dependent term $cos(\pi x/L)$ is dropped because of the 2-dimensional flow assumption. The characteristic equation is given by

$$(m + \frac{2\rho}{\kappa})\omega^2 - 4\rho V\omega + 2\kappa\rho V^2 - D[(\pi/L)^2 + \kappa^2]^2 - (\pi/L)^2 T = 0.$$

From this quadratic equation, the frequency can be written as

$$\omega = \frac{4\rho V \mp \sqrt{(4\rho V)^2 - 4(m + 2\rho/\kappa)2\kappa\rho V^2 - D[(\pi/L)^2 + \kappa^2]^2 - (\pi/L)^2 T}}{2(m + \rho/\kappa)}.$$

The stability boundary condition is obtained as

$$\rho V^2 - \frac{1}{2\kappa}(1 + 2\rho/m\kappa)D[(\pi/L)^2 + \kappa^2]^2 + 92\pi/L)^2 = 0, \qquad (21)$$

where $\kappa = 2\pi/\lambda$, and

$$\lambda = 2L([\frac{TL^2}{\pi^2 D} + 1]^{-\frac{1}{4}}.$$

The critical flow speed V_c and critical dynamic pressure q_c can be calculated by equation (21), and flutter frequencies above the critical speed are given by

$$f_0 = \frac{V}{\lambda + \pi m/\rho}.$$

The elastic modulus E and poisson ratio ν can be evaluated from equations (18) and (19) based on the structural model of the sheet. For $m = 0.058kg/m^2$ and $L = 0.23m$, the stiffness D in terms of E and ν may vary with parameter tension T, porosity Ω, single fiber modulus E_f, and z-dimensional angular distribution, respectively. Critical speed for edge fluttering d and

respective frequencies can be obtained as a function of the paper's structural and physical properties.

First, we consider three cases corresponding to different z-directional orientation of fibers. Case A is that fibers are uniformly distributed in the 3-D space; in turn, Q_{20} and Q_{40} in $f(\theta, \phi)$ are zero. In case B, fiber orientation is symmetric in the x-y plane, Q_{20} and Q_{40}, which represent the anisotropic distribution in the z-direction, are fitted to the curve in Figure 8 of reference 6, which is a projection of z-directional distribution on the y-z plane, based on experiments by Hasuike et al [6] (we have re-normalized the curve). In case B Q_{20} and Q_{40} are -0.088 and 0.063, respectively. Case C is constructed by setting $Q_{20} = -0.120$ and $Q_{40} = 0.073$. The degree of z-directional orientation of fibers in case A is larger than in case B, and these in case B is larger than case C. This is because Q_{20} is essentially the statistical average of $P_{20}(x_i)$ (see equation (8)), where $x_i = cos(\theta_i)$, of all fibers, and the value of $P_{20}(x)$ increases monotonically with the absolute value of x. Therefore, Q_{20}, which is called z-directional ordering parameter by us, can be used to

measure the degree of z-directional orientation. Other parameters are fixed for these three cases as specified in Table 1. The single fiber modulus is selected as 77.3 GPa corresponding to chemical pulp according to references [7,8]. The calculation result for modulus of the sheet is 6.48 GPa, which is in a good agreement with experimental results [9].

Table 1.

$m(kg/m^2)$	$T(N/m)$	$E_f(GPa)$	Ω	$L(m)$
0.058	10	77.3	0.60	0.23

The results of critical speeds and frequencies for cases A, B, and C are collected in Table 2. The critical air speeds are plotted against the z-directional ordering parameter Q_{20} in Figure 1. Since we assume the flow irrotational, the critical dynamic pressure is given as $q_c = \frac{1}{2}\rho V_c^2$, where V_c is the critical speed of air. The critical air speed and fluttering frequency decrease as the z-directional ordering increases. This suggests that z-directional distribution of fibers should be avoided.

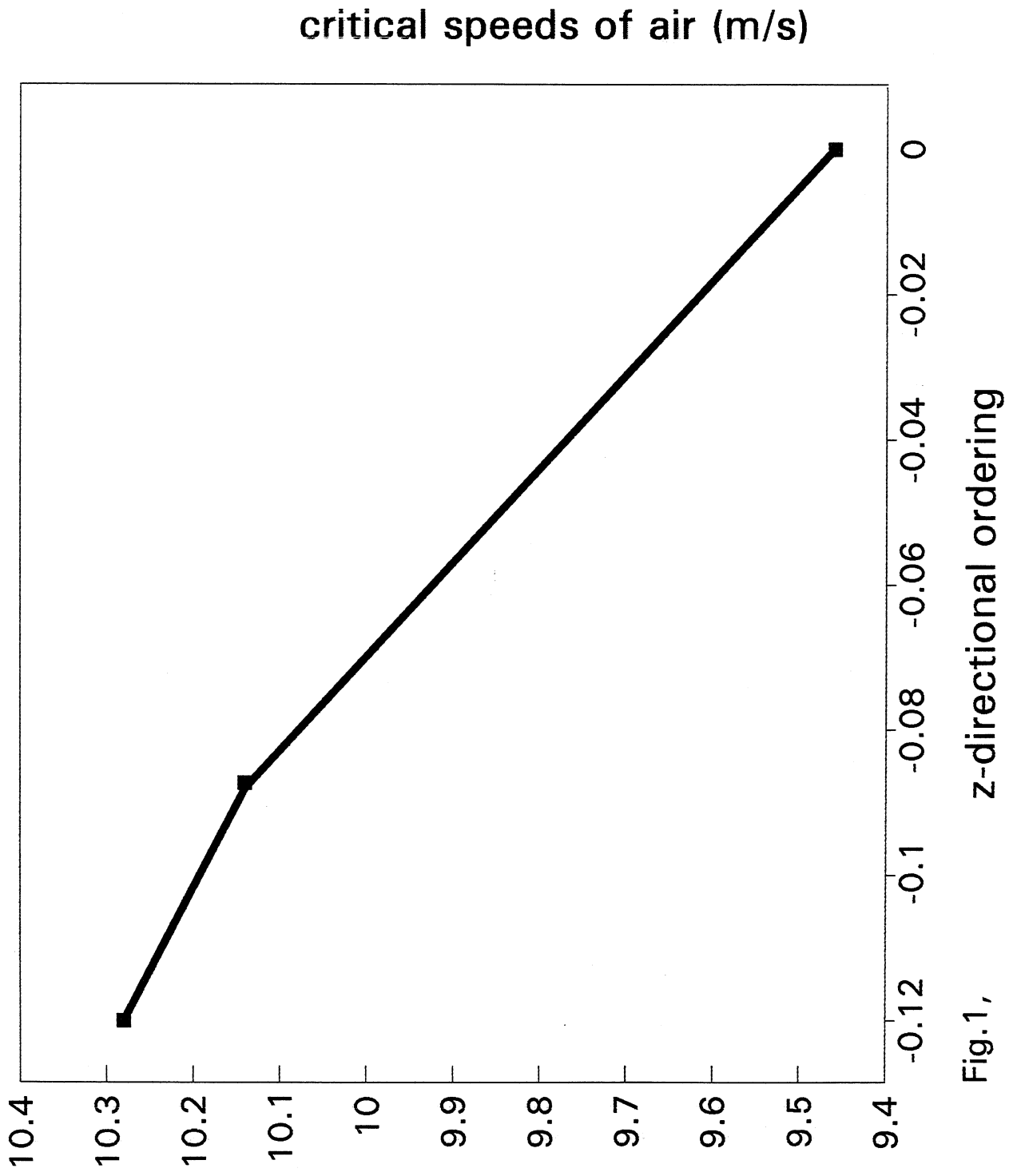
critical speeds of air (m/s)
10.4
10.3
10.2
10.1
10
9.9
9.8
9.7
9.6
9.5
9.4
-0.12
-0.1
-0.08
-0.06
-0.04
-0.02
0
z-directional ordering

Fig.1,

Table 2.

	Q_{20}	Q_{40}	$E(GPa)$	ν	$q_c(Pa)$	$V_c(m/s)$	f_0
case A	0.0	0.0	5.15	0.25	55.71	9.46	30.87
case B	-0.088	0.063	6.48	0.277	61.69	10.14	31.55
case C	-0.120	0.073	6.89	0.277	63.40	10.28	31.73

To investigate the effect of porosity at the onset of sheet flutter, the porosity Ω is set to different values, while Q_{20} and Q_{40} are the same as in case B. Other parameters are the same as those in Table 1. It is shown in Table 3 and Figure 2 that critical speed and frequency decrease as porosity increases. We can see that increasing voids is unfavorable for the dynamic stability of sheet in the paper machine.

Table 3.

	Ω	$E(GPa)$	$q_c(Pa)$	$V_c(m/s)$	f_0
case C	0.8	3.24	45.62	8.72	29.58
case D	0.7	4.86	54.26	9.51	30.70
case E	0.6	6.48	61.69	10.14	31.55
case F	0.4	9.72	74.46	11.14	32.85

Finally, critical speeds are calculated, while fiber lengths vary from 0.05 mm to 2 mm, and other parameters take the same values as in case B. The results are presented in Table 4 and plotted in Figure 3. We can see that

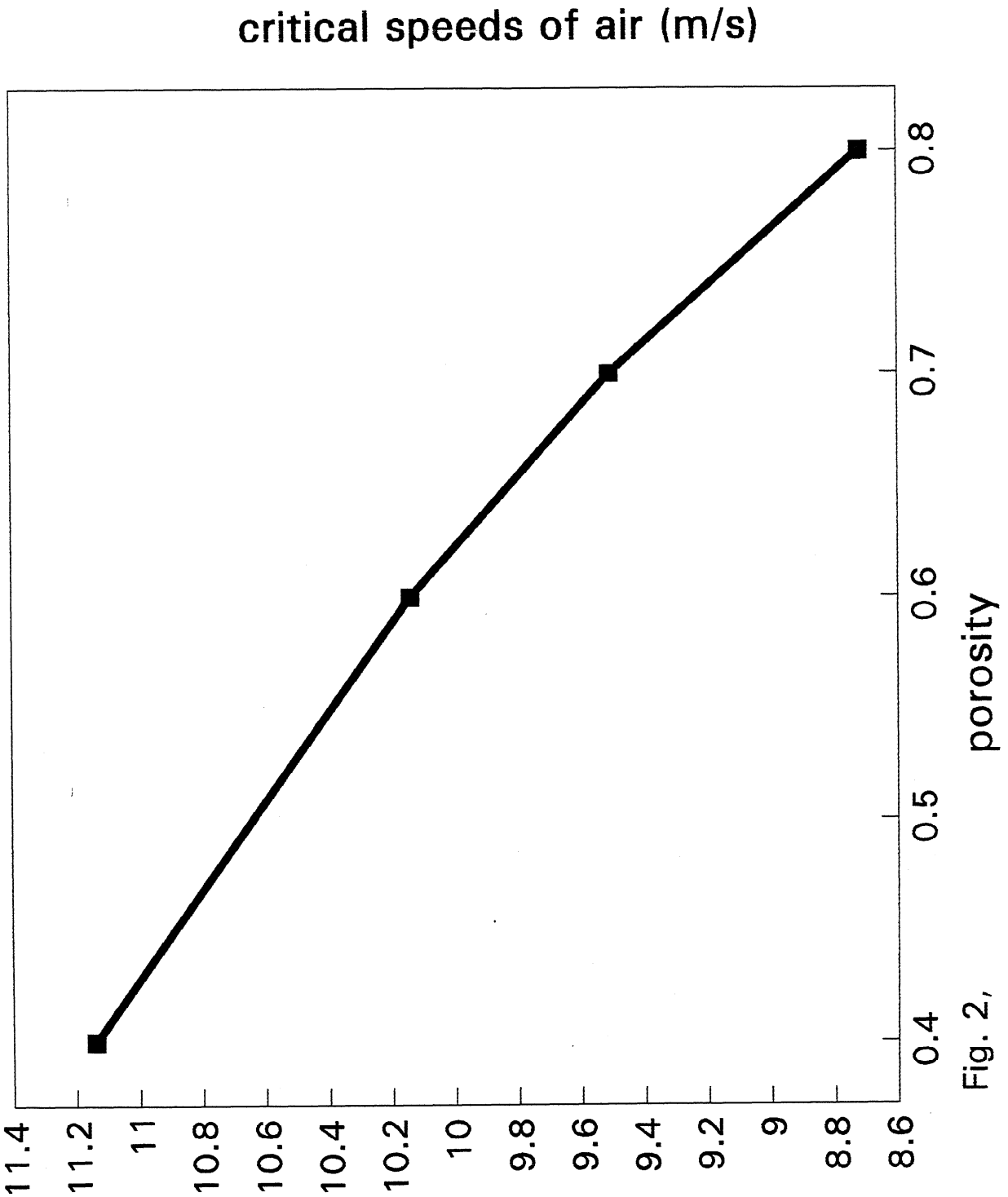
critical speeds of air (m/s)
11.4
11.2
11
10.8
10.6
10.4
10.2
10
9.8
9.6
9.4
9.2
9
8.8
8.6
0.4
0.5
0.6
0.7
0.8
porosity

Fig. 2,

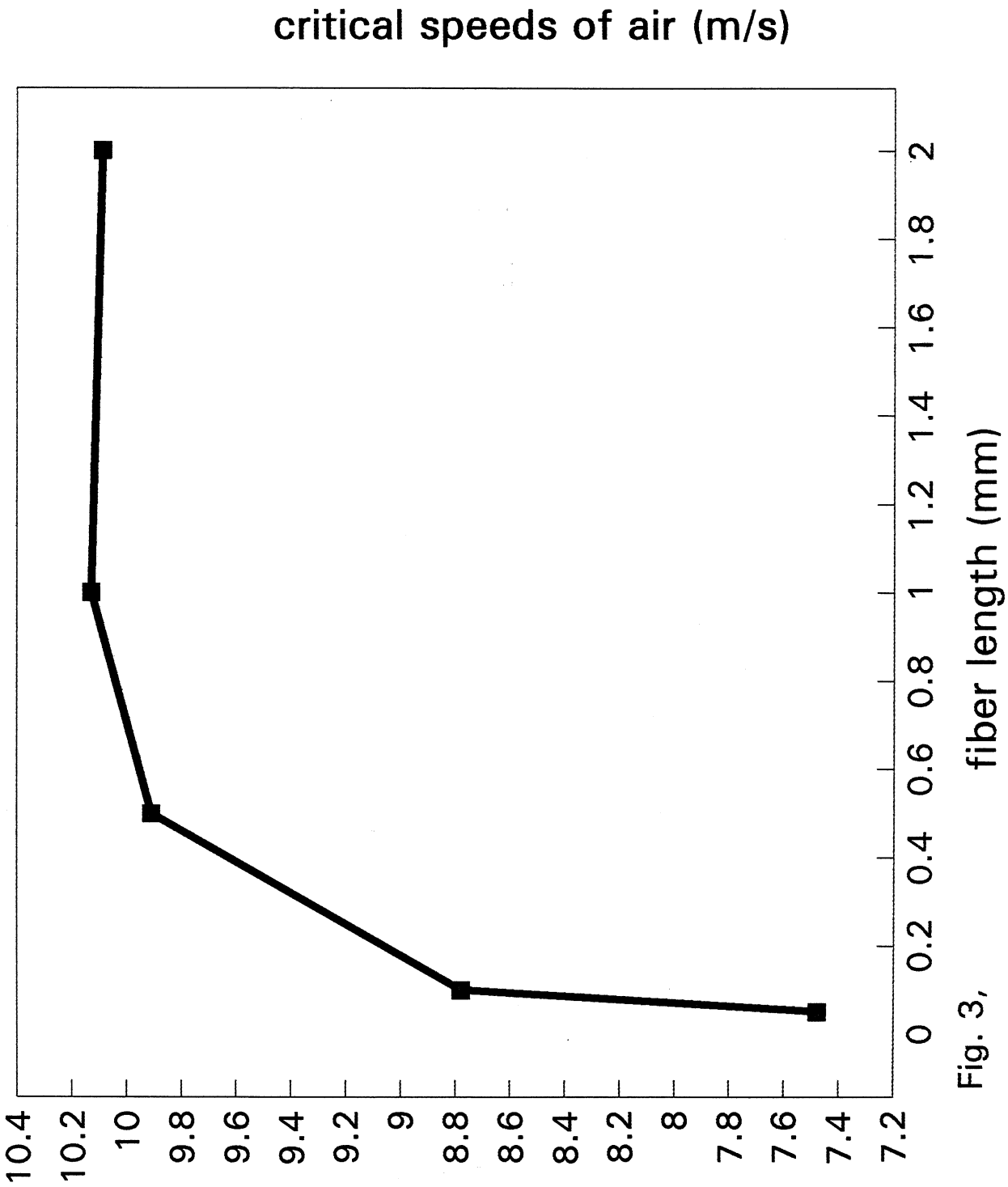
critical speeds of air (m/s)
10.4
10.2
10
9.8
9.6
9.4
9.2
9
8.8
8.6
8.4
8.2
8
7.8
7.6
7.4
7.2
0
0.2
0.4
0.6
0.8
1
1.2
1.4
1.6
1.8
2
fiber length (mm)

Fig. 3,

only fibers shorter than 0.5 mm have adverse effects on the stability of sheets. The instability is not affected by fibers longer than 1 mm.

Table 4.

	$l_0(mm)$	$E(GPa)$	$q_c(Pa)$	$V_c(m/s)$	f_0
case G	0.05	1.54	33.44	7.48	27.68
case H	0.1	3.36	46.25	8.78	29.67
case I	0.5	5.83	58.93	9.91	31.23
case J	1.0	6.16	60.36	10.13	31.40
case K	2.0	6.32	61.08	10.09	31.47

In all calculations, tension T is set to $10N/m$. For smaller tension, the critical speed would become more sensitive to the sheet structure. The two-dimensional assumption, that is $L >> \lambda$ used with potential theory, is only applicable for large tension. We are working on computational analysis of the full fluid flow equations to remove this and other restrictions from the analysis.

5 Conclusion

In order to analyze the effects of z-directional orientation of fibers on dynamic instability of sheet fluttering, a 3-D angular distribution function is

proposed for the first time. Both Cox's microstructure model of sheet and potential theory for the fluid flow are used to predict the critical speed of air in terms of physical characteristics of the sheet, such as, single fiber properties, porosity, and fiber orientation in the z-direction. It is found that critical speed decreases as z-direction orientation of fibers increases and that critical speed decreases as porosity increases and the fiber length decreases.

REFERENCES

1. Mujumdar, A.S. and Douglas, W.J.M. *Sevensk Paperstid*, 79 (**6**): 187 (1976).

2. Pramila, A., *Sheet Flutter & Windage Problems Seminar*, Tappi notes, 22, 1991.

3. Chang, Y.B. and Moretti, P.M., *Sheet Flutter & Windage Problems Seminar*, Tappi notes, 14, 1991.

4. Chang, Y.B. and Moretti, P.M., *Web Handling* ASME 67, 1992.

5. Cox, H.L., *British J. Appl. Phys.* **3**: 72 (1952).

6. Hasuike, M., Kawasaki, T., and Murakami, K., *J. Pulp and Paper Science*, vol. **18** (3), J114, (1992).

7. Subramanian, L., Carlsson, L.A., *Tappi* vol. **77**:11, 209 (1994).

8. Page, D.H., El-Hosseiny, F., and Lancaster, A.P.S., *Tappi* vol. **64**:4, 114 (1977).

9. Baum, G.A., Brennan, D.C., and Habeger, C.C., *Tappi* **64**(8) 97, (1981).

Deformable-Spatial-Domain/Space-Time (DSD/ST) Finite Element Computation for Unsteady Fluid and Elastic Membrane Interaction Problems

S.-J. Liang and G.P. Neitzel
The George W. Woodruff School of Mechanical Engineering
Georgia Institute of Technology

C.K. Aidun
Institute of Paper Science and technology

ABSTRACT

Flows involving moving boundaries and the associated hydrodynamic instabilities are encounted in many industrial, technology, and environmental applications. These include air-web dynamics, fluid-structure interactions, fluid-membrane interactions and phase change problems, etc. Direct numerical solution of the unsteady, highly non-linear equations governing even the most simplified two-dimensional models requires the dynamic evolution of both the flow field and the domain shape be determined as part of solution, since neither is known a priori. This paper describes a numerical algorithm based on the Deformable-Spatial-Domain/Space-Time (DSD/ST) finite element method for unsteady incompressible, viscous fluid and elastic membrane interaction. The unsteady Navier-Stokes and elastic membrane equations are solved separately and converge iteratively on a solution which satisfies both for every time instant. The resulting system equations, $Ax = b$, are solved by the GMRES technique with incomplete decomposition (ILU) preconditioner. Computed results demonstrate the capabilities and accuracy of the method for problems approaching ultimate steady-state as well as the time-dependent one.

INTRODUCTION

Flows involving moving boundaries and the associated hydrodynamic instabilities interactions are encounted in many industrial, technology, and environmental applications. One such application is in thin-film coating systems where a viscous fluid is applied on a flat, deformable substrate such as paper, photographic film, plastic or magnetic tapes [1-4]. The idea mode of fluid flow in most thin-film coating systems is two-dimensional, laminar, steady state. Even a small non-uniform deformation of the substrate and/or the coating element due to flow instabilities and flow-elasticity interactions could result in non-uniform

coated thickness and other defects. Flow instabilities and non-uniform hydrodynamic forces on the substrate increase with the coating application speed. But the demand for higher production rate and better quality require higher coating speeds with a laminar, stable two-dimensional steady-state flow. Our goals are to develop a numerical algorithm to study the fluid-membrane interaction and understand the physics of the associated hydrodynamic instabilities [5-7], in particularly to investigate the transient behavior.

Many other numerical methods have been devised to study problems with moving boundaries. These include, but are not limited to, the finite difference/element arbitrary Lagrangian-Eulerian [8-14], deformable cell methods [15] as well as the marker-and-cell [16-18] and related volume-of-fluid method [19], and boundary element methods [20-22]. Additionally, global mapping of an irregular and changing flow domain to a rectangular space [23,24] on which stand finite difference/finite volume discretization can be applied has also been successfully [25-27]. In this study, a numerical algorithm based on the Deformable-Spatial-Domain/Space-Time (DSD/ST) finite element method [28,29] is developed to study the fluid-membrane interaction. Similar studies for steady fluid-membrane interaction employing finite-element method [30] and finite-volume method [31] have been reported recently.

The Deformable-Spatial-Domain/Space-Time (DSD/ST) formulation has been successfully applied for the computation of unsteady flows involving free surfaces, two-liquid interfaces, moving mechanical components, and fluid-structure and fluid-particle interactions [28,29]. In the original DSD/ST method, the stabilized finite element formulation of the governing equations is written over the space-time domain of the problem and therefore, the deformation of the spatial domain with respect to time is automatically taken into account. With the advanced stabilized techniques [32-37] used in the DSD/ST formulation, the numerical stability challenges involved in the problem are overcome with minimal numerical dissipation and therefore, with minimal loss of accuracy.

The space-time (continuous-in-time) finite element formulation has been successfully applied for various problems with fixed spatial domain [32-37]. The basics of the method, it's implementation, and the associated stability and accuracy analysis can be found in these references. In a parallel development, the discontinuous-in-time space-time method have been gaining popularity for fixed domain problems, as an alternative to the common semidiscrete (finite difference/element in space, finite difference in time) approach. It's advantage is the finite element interpolation functions are discontinuous in time so that the fully discrete equations are solved one space-time slab at a time, and this makes the computations feasible.

Here, we implement the DSD/ST method, but do not include the stabilized techniques used in the original DSD/ST method, and use some numerical examples to demonstrate the capabilities and accuracy of the method.

Governing Equations and Boundary Conditions

The system of unsteady incompressible, viscous fluid and elastic membrane is outlined as the following:

The Navier-Stokes equations

We consider an incompressible, viscous fluid occupying at an instant $t \in [0, T_\infty]$ a bounded region Ω_t in $R^{n_{sd}}$, with boundary Γ_t, where n_{sd} is the number of space dimensions. The Navier-Stokes equations which describe the flow of a unsteady, viscous, incompressible Newtonian fluid with constant properties, written in terms of primitive variables are

$$\rho\left(\frac{\partial \mathbf{u}}{\partial t} + \mathbf{u}\cdot\nabla\mathbf{u}\right) - \nabla : \sigma = 0\,, \quad on\ \Omega_t\ \forall t \in [0, T_\infty]\,, \tag{1}$$

and

$$\nabla\cdot\mathbf{u} = 0\,, \quad on\ \Omega_t\ \forall t \in [0, T_\infty]\,, \tag{2}$$

where ρ is the fluid density, and σ is the stress tensor given as

$$\sigma = -p\mathbf{I} + 2\mu\,\varepsilon(\mathbf{u})\,, \tag{3}$$

with $$\varepsilon(\mathbf{u}) = \frac{1}{2}\left(\nabla\mathbf{u} + (\nabla\mathbf{u})^T\right). \quad (4)$$

Here μ represents the fluid viscosity, while $\mathbf{I}$ denotes the identity tensor.

The boundary conditions relating to the momentum equations commonly employed are either the specification of the velocity components (Dirichlet type)

$$\mathbf{u} = \mathbf{g}, \quad on\ (\Gamma_t)_g, \quad (5)$$

or specification of the surface stresses

$$\mathbf{n}\cdot\sigma = \mathbf{h}, \quad on\ (\Gamma_t)_h, \quad (6)$$

where $\mathbf{n}$ is the outward unit normal vector to the boundary, Γ_t. $(\Gamma_t)_g$ and $(\Gamma_t)_h$ are complementary subsets of the boundary Γ_t.

The initial condition consists in the specification of the velocity $\mathbf{u}(x,0) = \mathbf{u}_0$. The initial velocity field $\mathbf{u}_o$ is assume to be solenoidal, i.e.,

$$\nabla\cdot\mathbf{u}_0 = 0, \quad \text{on } \Omega_0 \quad (7)$$

Noted that no initial conditions are required for the pressure; the initial pressure, p_o, is contained implicitly in Eqs. (1) and (2), for a given $\mathbf{u}_o$. The role of the pressure is that of adjusting itself instantaneously in order that mass conservation be satisfied at any time. This behavior is related to the well know fact that in an incompressible fluid the value of the speed of sound becomes infinite.

The membrane equation

The membrane equation describing the deformable boundary, $(\overline{\Gamma}_t)_g \in (\Gamma_t)_g$, is given as

$$m\frac{d^2\delta}{dt^2} + T\frac{\frac{d^2\delta}{dx^2}}{\left[1+\left(\frac{d^2\delta}{dx^2}\right)^2\right]^{3/2}} + \frac{d^2}{dx^2}\left(EI\frac{d^2\delta}{dx^2}\right) = \sigma, \quad (8)$$

$$on\ x_L \le x \le x_R\ \forall\ t \in [0, T_\infty]$$

with the following boundary conditions:

$$\delta)_{x=x_L} = \delta_L, \qquad \delta)_{x=L} = \delta_R, \text{ and}$$
$$\left.\frac{d^2\delta}{dx^2}\right)_{x=x_L} = M_{x_L}, \quad \left.\frac{d^2\delta}{dx^2}\right)_{x=x_R} = M_{x_R}. \tag{9}$$

where m is the mass, T is the surface tension, E is the modules of elasticity, I is the second moment of area, and δ is the displacement.

As initial condition, displacements and velocities at t = 0 are specified for the membrane:

$$\delta(t=0) = \delta_o \quad \text{and} \quad \frac{d\delta(t=0)}{dt} = \frac{d\delta_o}{dt} \tag{10}$$

Finite-Element Formulation

In order to construct the finite element function spaces for DSD/ST method, we partition the time interval $[0,T_\infty]$ into subintervals $I_n =]t_n, t_{n+1}[$, where t_n and t_{n+1} belong to an ordered series of time levels $0 = t_0 \prec t_1 \prec \cdots \prec t_{N-1} \prec t_N = T_\infty$. Let Ω_t^h be the approximation to Ω_t in I_n, and let Γ_t^h be the boundary of Ω_t^h. Also let $\Omega_n = \Omega_{t_n}$ and $\Gamma_n = \Gamma_{t_n}$. We will define the space-time slab Q_n as the domain enclosed by the surface Ω_n , Ω_{n+1} and P_n, where P_n is the surface described by the boundary Γ_t^h as t travels I_n.

As is the case with Γ_t, P_n can be divided into $(P_n)_g$ and $(P_n)_h$ with respect to the type of boundary condition (Dirichlet and Neumann) being applied. For each space-time slab, Q_n, we define the following finite element interpolation function spaces for the velocity and pressure:

$$\left(S_{\mathbf{u}}^h\right)_n = \left\{\mathbf{u}^h \middle| \mathbf{u}^h \in \left[H^{2h}(Q_n)\right]^{n_{sd}},\ \mathbf{u}^h \equiv g^h \ \text{ on } (\mathrm{P_n})_g\right\} \tag{11}$$
$$\left(V_{\mathbf{u}}^h\right)_n = \left\{\mathbf{u}^h \middle| \mathbf{u}^h \in \left[H^{2h}(Q_n)\right]^{n_{sd}},\ \mathbf{u}^h \equiv 0 \ \text{ on } (\mathrm{P_n})_g\right\} \tag{12}$$
$$\left(S_p^h\right)_n = \left(V_p^h\right)_n = \left\{q^h \middle| q^h \in \left[H^{1h}(Q_n)\right]\right\} \tag{13}$$

Here $H^{1h}(Q_n)$ and $H^{2h}(Q_n)$ represent the finite dimensional function space with first- and second-order polynomials in space over the space-time slab Q_n. Over the parent (element) domain, this space is formed by using second-order (bi-quadratic) polynomials

for velocity and first-order (bilinear) polynomials for pressure in space, and zero-order polynomials in time. Globally, the interpolation functions are continuous in space but discontinuous in time.

Equations determining the value of unknowns *u, v and p* are derived using the DSD/ST method. The unsteady Navier-Stokes equations are multiply by the finite element basis functions and integrated over the space-time slab Q_n. Values of the unknowns are found such that these residuals vanish. The DSD/ST formulation for the Navier-Stokes equations can be written as follow:

given $\left(\mathbf{u}^h\right)_n^-$, find $\mathbf{u}^h \in \left(S_{\mathbf{u}}^h\right)_n$ and $p^h \in \left(S_p^h\right)_n$, such that $\forall \mathrm{w}^h \in \left(V_{\mathbf{u}}^h\right)_n$, $\forall \mathrm{q}^h \in \left(V_p^h\right)_n$

$$\begin{aligned}
&\int_{Q_n} w^h \cdot \rho\left(\frac{\partial \mathbf{u}^h}{\partial t} + \mathbf{u}^h \cdot \nabla \mathbf{u}^h\right) dQ + \int_{Q_n} \varepsilon\left(w^h\right) : \sigma\left(p^h, u^h\right) dQ \\
&+ \int_{Q_n} q^h \rho \nabla \cdot \mathbf{u}^h dQ + \int_{\Omega_n} \left(w^h\right)_n^+ \cdot \rho\left(\left(\mathbf{u}^h\right)_n^+ - \left(\mathbf{u}^h\right)_n^-\right) d\Omega \\
&= \int_{(\mathrm{P_n})_h} w^h \cdot \mathbf{h}\, \mathrm{dP} \quad \forall \mathrm{w}^h \in \left(V_u^h\right)_n \quad \forall \mathrm{q}^h \in \left(V_p^h\right)_n
\end{aligned} \tag{14}$$

This procedure is applied sequentially to all the space-time slabs Q_0 , Q_2 , ..., Q_N.

In the variational formulation given by Eq. (14), the following notations are used:

$$\left(\mathbf{u}^h\right)_n^{\pm} \equiv \lim_{\varepsilon \to 0} \mathbf{u}\left(\mathrm{t_n} \pm \varepsilon\right), \tag{15}$$

$$\int_{Q_n} (\cdots) dQ \equiv \int_{t_n} \int_{\Omega_t^h} (\cdots) d\Omega dt \tag{16}$$

$$\int_{P_n} (\cdots) dQ \equiv \int_{t_n} \int_{\Gamma_t^h} (\cdots) d\Gamma dt \tag{17}$$

Similarly, the elastic membrane equation is discretized using the DSD/ST finite element formulation with the bilinear basis function $\overline{w^h}$

$$\int_{t_n}^{t_{n+1}} \int_{t_n}^{t_{n+1}} \overline{w^h} \left(m \frac{d\dot{\delta}^h}{dt} - T \left(\frac{\dfrac{d^2\delta^h}{dx^2}}{\left[1 + \left(\dfrac{d^2\delta}{dx^2}\right)^2\right]^{3/2}} \right) + \frac{d^2}{dx^2}\left(EI \frac{d^2\delta^h}{dx^2} \right) - \sigma^h \right) dx dt = 0 \tag{18}$$

The location of the membrane is updated using the following relation:

$$\delta_n^h = \delta_{n-1}^h + \frac{\Delta t}{2}\left(\dot{\delta}_n^h + \dot{\delta}_{n-1}^h\right) \tag{19}$$

The Navier-Stokes and elastic membrane equations are solved separately and converge iteratively (decoupled) on a solution that satisfies both for every time instant. The resulting system equations, Ax = b, are solved by the GMRES technique [38] with incomplete decomposition (ILU) preconditioner. The computations start with the initial condition

$$\left(u^h\right)_0^- \equiv u_0, \quad \left(\delta^h\right)_0^- \equiv \delta_0 \quad and \quad \left(\dot{\delta}^h\right)_0^- \equiv \dot{\delta}_0^h, \tag{20}$$

and initial domain Ω_0, $\left(\Gamma_0\right)_g$, $\left(\Gamma_0\right)_h$ *and* $\left(\overline{\Gamma}_0\right)_g$.

Preliminary Results

The following numerical examples are presented to demonstrate the capability and accuracy of the DSD/ST finite element method, and it's application of the fluid-membrane interaction problem.

A. One-dimensional wave equation.

The one-dimensional, time-dependent, pure convection problem with constant convection velocity, u, and boundary conditions considered are given as

$$\frac{\partial T}{\partial t} + u\frac{\partial T}{\partial x} = 0, \quad on\ \Omega_t = [0,1]\ \forall\ t \in [0,T] \tag{21}$$

$$T(0,t) = 1 \quad \text{and} \quad T(1,t) = 0 \tag{22}$$

The initial condition is a discontinuity spread across one spatial element.

$$T(x,0) = \begin{cases} 1 & \text{for } 0 \le x \le 0.4 \\ 0 & \text{otherwise} \end{cases} \tag{23}$$

The comparison of the conventional method (FE in space and FD in time) and the DSD/ST finite element method is performed. Computed results with 100 uniform elements and $\Delta t = 0.01$ are given in Figure 1 for both methods. When the fixed mesh method is used, the discontinuity becomes smoother and smoother due to the numerical dissipation as time marching, as shown in Figure 1-(a). The effect of reflection on the open boundary is also noticeable. When the mesh is moved with the convection velocity, u, the local

convection effect (relative to the mesh) is minimized and the exact solution is obtained, as shown in Figure 1-(b).

B. Driven-cavity flow

A closed square cavity, as shown in Figure 2-(a), with the top plate being impulsively set into a motion with $U(x,H,t)=1$ at time = 0^+ is investigated. $\mathrm{Re}=\frac{\rho u_r l_r}{\mu}$ based on the reference velocity, u_r = U(x,H,t), and reference length, l_r = L, is 100. The cavity is 'loaded' on a 'truck' traveling with the same speed of the lid. Consequently the absolute velocity of the lid is 2 times of a stationary cavity.

A uniform 17x17 grid with Δt = 0.01 is employed to solve this problem. The steady-state solution of translating cavity is compared with the solution of the stationary cavity, and the two results are found to converge to virtually the same steady-state solution, as shown in Figure 3.

C. Couette flow between two flat parallel walls

The next problem considered is the transient developing flow between two parallel flat walls from rest by the lower wall being impulsively set into constant motion at time = 0^+. Since the convection terms vanish and the pressure is constant in the whole domain, the momentum equation for the first velocity component u(t,x,y) simplifies to

$$\frac{\partial u}{\partial t}=\frac{\partial^2 u}{\partial y^2} \tag{24}$$

with the second component v(t,x,y) vanishing identically.

On a two-dimensional unit square domain as illustrated in Fig. 2-(a), the associated boundary and initial conditions adopted are

$$u(t,x,0)=1, \quad u(t,x,1)=0, \text{ and } \quad u(0,x,y)=0. \tag{25}$$

This problem admits an infinite series solution, [39],

$$u(t,x,y)=1-y-2\sum_{n=1}^{\infty}\frac{1}{n\pi}\exp\left(-n^2\pi^2 t\right)\sin(n\pi y) \tag{36}$$

A uniform mesh of 9x9 grid is employed to solve this problem with constant $\Delta t = 0.001$. Inlet $(\overline{DA})$ and outlet $(\overline{BC})$ conditions are chosen as free natural conditions, $\frac{\partial u}{\partial n} = 0$. The computed results are in excellent agreement with the analytic solutions as presented in Figure 4.

D. Fluid-membrane interactions

The model problem for the fluid-membrane interaction is schematically represented in Figure 2-(b). The length of the cavity is unit one in x- and y-direction initially. There is an opening with length of a quarter and end points at $(x_C, y_C) = (1, 0.25)$ and $(x_D, y_D) = (1, 0.5)$. The membrane is simple supported, i.e., $\delta(x = 0) = \delta(x = L) = 0$ and $M(x = 0) = M(x = L) = 0$. The fluid-membrane interaction is started by the top plate motion and external applied pressure, P_e. On the rigid boundaries $\overline{BC}$, $\overline{DE}$, $\overline{EF}$, *and* $\overline{EA}$ no-slip condition is applied, on the opening boundary, $\overline{CD}$, stress-free condition is applied. The shape and motion of the membrane, $\overline{AB}$, are unknown in priori, and have to be determined as part of the solution.

Parameters used for computations are: $\rho = 1$, $\mu = 0.01$, m=1, T=0.0001 EI=0 and $P_e = 0$. A uniform 33x33 grid with $\Delta t = 0.01$ is employed. Both the flow approaching ultimate stead-state and time-dependent are investigated.

(a) The steady-state case:

The cavity is a unit square initially. Flow is started by the motion of the top plate, $U(t) = 1$. The Reynolds number based on the velocity of the motion of the top platre and the unit length is 100. Computed steady-state streamline and pressure fields are given in Figure 5. The pressure field is very different from that of the "standard" driven-cavity flows (not including the membrane), mainly because of the pressure release due to the opening. The transient behavior of the membrane for different time instants are shown in Figure 6. The final shape of the membrane becomes s-shaped, with the maximum

deformation about 8%. The interaction of fluid and elastic membrane is evident in particularly the short period after the initiation of the top plate motion. When the flow starts to develop, pressure effect acts on the membrane immediately. Pressure variations dominate the deformation of the membrane. An inflection point closes the lower, right corner is observed. It's appearance mainly due to the impinging flow hits the membrane there. There is a small secondary near the lower, right corner. As the flow continues to develop, flow and membrane approach equilibrium eventually. The transient behavior approaching the steady-state is very different from the "standard" cavity-driven flow. It takes much longer time for the fluid-membrane system to reach the steady-state compared with that of the "standard" driven-cavity flow, which depends on the time scale of both the fluid and elastic membrane.

(b) Time-Dependent case:

Similar case as previous one, except the top plate moves with $U(t) = \sin\left(\frac{2\pi}{T_f}\right)$ and $T_f = 1$ is considered next. Computed results are presented in Figures 7-11. Figure 7 shows the time history of the pressure and displacement of the membrane at three different locations, i.e., 0.25, 0.5 and 0.75, respectively. Fluid and membrane response with the external forcing closely, though the phase shift at different locations is noticeable for both pressure and displacement. The membrane shapes at some different time instants are given in Figure 8. The variation of the membrane shape mainly occurs at the left half, since the opening at the right side of the cavity relaxes the pressure change at the right half. The time history of the stain rate (time rate of the membrane length) of the membrane is given in Figure 9. There is a sudden change of the strain rate when the motion of the top plate changes the direction. The streamlines and pressure contours at t = 4.25 and 4.75, corresponding to maximum and minimum velocity of the top plate motion, are given in

Figures 10 and 11. Though the streamlines are very different at t = 4.25 and 4.75, the pressure contours are very similar, due to the pressure release of the opening there.

Conclusion

We employ the Deformable-Spatial-Domain/Space-Time (DSD/ST) finite element method to study unsteady flows involving moving boundaries. Based on the space-time finite element formulation, the deformation of the spatial domain with respect time is automatically taken into account. We use some model problems - one-dimensional, two-dimensional and deformable domain cases - to demonstrate it's capabilities. Finally, we present the computed results from the fluid-membrane interaction, which both the problem of approaching ultimate steady-state and time-dependent are studied. This study constitutes the preparation phase for investigating coupled fluid-elasticity interactions and the associated hydrodynamic instabilities.

References

[1] Pramila, A., "Sheet flutter and the interaction between sheet and air", TAPPI Journal, 69, 70-74, 1986.

[2] Saito, H. and L.E. Scriven, "Study of coating flow by the finite element method", Journal of Computational Physics, 42, 53-76, 1981.

[3] Kistler, S.F. and L.E. Scriven, "Coating flow", in J.R.A. Pearson and S.M. Richardson (eds.) **Computional Analysis of Polymer Processing**, Applied Science Publishers, London, 243-299, 1983.

[4] Christoudoulou, K.N. and L.E. Scriven, "The fluid mechanics of slide coating", Journal of Fluid Mechanics, 208, 321-354, 1989.

[5] Aidun, C. K., "Principles of hydrodynamic instability: application in coating systems. Part 1: Background", TAPPI Journal, 74, 213-219, 1991.

[6] Aidun, C. K., "Principles of hydrodynamic instability: application in coating systems. Part 2: Examples of flow instability", TAPPI Journal, 74, 213-220, 1991.

[7] Aidun, C. K., "Principles of hydrodynamic instability: application in coating systems. Part 3: A generalized view of instability and bifurcation", TAPPI Journal, 74, 209-213, 1991.

[8] Harlow, F.H. and A.A. Amsden, "A numerical fluid dynamics calculation method for all flow speed", Journal of Computational Physics, 8, 197-213, 1971.

[9] Hirt, C.W., A.A. Amsden and J.L. Cook, "An Arbitrary Lagrangian-Eulerian computing method for all speeds", Journal of Computational Physics, 14, 227-253, 1974.

[10] Pracht, W.E., "Calculating three-dimensional fluid flows at all speeds with an Eulerian-Lagrangian computing mesh", Journal of Computational Physics, 17, 132-159, 1975.

[11] Chan, R. K.-C., "A generalized Arbitrary Lagrangian-Eulerian method for incompressible flows with sharp interfaces", Journal of Computational Physics, 17, 311-331, 1975.

[12] Hughes, T.J.R., W.K. Liu and T.K. Zimmermann, "Lagrangian-Eulerian finite element formulation for incompressible viscous flows", Computer Methods in Applied Mechanics and Engineering, 29, 329-349, 1981.

[13] Huerta, A. and W.K. Liu, "Viscous flow with large free surface motion", Computer Methods in Applied Mechanics and Engineering, 69, 277-324, 1988.

[14] Ramaswamy, B. and M. Kawahara, "Arbitrary Lagrangian-Eulerian finite element method for unsteady, convective, incompressible viscous free surface flows", International Journal for Numerical Methods in Fluids, 7, 1053-1075, 1987.

[15] Mizuta, Y., "Generalized boundary conditions on the basis of a deformable-cell method: Free surface, density interfaces and open boundaries", Computers & Fluids, 19, 377-385, 1991.

[16] Daly, B.J., "A technique for including surface tension effects in hydrodynamic calculations", Journal of Computational Physics, 4, 97-117, 1969.

[17] Chan, R. K.-C. and R.L. Street, "A computer study of finite amplitude water waves", Journal of Computational Physics, 6, 68-94, 1970.

[18] Viecelli, J.A., "A computing method for incompressible flows bounded by moving walls", Journal of Computational Physics, 8, 119-143, 1971.

[19] Hirt, C.W. and B.D. Nichols, "Volume of fluid (VOF) method for the dynamics of free boundaries", Journal of Computational Physics, 39, 201-225, 1981.

[20] Brebbia, C.A., **The Boundary Element Method for Engineers**, Pentech, London, 1978.

[21] Tanner, R.I., "Extrudate swell", in J.R.A. Pearson and S.M. Richardson (eds.) **Computational Analysis of Polymer Processing**, Applied Science Publishers, London, 63-138, 1983.

[22] Yuan, Y. and D.B. Ingham, "The numerical solution of viscous flows with a free surface", in L.C. Wrobel and C.A. Brebbia (eds.), **Computational Modelling of Free and Moving Boundary Problems**, Computational Mechanics Publications, Southampton, 325-340, 1991.

[23] Thompson, J.F. and Z.U.A. Warsi, "Boundary-fitted coordinate systems for numerical Solution of Partial Differential Equations-A Review", Journal of Computational Physics, 47, 1-108, 1982.

[24] Ryskin, G. and L.G. Leal, "Orthogonal mapping", Journal of Computational Physics, 50, 71-100, 1983.

[25] Ryskin, G. and L.G. Leal, "Numerical solution of free-boundary problems in fluid mechanics. Part 1. The Finite-Difference Technique", Journal of Fluid mechanics, 148, 1-17, 1984.

[26] Ryskin, G. and L.G. Leal, "Numerical solution of free-boundary problems in fluid mechanics. Part 2. Bouyance-driven motion of a gas bubble through a quiescent liquid", Journal of Fluid Mechanics, 148, 19-35, 1984.

[27] Ryskin, G. and L.G. Leal, "Numerical solution of free-boundary problems in fluid mechanics. Part 3. Bubble deformation in an axisymmetric straining flow", Journal of Fluid Mechanics, 148, 37-43, 1984.

[28] Tezduyar, T.E., M. Behr, and J. Liou, "A new strategy for finite element computations involving moving boundaries and interfaces - The deformable-spatial-domain/space-time procedure: I. The concept and the preliminary numerical tests", Computer Methods in Applied Mechanics and Engineering, 94, 339-351,1992.

[29] Tezduyar, T.E., M. Behr, S. Mittal, and J. Liou, "A new strategy for finite element computations involving moving boundaries and interfaces - The deformable-spatial-

domain/space-time procedure: II. Computation of free-surface flows, two-liquid flows, and flows with drifting cylinders", Computer Methods in Applied Mechanics and Engineering, 94, 353-371, 1992.

[30] Rast, M.P., "Simultaneous solution of the Navier-Stokes and elastic membrane equations by a finite element method", International Journal for Numerical Methods in Fluids, 9, 1115-1135, 1994.

[31] Smith, R. and W. Shyy, "A computational model of flexible membrane wings in steady laminar flow", AIAA Journal, under review.

[32] Nguyen, H. and J. Reynen, "A space-time least-square finite element scheme for advection-diffusion equations", Computer Methods in Applied Mechanics and Engineering, 42, 331-342, 1984.

[33] Brooks, A.N. and T.J.R. Hughes, "Streamline-upwind/Petro-Galerkin formulations for convection dominated flows with particular emphasis on incompressible Navier-Stokes equations", Computer Methods in Applied Mechanics and Engineering, 32, 199-259, 1982.

[34] Hughes, T.J.R., L.P. Franca, and M. Mallet, "A new finite element formulation for computational fluid dynamics: VI. Convergence analysis of the generalized SUPG formulation for linear time-dependent multi-dimensional advective-diffusive systems", Computer Methods in Applied Mechanics and Engineering, 63, 97-112, 1987.

[36] Hughes, T.J.R., L.P. Franca, and G.M. Hulbert, "A new finite element formulation for computational fluid dynamics: VIII. The Galerkin/least-squares method for advective-diffusive equations", Computer Methods in Applied Mechanics and Engineering, 73, 173-189, 1989.

[35] Hughes, T.J.R. and G.M. Hulbert, "Space-time finite element methods for elastodynamics: Formulations and error estimates", Computer Methods in Applied Mechanics and Engineering, 66, 339-363, 1988.

[37] Bell, B.C. and K.S. Surana, "A sapce-time coupled p-version least squares finite element formulation for unsteady fluid dynamics problems", International Journal for Numerical Methods in Fluids, 9, 1115-1135, 1994.

[38] Saad, Y. and M.H. Schultz, "GMRES: A generalized minimal residual algorithm for solving nonsymmetric linear systems", Journal on Scientific and Statistical Computing, 7, 856-869, 1986.

[39] Schlichting, H., **Boundary-Layer Theory**, McGraw-Hill, New York, 1968.

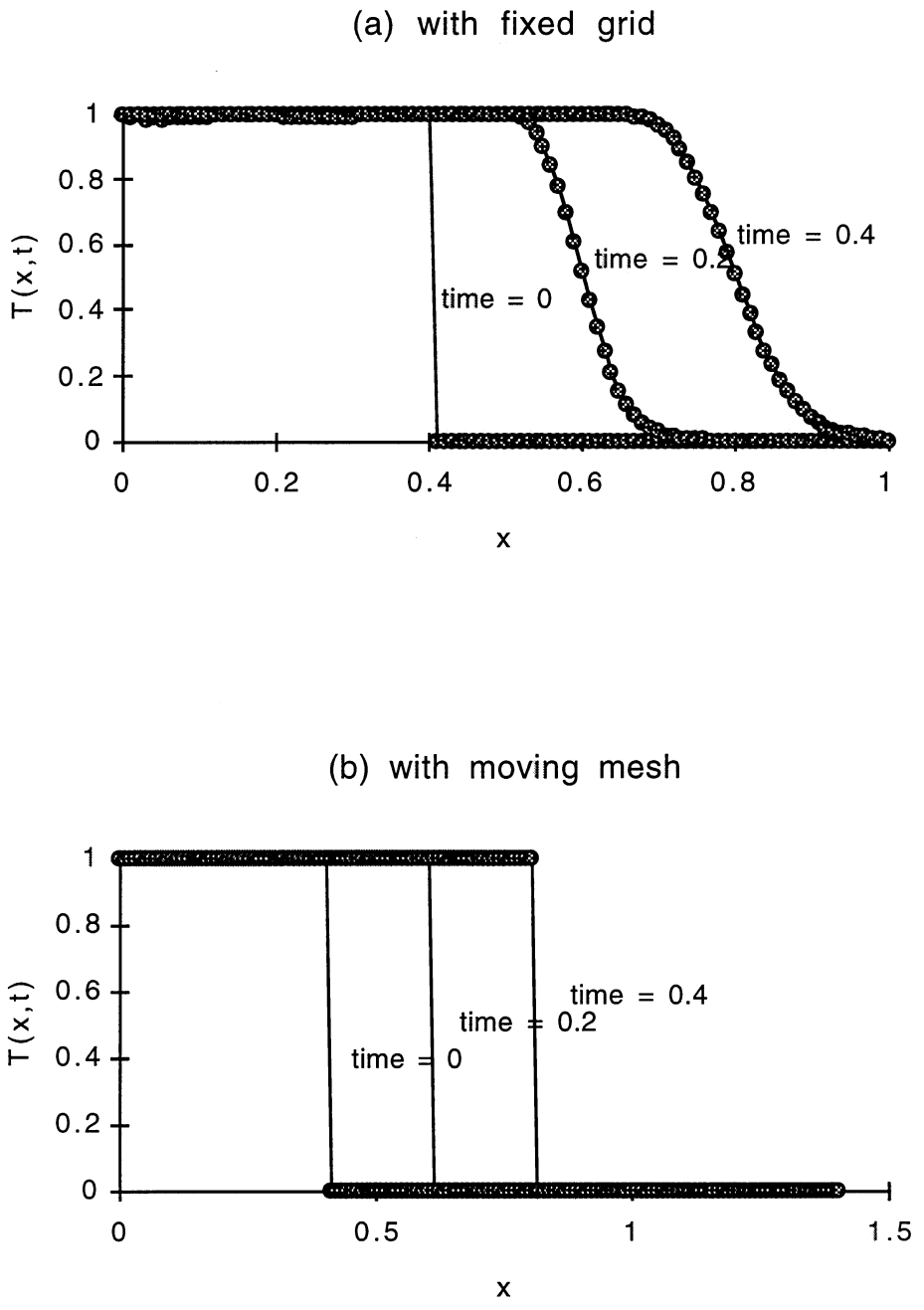

Figure 1. One-dimensional convection of a discontinuity: initial condition and the solution at time = 0.2 and time = 0.4 with fixed and moving meshed.

(a) Driven-cavity flow

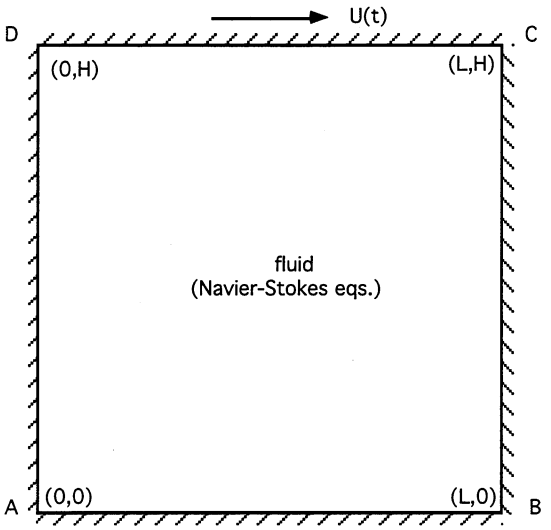

(b) Fluid-membrane interaction

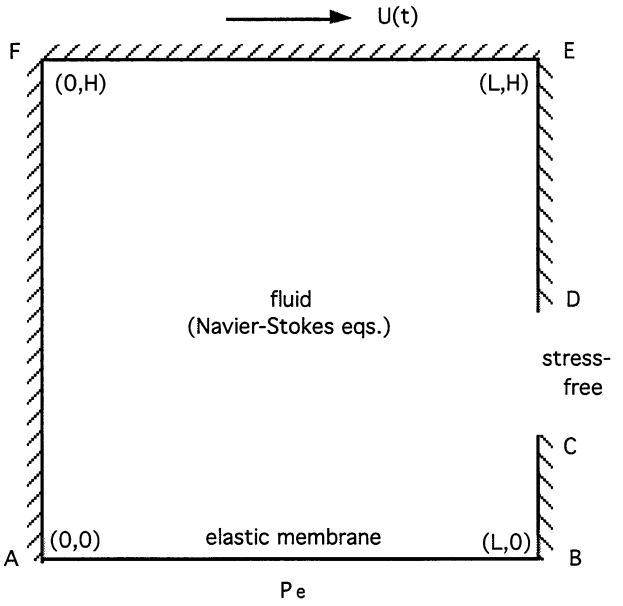

Figure 2. Schemetic representation of the model problem for (a) driven-cavity flow and (b) fluid-membrane interaction.

Fixed Mesh

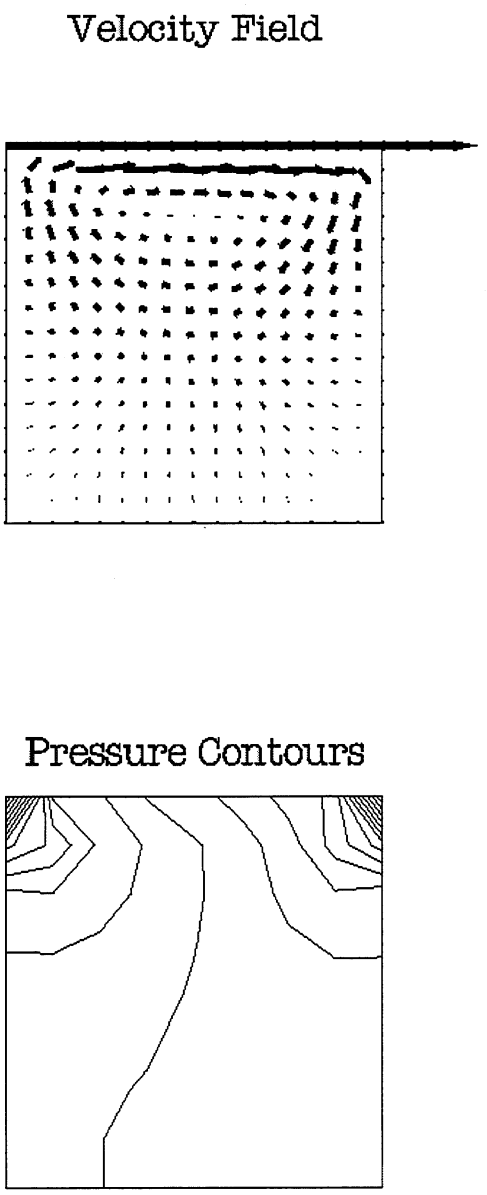

Figure 3-(a). Stationary cavity: velocity and pressure fields (steady-state solution).

Moving Mesh

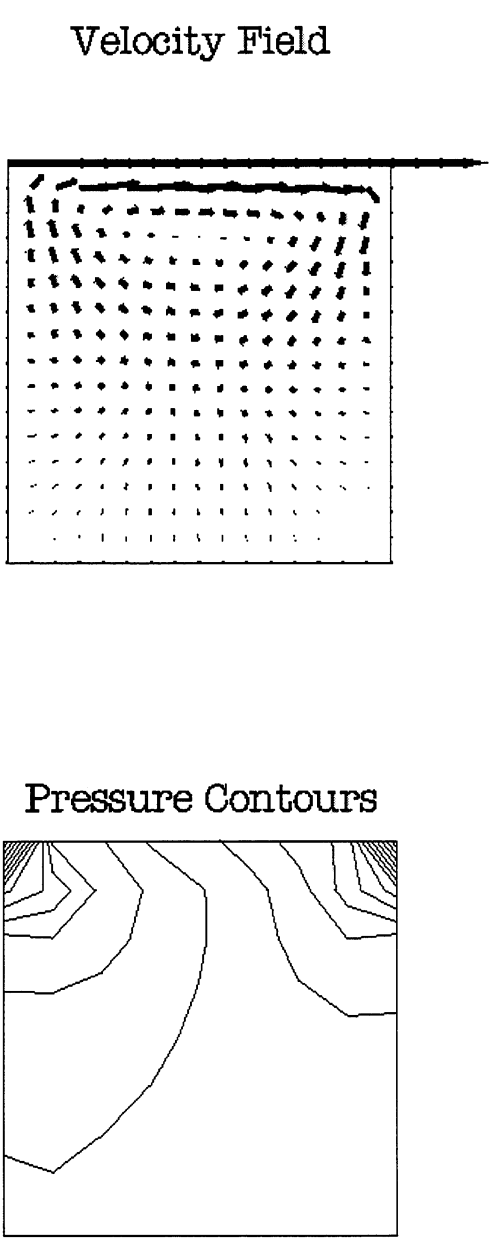

Figure 3-(b). Translating cavity: velocity and pressure fields (steady-state solution).

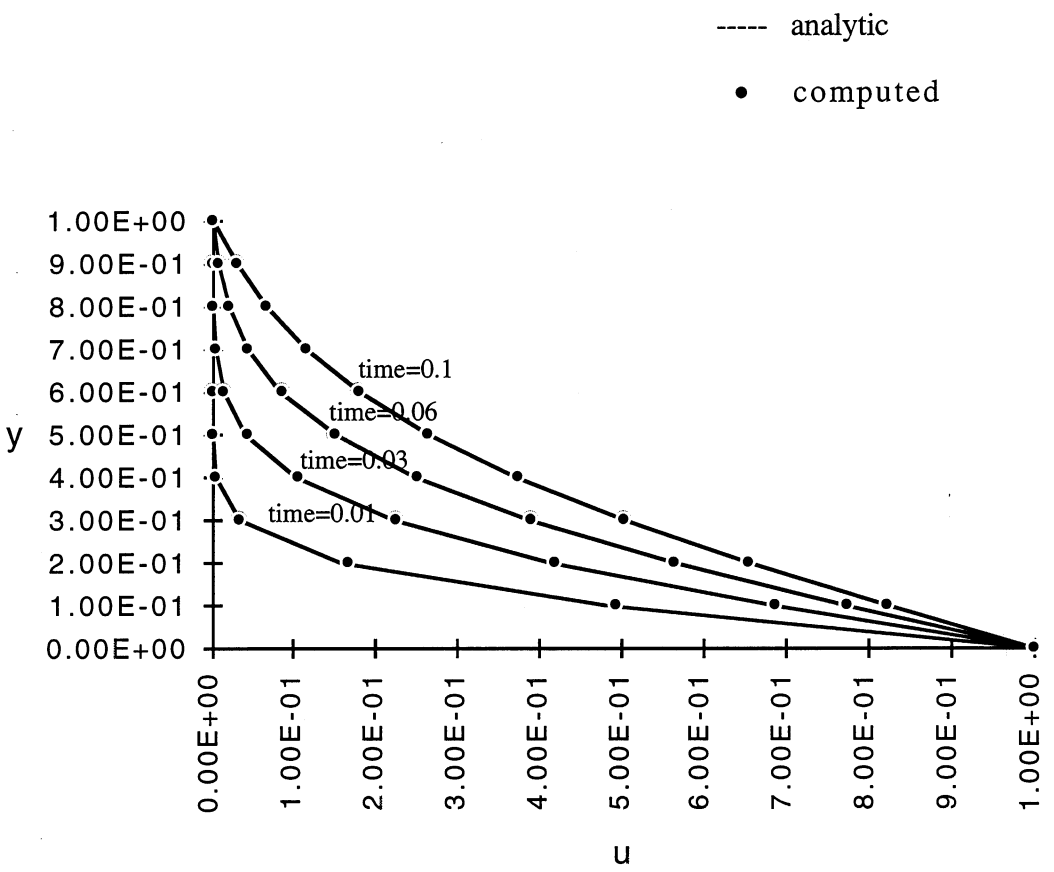

Figure 4. Starting transient Couette flow with $\Delta t = 0.001$.

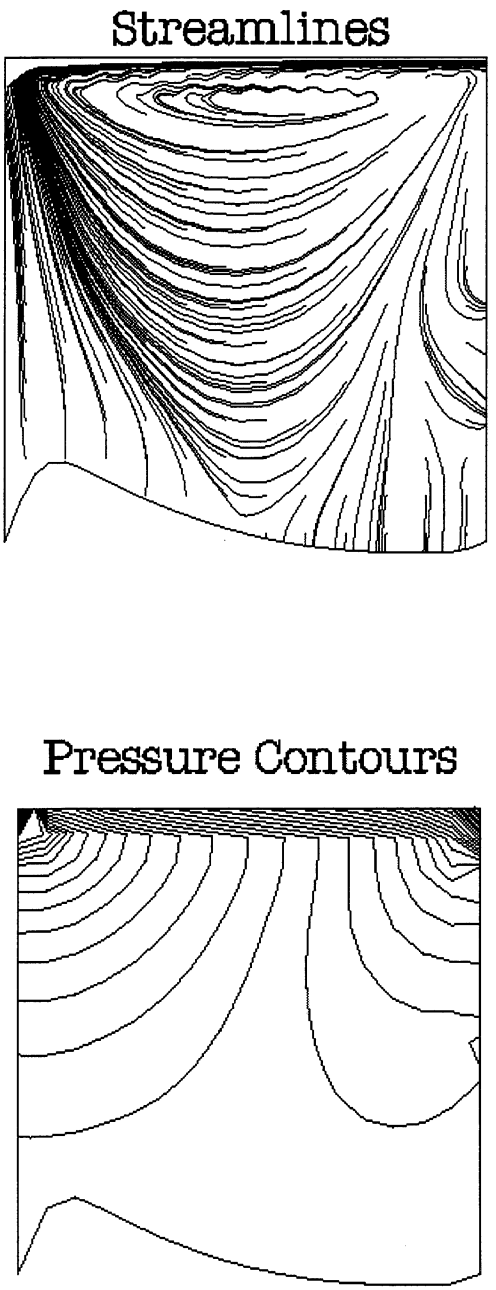

Figure 5. The steady-state solution of streamline and pressure contours for the fluid-membrane interaction problem.

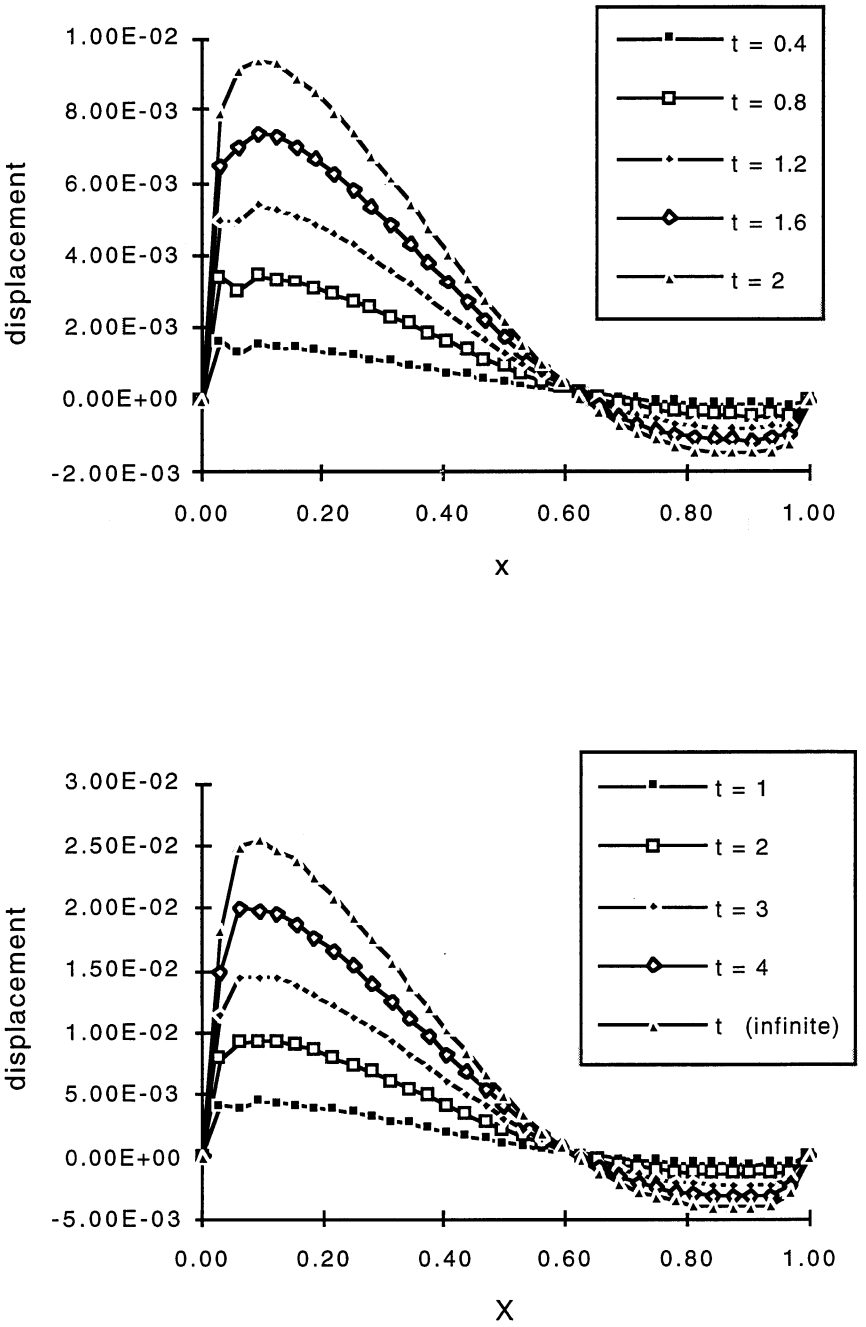

Figure 6. The membrane shape at different time instants for fluid-membrane interaction approaching steady-state.

(a) Pressure time history at x = 0.25, 0.5 and 0.75.

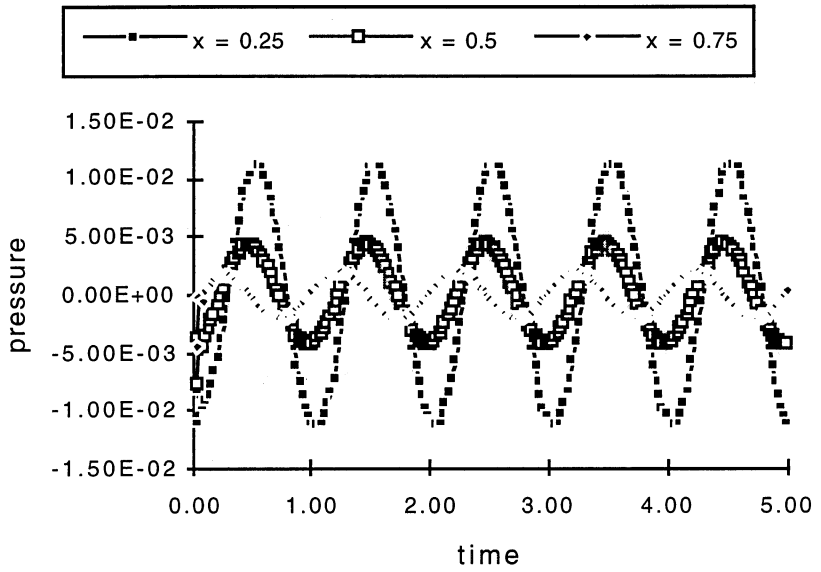

(b) Displacement time history at x = 0.25, 0.5 and 0.75.

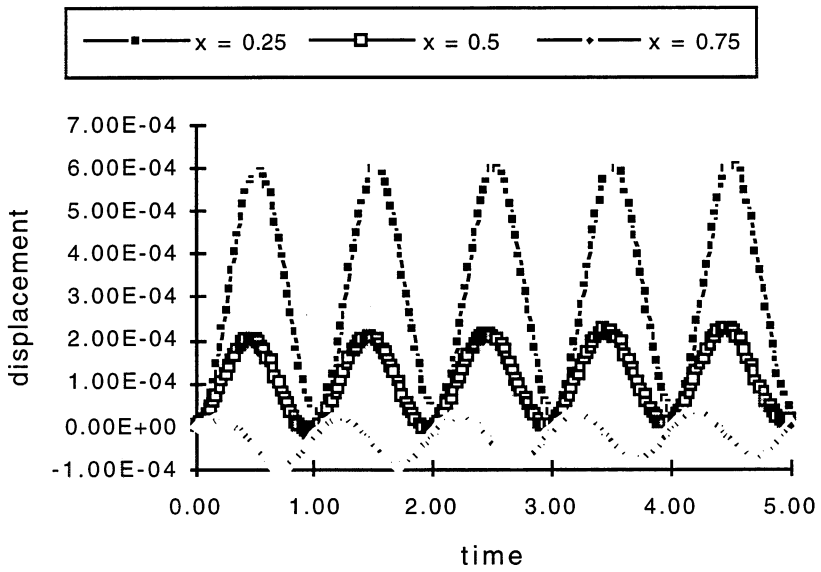

Figure 7 Time history of pressure and displacement on the membrane at x = 0.25, 0.5 and 0.75.

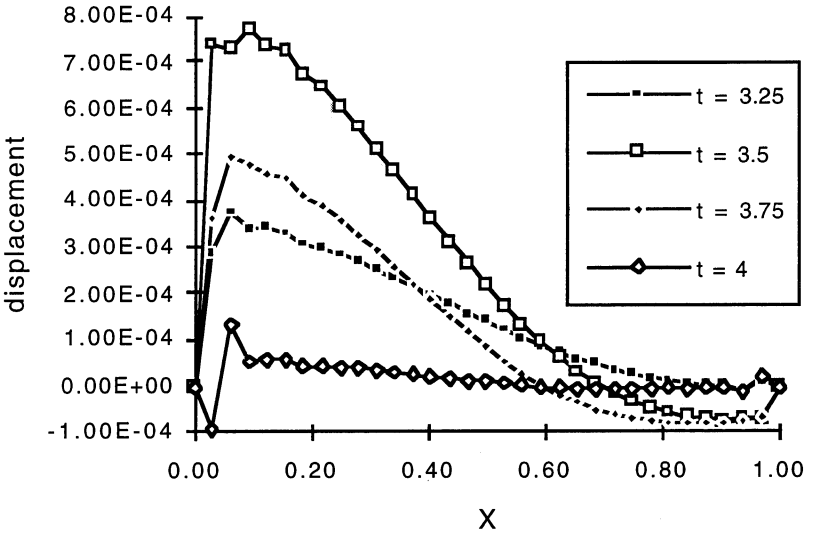

Figure 8 The membrane shape at different time instants for sinusoidal forcing case.

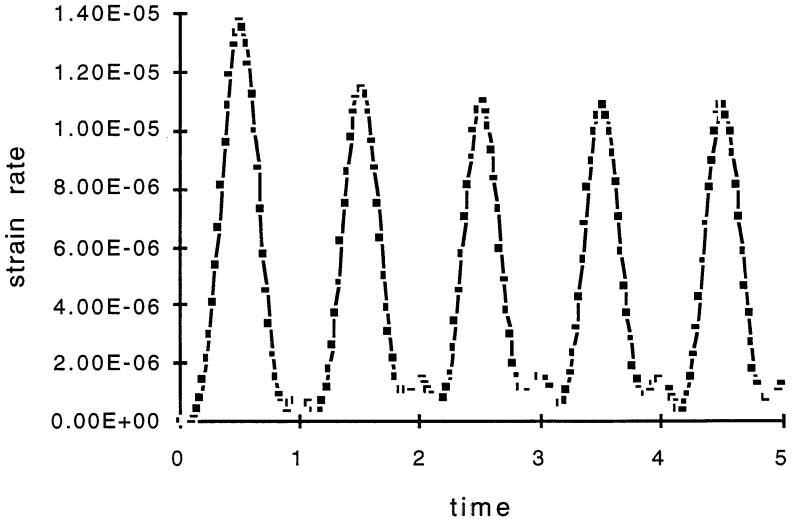

Figure 9 Time history of the strain rate of the membrane for sinusoidal forcing case.

t = 4.25

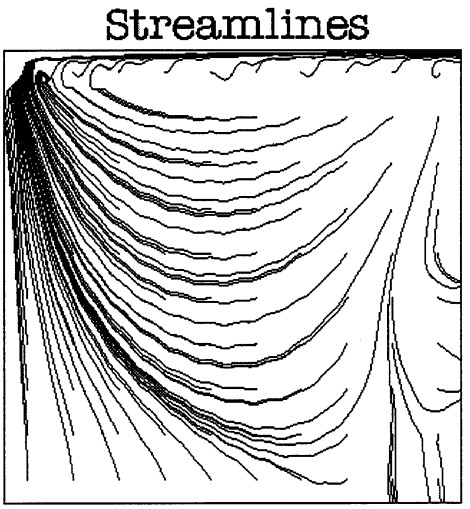

t = 4.75

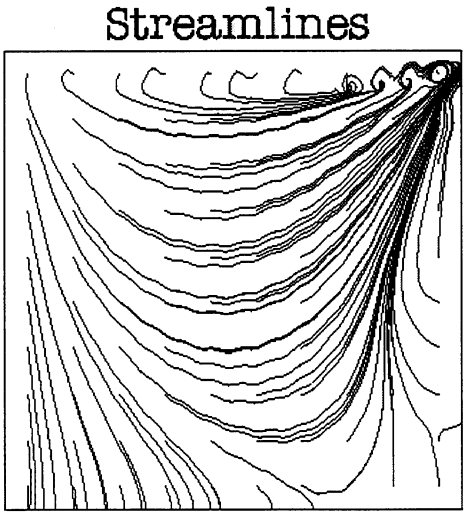

Figure 10 The streamlines at time = 4.25 and 4.75 of sinusoidal forcing case.

t = 4.25

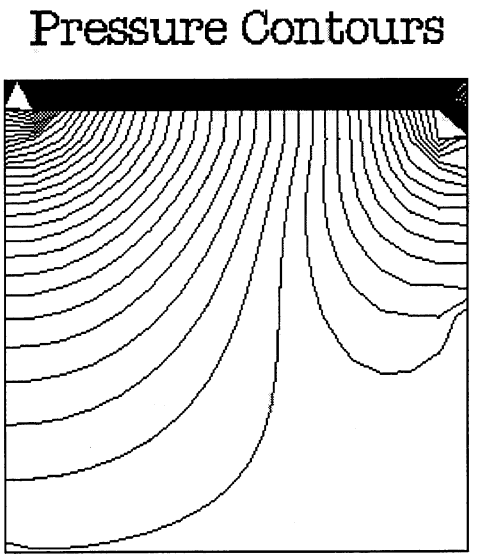

t = 4.75

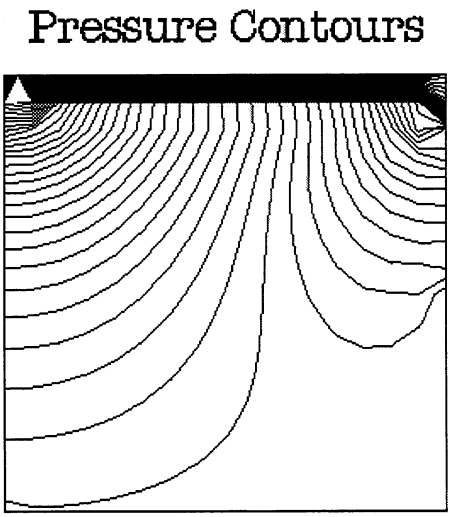

Figure 11 The pressure contours at time = 4.25 and 4.75 of sinusoidal forcing case.

SENSOR DEVELOPMENT

STATUS REPORT

FOR

PROJECT F020

Douglas Coffin

March 20 - 21, 1995

Institute of Paper Science and Technology
500 10th Street, N.W.
Atlanta, Georgia 30318

TECHNICAL PROGRAM REVIEW

Project Title: Sensor Development

Project Code: SENSOR

Project Number: F020

Project Staff: Douglas W. Coffin

Project Budget: $77,278

OBJECTIVE

The objective of this program it to build a science base of information and tools leading to the development of new sensors for the paper industry. The sensor technology obtained from this research effort will increase the efficiency of a process as well as increase the quality of the product.

SUMMARY

At the Spring 1994 meeting of the Process Simulation and Control PAC meeting, the need for sensor development in the paper industry was addressed. This led to the development of statements on four sensors chosen by the committee for consideration. The four sensors were as follows: Web Permeability Sensor, CD Jet Velocity Sensor, Black Liquor Heating Value Sensor, Recycled Pulp Fines and Contaminants Sensor. The present dues-funded project, Sensor Development, was initiated at this time and work began in August of 1994. These four sensors were reviewed, and the research possibilities were addressed at the Fall PAC meeting.

During the Fall meeting of the Process Simulation and Control PAC, it was decided that the sensor needs of the industry should be investigated. In order to narrow the scope of these industry needs, emphasis was placed on sensor needs in and around the papermachine. It was proposed that an informal survey of papermakers be conducted to

determine what problems they deemed important and where sensor development was needed. This survey was modeled after a successful survey of industry needs and problems pertaining to dimensional stability.

The survey on sensor needs did not lead to any conclusions on sensor needs , and no one area of development stood out as the most important issue. In fact, it was very difficult to find people willing to discuss sensor needs in detail. One general conclusion that could be drawn from the telephone conversations was that any sensor development that helps increase the efficiency of the papermachine or increases the quality of paper would be useful to the paper industry. Areas of research on sensors for the pulp and paper industry has been the focus of several papers and workshops in the recent past [1-8]. A summary of these needs is given in the background section.

It appears that many different areas could be addressed for sensor development; all with equal value to the industry. It is proposed that this research project center on sensors that would indicate moisture levels, drying rates, and shrinkage of the sheet. This would address some of the issues that have been noted as important to the papermaker. This information could be used in the control of the process to increase the efficiency of the process and the quality of the sheet. Research efforts in this area would compliment the dues-funded project on dimensional stability while maintaining a distinct objective towards sensor development.

In addition to developing new sensors, effort must be put into developing control strategies. For increased value of a new sensor, the sensed data should aid in the control of the process. Control strategies must be developed in conjunction with new sensors. For example, moisture levels, drying rate, and shrinkage of the sheet all influence the overall quality of the sheet and especially influence the dimensional stability of the sheet.

If one or all of these quantities could be sensed and the measurements used in a control strategy, then the possibility exists for increasing the efficiency of the process and the quality of the product.

GOALS

Taking into account the information gained in the past year on sensor needs, the goals of this project are as follows:

1. Develop a sensor or group of sensors that can be used to increase the efficiency of the papermaking process and the quality of the product. Specifically, the areas of moisture control and sheet shrinkage on the papermachine will be addressed.

2. Develop control strategies that utilize the developed sensors.

3. Transfer the developed technology to industry.

For the coming year the tasks of the project are as follows:

1. Develop a research program for sensor development for such parameters as moisture level, drying rates, and shrinkage on the papermachine.

2. Conduct a thorough literature search to determine the existing state of knowledge in this area pertaining to sensors, other measurement techniques, and control strategies.

3. Begin developing new technology which is deemed necessary from the results of the literature search.

BACKGROUND

Sensors provide essential information about the state of a process and are the key to automatic control of a process. On-line sensors provide rapid feedback to the operators and the data collected from these sensors can be used to maintain the process at normal operating conditions. Without sensors, it is improbable that today's papermachines could run at current speeds while maintaining product quality.

Even though the sensors available today are of great benefit to the papermaker, many sensors still do not meet expectations. The papermaker still has many needs that could be fulfilled by new or improved sensors that add insight into the process of papermaking.

The sensor needs of the paper industry have been addressed many times. In 1986, Rutledge [1] listed some specific needs including consistency gages which measure both filler and fiber and printability meters. Rutledge [1] suggests that "optical sensors, electro-optic sensors and fiber optic sensors are needed for rapid response and measurement."

In 1988 the National Science Foundation sponsored a workshop on the research needs of the pulp and paper industries [2]. As a result of this workshop, three categories for new or improved on-line sensors were listed as being essential for control systems to reach their full potential. The three categories were as follows: pulp quality characteristic sensors, process sensors, sensors for product quality characteristics. A list of 46 sensors were discussed by a panel of industrial experts. It is interesting to note that Hwalek, who recorded the workshop discussion [2], notes that "there was little consensus as to which are the most important variables to monitor in order to measure paper sheet and pulp quality."

TAPPI sponsored a workshop of paper industry research needs in 1992 [3], and the research needs in the area of sensors and process control were addressed. A list of high, medium, and low priority sensor needs was developed. For example, high priority items pertaining to moisture and drying were on-line freeness, dry line detector, drainage, CD shrinkage, and MD wet straining.

In 1993 the U.S. Department of Energy Office of Industrial Technologies sponsored a workshop entitled "Paper Mill of the Future" [4]. The purpose of this workshop was to act as a catalyst to develop a vision of the pulp and paper industry that could exist by the year 2020. During this workshop a group was formed to discuss papermaking technologies. Twenty-one potential technologies that could lead to reduced energy utilization and environmental impact were suggested. Each of these areas was assessed against potential for energy reduction, economic return, and environmental benefits. The list of twenty-one technologies was narrowed down to nine key technologies worthy of immediate attention. Finally, these nine key technologies were ranked from highest to lowest priority based on the probability of success associated with the technology and the benefit to be gained from each key technology. The highest ranking priority was the development of sensors and controls that minimize process and product variability. This report [4] states the following: current sensors are inadequate, a need exists for rapid and robust measurements, and total sheet measurements are needed. An outgrowth of this program was a document entitled *Agenda 2020*. *Agenda 2020* is a vision statement for the future of the forest products industry. One of the high priority areas for cooperative research given in *Agenda 2020* is sensors and control. The U.S. DOE has pledged to allocate government funds to support cooperative research in the pulp and paper industry [5].

National Institute of Standards and Technology (NIST) is considering an Advanced Technology Program [6] on sensors and controls in the medical device and bulk processing industries, including the pulp and paper industry. A workshop was held in 1994, and the needs for new sensors and control systems in the paper industry were presented. After the workshop, white papers were submitted to NIST, and a report was prepared for consideration as an ATP. The white papers addressing sensors and control systems for the pulp and paper industry [7,8] emphasized the importance of sensors and control systems to reduce operating costs, improve production, improve quality, and reduce environmental impact. These reports also state that although existing sensors and control systems have been of great benefit to the paper industry, much more research is needed to make further gains. Table 1 provides a list of sensor needs as reported in IPST's white paper [7]. This list was originally compiled for the Process Simulation and Control PAC from the data given in reference [3].

It is clear that the Paper Industry is dedicated to research efforts to develop new sensors. In addition, it appears that the government is dedicated to assisting the paper industry in improving sensor technology. As shown in Table 1, there are many technological issues that could be overcome with the development of new sensors.

Table 1. Sensor Needs in the Pulp and Paper Industries

Sensors

Woodyard
chip moisture
chip thickness
chip density
chip mean particle length and distribution
bark content

Pulping
digester level
residual alkali
lignin content
pulp viscosity
shives level
dissolved solids

Bleach Plant
flow meters
consistency
fiber properties
brightness
pH
pitch content
dirt particles

Recovery
black liquor viscosity
black liquor heating value
RB temperature
chloride in black liquor
droplet size
leak detection systems
TRS/opacity on stacks
causticizing efficiency
kiln temperature
lime availability
lime particle size
lime moisture content

Papermaking
recycled fiber content
broke brightness
refined stock properties
surface energy
freeness
wet fiber flexibility
porosity/formation
dry-line detection
fiber orientation
MD/CD/ZD strength or stiffness
curl
mottle
gloss
coating weight
ash content
web tension
drainage
rush/drag ratio
CD jet profile
CD shrinkage
coating quality

REFERENCES

1. Rutledge, W., "Recent Developments and Needs in Sensors for Sheet Products," *Selected Papers from the Sixth IFAC/IFIP/IMEKO Conference*, Akron, Ohio, October 27-29, 1986, Edited by A. Kaya and T. J. Williams, Pergamon Press, pp. 23-27.

2. *Research Needs in the Pulp and Paper and Related Industries,* a Report of an Industrial Workshop sponsored by the National Science Foundation, University of Maine, July 12-13, 1988.

3. *Proceedings of Paper Industry Research Needs Workshop*, sponsored by TAPPI, State University of New York, May 26-28, 1992.

4. Fleischman, E. and Sobcynski, S., *Pulp and Paper Mill of the Future: A Workshop*, Final Report, October 1993.

5. Burke, D. J., "DOE to Fund Pulp and Paper Research," *TAPPI Journal*, Vol. 78, No. 2, February 1995, pp. 28-29.

6. Repka J. R., *Sensors and Control Systems: Their Applications in the Medical Device and Bulk Processing Industries*, National Institute of Standards and Technology proposal for focused program, 1994.

7. *A Pulp and Paper Industry White Paper: An Advanced Technology Program to Stimulate the Development of Improved Measurement Sensors and Control Systems for the Paper Industry*, presented by The Institute of Paper Science and Technology, September 1994.

8. *Pulp and Paper Industry White Paper: In Response to ATP Sensors Workshop*, submitted by Measurement Technology Committee of the American Forest and Paper Association, July 1994.